Design and Synthesis of Donor-Acceptor π-Conjugated Systems

Craig Yu

Thesis submitted to the

Faculty of Graduate and Postdoctoral Studies

University of Ottawa

in partial fulfillment of the requirements for the degree of

Master of Science in Chemistry

Department of Chemistry and Biomolecular Sciences

Ottawa-Carleton Chemistry Institute

Faculty of Science

University of Ottawa

Table of Contents

Abstract

Organic π-conjugated molecules have garnered significant attention in the past twenty years for their potential applications in low-cost, lightweight, and flexible electronic devices. In particular, donor-acceptor (D-A) systems that involve the combination of electron-rich and electron-poor moieties in a molecule have been extensively studied due to tunability in intramolecular orbital interactions and materials properties. The theme of the current thesis is on the investigations of three different forms of D-A systems. Chapter 2 focuses on the design and synthesis of halogen-bonded organic frameworks using π-conjugated precursors as halogen bond donors and acceptors. The resulting co-crystals were subjected to single-crystal, thermal stability, and solid-state photophysical studies. In chapter 3, a series of D-A π-conjugated small molecules containing triphenylamine as the donor and an SF_5 group as the acceptor was designed. The investigations include their synthesis, intramolecular orbital interactions, and photophysical properties. Chapter 4 introduces a pyrazine-containing D-A polymer using two metal-free polymerization methods, and the photophysical properties of the polymer can be significantly tuned using postpolymerization techniques.

Acknowledgments

I would like to begin by thanking my supervisor, Prof. Julian Chan, for accepting me into his research group and providing his advisory throughout my time in his group. I have learned a great deal about organic synthesis and materials chemistry from you. I would like to thank my committee members, Prof. David Bryce and Prof. Stephen Newman for their support and insights toward my research. I am also thankful for all the professors whom I had for my graduate courses, Prof. Jaclyn Brusso, Prof. Louis Barriault, Prof. Fabien Gagosz, Prof. Derek Pratt, and Prof. Abdelhamid Sayari. Your lectures on materials chemistry and organic chemistry gave me the fundamental knowledge and inspirations for my research.

I am truly grateful to all the members, both former and present, of the Chan group, for providing a space where we could learn from each other, support each other through stressful times, and celebrate each other's achievements. I would like to give special thanks to my colleagues and dear friends Guoxian Zhang and Dr. Prabhat Gautam who made my graduate experience extremely enjoyable and gave me strength and support throughout my degree. I will forever cherish our friendship, and the time we spent inside and outside the lab.

I need to thank our talented crystallographer, Dr. Bulat Gabidullin, for solving all my crystal structures and providing me the data. My thesis would not have been complete without your hard work and our frequent discussions.

I cannot go without thanking all my family members, especially my father and grandfather, for your constant support since the first day of my M.Sc. program. I would like to thank all my friends, especially Jay, Joe, Jason, and Johnson, who are currently pursuing their graduate studies at other schools. Thank you for your encouragements and making me laugh every time we talk, I wish you all the best for your studies. Lastly, I would like to express my gratitude to my girlfriend, Gwen, who encouraged and supported me through thick and thin. Thank you for constantly reminding me to become the best version of myself. My graduate experience would not have been the same without you.

Abbreviations

OPV	Organic photovoltaic
OFET	Organic field-effect transistors
OLED	Organic light-emitting diode
DCM	Dichloromethane
THF	Tetrahydrofuran
DMF	*N*, *N*-dimethylformamide
TMS	Trimethylsilyl
TCNE	Tetracyanoethylene
TCNQ	Tetracyanoquinodimethane
COF	Covalent-organic framework
HB	Hydrogen bond
XB	Halogen bond
UV	Ultraviolet
IUPAC	International Union of Pure and Applied Chemistry
PVA	Pyridylvinylanthracene
TPA	Triphenylamine
IP	Ionization potential
D-A	Donor-acceptor
HOMO	Highest occupied molecular orbital
LUMO	Lowest unoccupied molecular orbital
TFTIB	1,3,5-trifluoro-2,4,6-triiodobenzene
TFDIB	1,2,4,5-tetrafluoro-3,6-diiodobenzene
1,4-BPB	1,4-di(pyridin-4-yl)benzene
1,4-BPEB	1,4-bis(pyridin-4-ylethynyl)benzene
2,5-BPET	2,5-bis(pyridin-4-ylethynyl)thiophene
N,N'-PNDI	2,7-di(pyridin-4-yl)benzo[lmn][3,8]phenanthroline-1,3,6,8(2H,7H)-tetraone

Experimental Section

NMR Spectroscopy

^{1}H, ^{13}C, and ^{19}F NMR spectra were recorded on the Bruker AVANCE II 400 MHz, and the Bruker AVANCE II 300 MHz NMR spectrometer. Chemical shifts were reported relative to TMS (^{1}H: δ = 0.00 ppm), $CDCl_3$ (^{1}H: δ = 7.26 ppm; ^{13}C: δ = 77.0 ppm), and $(CD_3)_2CO$ (^{1}H: δ = 2.05 ppm; ^{13}C: δ = 29.84 ppm). An external reference was used for ^{19}F NMR spectra, where the chemical shifts were reported relative to C_6F_6 (^{19}F: δ = -164.9 ppm).

Mass Spectrometry

High-resolution mass spectrometry was recorded on the Kratos Concept Magnetic Sector Electron Impact mass spectrometer. The samples were submitted to Dr. Sharon Curtis of the John L. Holmes Mass Spectrometry Facility at the University of Ottawa for electron impact experiments.

UV-vis Spectroscopy

The solution-state UV-vis spectra were recorded on the Cary 60 UV-vis spectrophotometer, and the solid-state UV-vis spectra were recorded on the Cary 7000 UV-vis spectrophotometer.

Fluorescence Spectroscopy

The solution-state and solid-state photoluminescence spectra were recorded on the Horiba Fluorolog-3 spectrofluorometer. The slit width for the emission was set at 1 mm.

Single-Crystal X-Ray Diffraction

Single-crystal X-ray diffraction data was collected on a Bruker APEX II diffractometer with graphite-monochromatized Mo-Kα radiation (λ= 0.71073 Å). Data collection and processing were performed using the Bruker APEX II software package. Semi-empirical absorption corrections based on equivalence reflections were applied. The structure was solved by direct methods and refined with full-matrix least-squares procedures using SHELX and WinGX. All non-hydrogen atoms were refined anisotropically. The positions of all hydrogen atoms were calculated based on the geometry of related non-hydrogen atoms. No restraints or constraints were applied during the refinement. The SCXRD experiments were conducted by Dr. Bulat Gabidullin in the X-ray Core Facility at the University of Ottawa.

Powder X-Ray Diffraction

The powder X-ray diffraction studies were carried out on a Rigaku Ultima IV diffractometer, and the experiments was conducted by Dr. Bulat Gabidullin in the X-ray Core Facility at the University of Ottawa.

Computational Calculations

The density functional theory (DFT) calculations for molecules containing C, H, N, F, S, O atoms were carried out at the B3LYP level of theory using the Gaussian09 program,[1,2] and LANL2DZ level of theory was employed for I atoms. A basis-set of 6-31G was used for all calculations, and a dispersion correction of (d,p) was used for the halogen-bonded network calculations. All molecules and complexes were first constructed in the GaussView program and later optimized using the Gaussian09 program.

References

(1) Becke, A. *J. Chem. Phys.* **1993**, *98*, 5648–5652.

(2) M. J. Frisch, G.; Trucks, W.; Schlegel, H. B.; Scuseria, G. E.; Robb, M. A.; Cheeseman, J. R.; Scalmani, G.; Barone, V.; Mennucci, B.; Petersson, G. A.; Nakatsuji, H.; Caricato, M.; Li, X.; Hratchian, H. P.; Izmaylov, A. F.; Bloino, J.; Zheng, G.; Sonnenberg, J. L. *Gaussian 09, Revision A. 1; Gaussian*; **2009**.

Chapter 1. Introduction

1.1 π-Conjugated Organic Materials

The ground-breaking discovery of electrical conductivity in polyacetylene upon I_2 vapor doping by Alan Heeger, Alan MacDiarmid, and Hideki Shirakawa not only led to the 2000 Nobel Prize in Chemistry, but also marked the beginning of the entire field of π-conjugated organic materials.[1] In subsequent years, numerous novel π-conjugated molecules (organic molecules that contain overlapping *p*-orbitals on adjacent atoms) such as polythiophene and oligoacenes have been developed (**Figure 1.1**), and their optical and electronic properties have also been intensively studied.[2] It is realized that the organic π-conjugated molecules can behave as semiconductor and metallic conductor materials and achieve a broad range of optical absorption, charge storage, and charge mobility. Thus, the discovery enabled the applications of the organic π-conjugated molecules in organic electronics and photonics, such as organic photovoltaics (OPVs), organic field-effect transistors (OFETs), and organic light-emitting diodes (OLEDs) (**Figure 1.2**).[3–5]

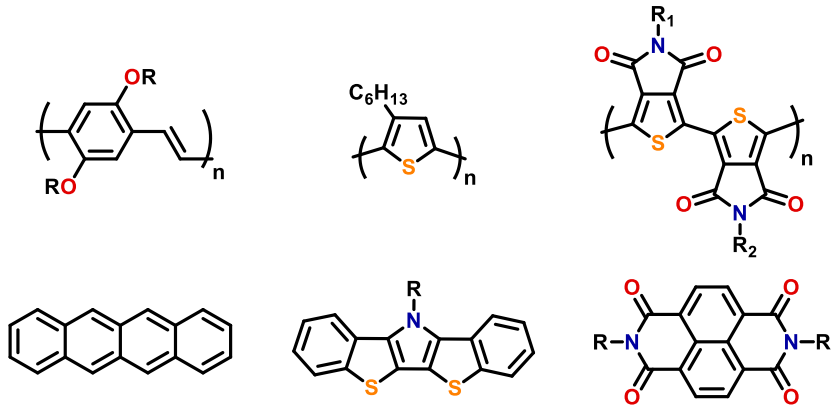

Figure 1.1. Examples of π-conjugated functional organic materials.

The π-conjugated organic materials are of considerable interest due to their low cost of synthesis, tunability, and mechanical flexibility, as compared to the traditional inorganic-based electronic materials such as silicon.[6] Unlike the synthesis of silicon-based materials, which requires high temperature (T= 500˚C),[7] π-conjugated organic materials can be readily synthesized through robust organic transformations such as Pd-catalyzed cross-coupling reactions, which reduces the cost of synthesis of the materials.[8] The development of modern organic synthetic methods also allows facile functionalization of the organic materials to tune their optical and electronic properties.[9] Inorganic-based materials are generally hard and brittle, while organic materials, on the other hand, resemble plastics in that they are mechanically flexible in nature, a desirable feature for developing next-generation, large-area flexible electronics.[10]

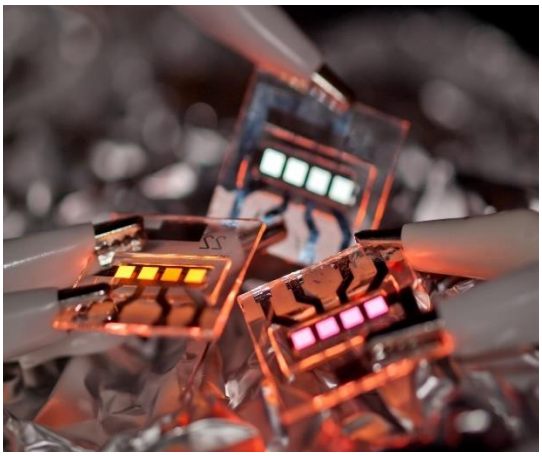

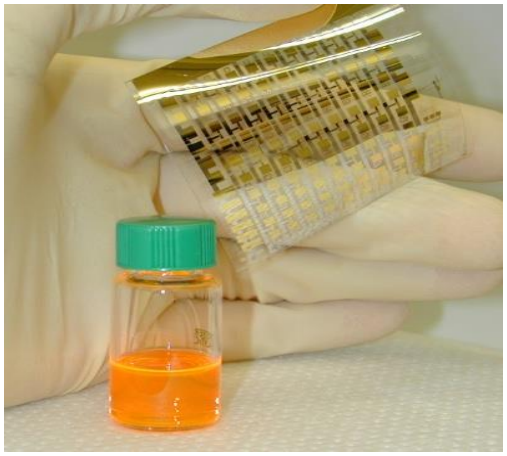

Figure 1.2. Left: An image of OLED devices. Photo: IAPP. Right: A Thin-film OFET device and a semiconductor solution. Photo: University of Stuttgart.

Despite its rapid development, the performance of contemporary π-conjugated organic materials is still inferior to that of silicon-based materials. The low power conversion efficiency of OPVs and low charge mobility of OFETs devices make their commercialization far from reality. Although the performance of state-of-the-art organic electronic materials does not exceed that of silicon-based materials, improvement of their optoelectronic properties through chemical modifications and device fabrication techniques can be complementary to silicon-based materials, which can reduce the cost and enable new device functionalities such as mechanical flexibility and impact resistance.[11] A significant amount of effort in the current quest for high-performance π-conjugated organic materials is focused on, but not limited to three categories, π-conjugated organic polymers, small molecules, and covalent organic frameworks. Each type of organic π-conjugated system has its unique potential and areas of improvement; thus, intensive research is required to thoroughly investigate and improve the properties of each system and utilize their advantages to develop high-performance materials.

1.2 π-Conjugated Systems

1.21 π-Conjugated Polymers

The π-conjugated polymer systems contain a π-conjugated backbone in which the π-orbitals are extended throughout the entire polymer chain to enable intramolecular charge-transfer, and optical absorption,[12] and the conjugation units commonly include aromatic rings, heterocycles, olefinic and acetylenic groups. The π-conjugated polymers are often functionalized with solubilizing substituents such as hydrocarbon chains that promote solution-processability during device fabrications, and the enhancement of intermolecular interactions in the solid-state.[13]

The performance of π-conjugated polymer-based materials also depends on properties such as the molecular weight and the distribution of molecular weight, called the dispersity ($Đ$). Polymers with high

molecular weight have longer conjugation length which improves the charge-transport property and broadens the optical absorption. Polymerization methods for the synthesis of high molecular weight π-conjugated polymer is also an active area of research. It is also important to minimize $Đ$ so that the polymers have similar chain lengths and unwanted small molecules and oligomers are excluded from the polymer mixture. Polymers with low $Đ$ have smooth morphologies and fewer surface defects, which is desirable for charge-transport properties and optical absorptions.[11]

The intrinsic drawback of the polymeric systems is their low crystallinity. The low crystalline, and highly amorphous solid-state morphology could lead to isotropic charge transport characteristics, which ultimately results in lowering of the materials performance.[14] However, polymers generally form good quality thin-films with smooth and uniform surface due to their high viscosity, which is excellent for device fabrication and performance.[11]

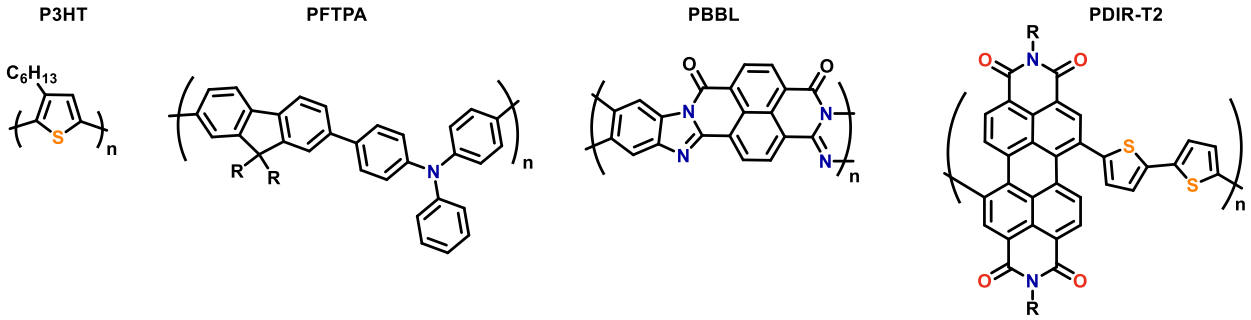

Figure 1.3. The structures of P3HT, PFTPA, PBBL, and PDIR-T2.

To date, numerous π-conjugated polymers have been designed and synthesized, from electron-rich systems such as poly(3-hexylthiophene) (P3HT) and fluorene/triphenylamine co-polymer poly(9,9-dialkylfluorene-alt-triphenylamine) (PFTPA), electron-deficient systems like poly(benzobis-imidazobenzophenanthroline) (PBBL), as well as donor-acceptor polymers such as poly(*N,N'*-dialkylperylenedicarboximide-dithiophene) (PDIR-T2) (**Figure 1.3**). The polymerization of the π-conjugated polymers is commonly done by Pd-catalyzed polycondensation such as Stille polycondensation and Suzuki polycondensation.[15,16] Recent progress on Pd-catalyzed direct arylation polycondensation has also been extensively researched, and high molecular weight and low dispersity polymers can be efficiently synthesized using these methods.[17]

1.22 π-Conjugated Small Molecules

The development of π-conjugated small molecules in organic electronics is also an extremely active area of research. Compared to the polymeric systems, π-conjugated small molecules can be readily purified by traditional column chromatography and crystallization techniques, which are not applicable to the polymeric systems. The elimination of impurities from organic materials is essential since they lead to

charge-carrier traps, which diminish the performance of the device. The π-conjugated small molecules can also achieve high crystallinity by solution-grown crystallization and vacuum deposition techniques. In electronic devices such as OFETs, the performance of the device depends on the intermolecular transport of the charge-carriers, and the efficiency of charge-transport depends on the organization of molecular arrangement in the solid-state. Highly crystalline molecules facilitate efficient intermolecular charge-transport, thus improves the performance of the electronic materials. To date, the highest performing OFET materials are small molecules such as crystalline pentacene and rubrene (**Figure 1.4**).[14]

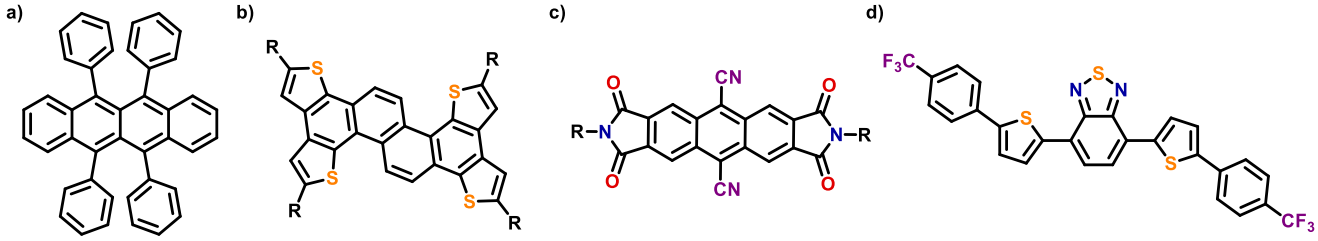

Figure 1.4. Structures of a) rubrene, b) electron-rich, c) electron-deficient, and d) donor-acceptor π-conjugated small molecules.

A large number of π-conjugated small molecules have been reported in the literature, and their application spans multiple areas such as OFETs, OPVs, OLEDs, and organic lithium-ion batteries. The design principle of π-conjugated small molecules is similar to that of polymeric systems, where electron-rich, electron-deficient, and donor-acceptor moieties are designed for their specific functions (**Figure 1.4**). Electron-deficient π-conjugated materials in their charge-carrying state are prone to oxidation under ambient conditions by water and oxygen due to their role as the electron acceptor in the electronic device. Thus it is crucial to obtain low-lying LUMO energy levels to prevent such undesired reactions. The installation of certain functional groups that can tune the electronic property of small molecules is made convenient by modern synthetic techniques, and the functionalization with electron-withdrawing substituents such as -F, -CF_3, and -CN can effectively lower the LUMO energy levels and improve the performance and stability of the electron-deficient materials.[18]

1.23 Covalent Organic Frameworks

The covalent-organic frameworks (COFs) with π-conjugated monomer units typically form two-dimensional (2D) sheets (**Figure 1.5**). Similar to the polymeric system, COFs have continuous π-conjugation, but its conjugation extends in two dimensions. The 2D monolayer sheets stack on top of one another to form highly organized columnar structures, therefore giving rise to its crystallinity and porosity. The molecular arrangement of COF provides a unique continuous crystalline π-conjugated system, which is difficult to achieve with small molecule and polymeric systems.[19] In 2005, Yaghi and co-workers reported the synthesis of the first covalent-organic frameworks from the 1,4-phenylenediboronic acid precursor by condensation.[20] The resulting COF structures were found to have highly crystallinity and

micro/mesoporosity, as well as thermal stability up to 600˚C. This landmark study provided the synthetic method for COF and enabled the application of COF-based materials. The early applications of COF were in gas capturing/storage and heterogeneous catalysis due to the porous structures;[21] however, applications of COF in organic electronic materials have surfaced in recent years. COFs have been shown to be strongly emissive upon optical excitation, and possess good charge-mobility in OFET devices due to their molecular packing.[22,23] In 2017, redox-active COF materials were developed, and they have shown high capacitance which is promising for the supercapacitor applications.[24]

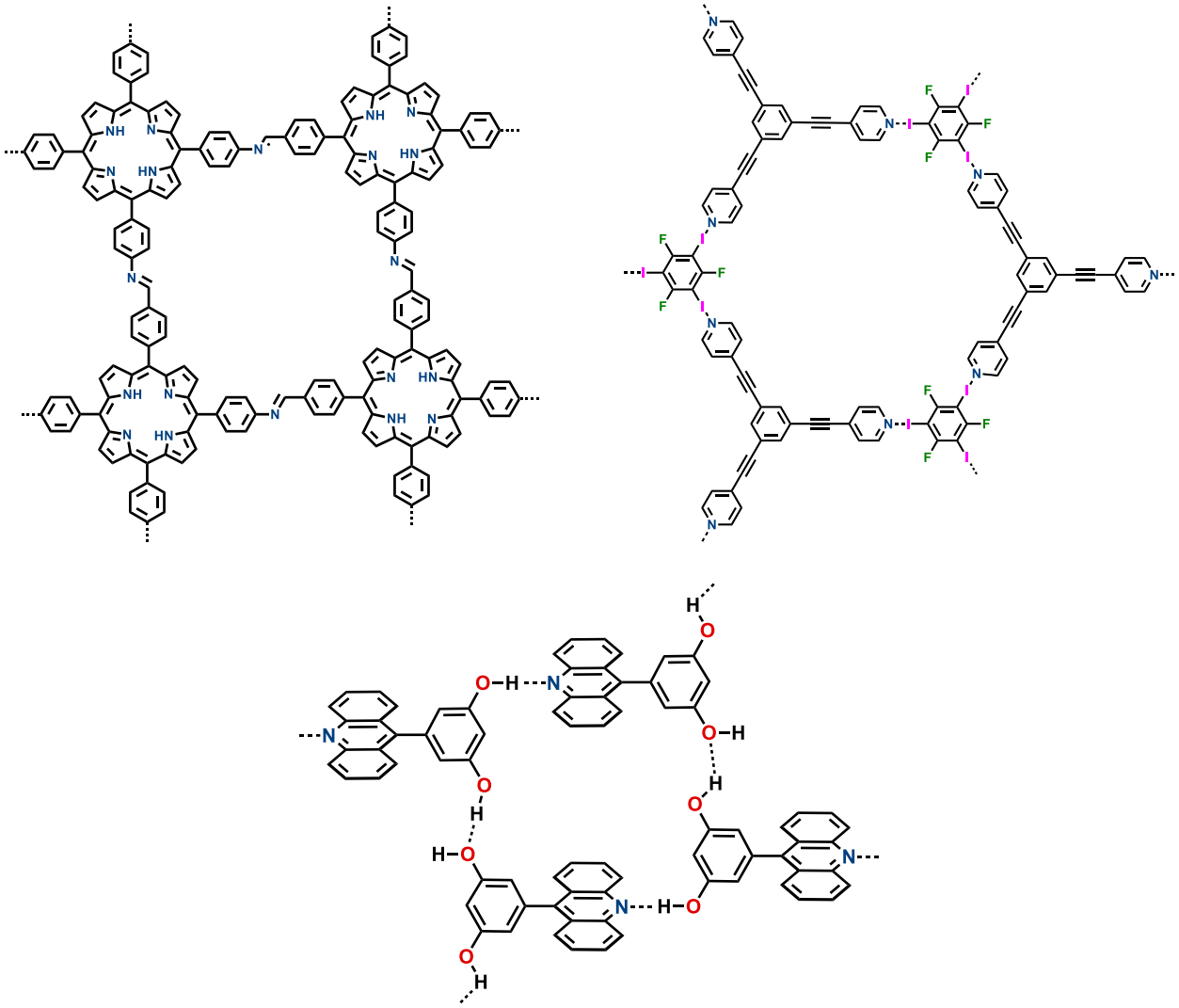

Figure 1.5. The molecular structure of a COF (left), the molecular structure of a halogen-bonded 2D network (right), and an example of a hydrogen-bonded network (bottom).

On the other hand, non-covalent organic frameworks are also being developed, where the chemical linkage between the monomer units are non-covalent in nature. One of the most utilized non-covalent interaction for the construction of non-covalent organic frameworks is the hydrogen bond (HB) (**Figure**

1.5). The π-conjugated monomer units need to contain an HB donor and an acceptor. The synthesis of the HB organic frameworks is typically done by solution-grown crystallization techniques between the HB donor and acceptor. The resulting crystalline structures have been studied for gas absorption/storage, light-emission, and OFET applications.[25–27] In addition to the HB organic networks, less studied interactions such as the halogen bond (XB) have also been developed, and highly ordered 2D XB π-conjugated organic frameworks were recently synthesized by electrical stimulation (**Figure 1.5**).[28]

1.3 Halogen-Bonded Organic Networks

1.31 A Brief History of the Halogen Bond

The first observation of XB interactions could be traced back to 1814, when J. J. Colin and J. L. Gay-Lussac reported the formation of a dark blue colored liquid upon combination of iodine and amylose.[29] Since then, many other XB complexes were reported, such as the observation of the formation of $NH_3 \cdots I_2$ complex by F. Guthrie in 1864,[30] and the quinoline and iodoform adduct by O. Rhoussopoulos in 1883.[31] Despite the ample number of reports on the observation of apparent XB interactions in the literature, systematic studies on the properties of the XB was not done until the 1950s when R. S. Mulliken studied the charge-transfer interactions between I_2 and a series of organic solvents using UV-vis spectroscopy, and O. Hassel obtained the first X-ray crystallographic data of an XB adduct and studied the strength and directionality of the novel interaction.[32,33] The term *halogen bond* was first coined by R. M. Hedges and co-workers when they studied the halogen-phosphine/sulfide oxides in 1961, to describe the interactions where the halogen acts as an electrophilic species, as an analogy to the role of hydrogen in hydrogen-bonding interactions.[34] As the nature of the XB interaction becomes clear thanks to the aforementioned fundamental studies, the number of papers containing the concept of XB has been increasing exponentially since the late 1990s.[35] The application of XB interactions spans across multiple fields of chemistry, including crystal engineering,[36] catalysis,[37] medicinal chemistry,[38] as well as materials chemistry.[39]

1.32 Nature of the Halogen Bond

The unified definition of XB was given by the IUPAC in 2009.[40] A typical XB is as shown in **Figure 1.6**, where R-X is the XB donor that contains the halogen atom X, which is electrophilic in nature, and an R group which is usually covalently bonded to atom X. The XB acceptor is denoted as Y, the species that contains a nucleophilic region, and it acts as a Lewis base that donates the electron density to the electrophilic XB donor in an XB interaction. To summarize the IUPAC definition in one sentence, an XB is where there is evidence of bond formation between a nucleophilic species Y and an electrophilic halogen atom X.

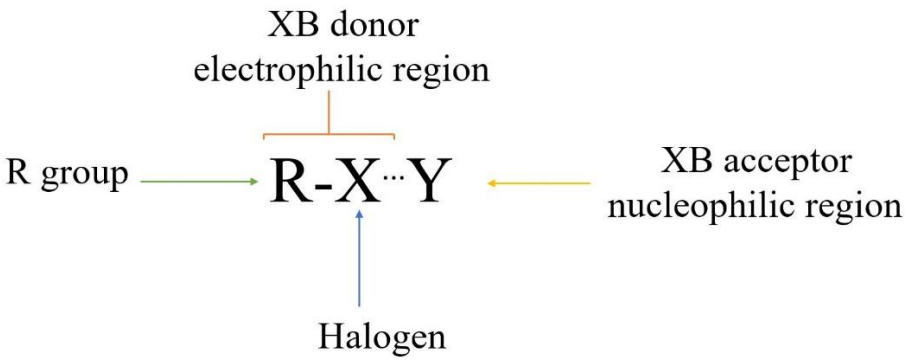

Figure 1.6. Schematic representation of the IUPAC definition of XB.

The highly anisotropic (directional) nature of the XB arises from its unique electrostatic potential on the XB donor. Owing to the polarizability of the covalently bonded halogen atom, it forms a nucleophilic belt that is orthogonal to the covalent bond, and an electrophilic region called the σ-hole where the XB interactions occur, and since XB only forms at the region, the resulting XB interactions are highly directional. A theoretical study by Politzer and co-workers demonstrated the concept perfectly, as the authors calculated the electrostatic potential surface of 1,2-diiodoperfluoroethane,[41] and observed the electrostatic potential surface shown in **Figure 1.7**. The fluorine atoms are electronegative, and as for the iodine atoms, nucleophilic belts that are perpendicular to the C-I bond are formed, and this region can potentially participate in hydrogen bonding interactions. A small electropositive region at the end of the iodine surface is formed and gives rise to the σ-hole, which is responsible for the formation of highly anisotropic XB interactions.

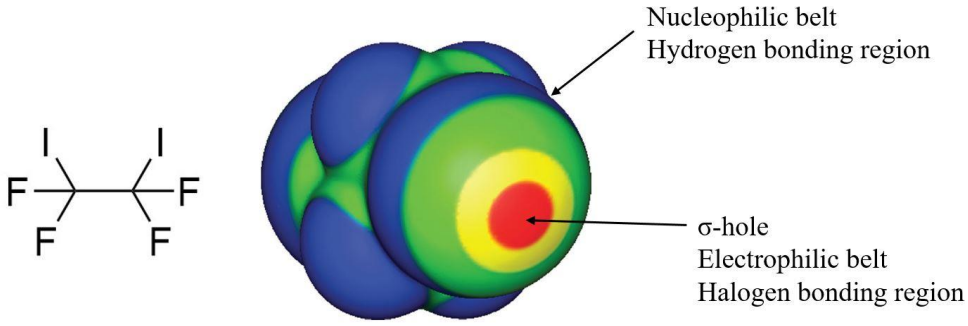

Figure 1.7. The electrostatic potential surface of 1,2-diiodoperfluoroethane calculated at the M06-2K/6-311G(d) level of theory. Color ranges, in kcal mol^{-1}, are red, greater than 25; yellow, between 15 and 25; green, between 0 and 15; blue, less than 0 (negative).[41] Figure was slightly modified from the original.

The strength of the XB is directly proportional to the size of the σ-hole and the size of the σ-hole is dependent on the polarizability of the halogen atom participating in the XB. A polarizability scale of the halogens is as such, F < Cl < Br < I, therefore, Br and I are commonly used as the XB donor to improve the strength of the XB. The hybridization of the C atom covalently bonded to the halogen can affect the strength of the XB, where *sp* hybridized carbon-X produces the strongest XB, follow by sp^2 carbons, and lastly, sp^3

carbons. The strength of the XB can also be affected by the electronic nature of the XB donor, the larger the difference in electronegativity between the R group and the X atom, the larger the σ-hole. A study by Bruce and co-workers in 2009 compared the XB distances among the iodobenzene XB donors with different degrees of fluorination and observed a decrease in the XB distance as the electronegativity of the R group increased.[42]

The electronic nature of the XB acceptor can affect the strength of XB as well. Since the XB acceptor acts as the Lewis base in the XB interaction, an increase in its nucleophilicity could improve the donor-acceptor interaction, and therefore, strengthen the XB. Common XB acceptors are the group V and VI atoms, such as N, O, and S, and due to the higher nucleophilicity of N, it forms stronger XB as compared to O and S.[43] It is recently found that polycyclic aromatic hydrocarbons can also act as the XB acceptor, where the π-electron clouds interact with the electrophilic XB donors, although the strength of the C-I$\cdots\pi$ is found to be much weaker than that of typical C-I$\cdots$N XB interactions.[44]

1.33 Applications of Halogen Bonding in Materials Chemistry

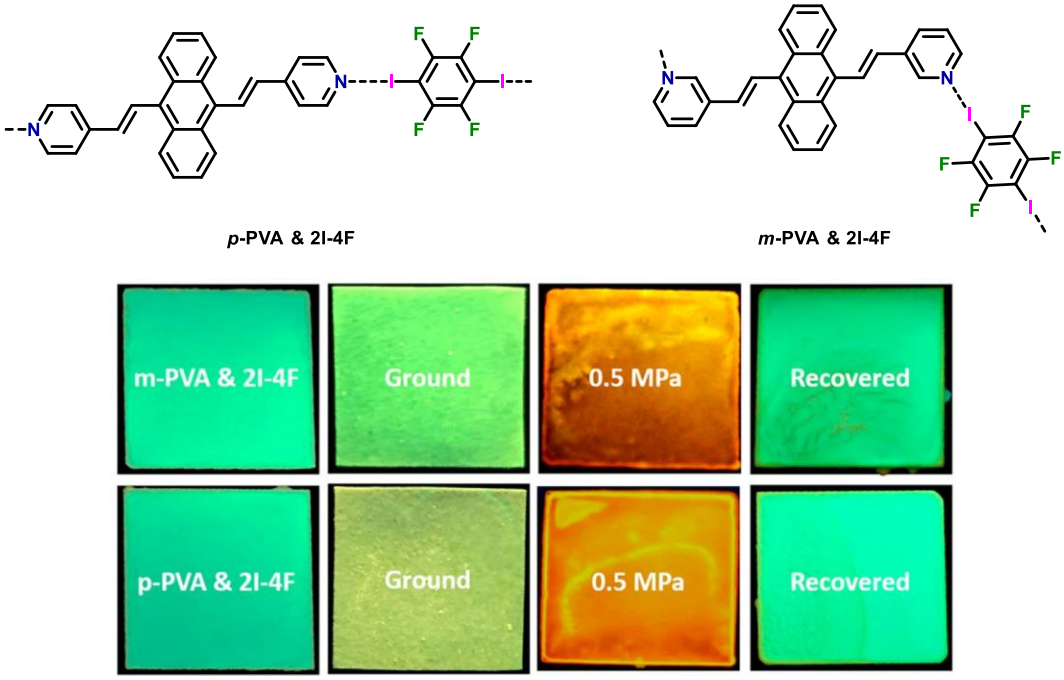

Figure 1.8. The structures of *p*-PVA & 2I-4F and *m*-PVA & 2I-4F, and their mechanofluorochromism and piezofluorochromism. The figure showed the fluorescent emissions of the two co-crystals in their crystalline states and ground states, illustrating the mechanofluorochromic effect. The ground crystals were then subjected to mechanical pressure of 0.5 MPa, whereby they demonstrated piezochromic properties. The co-crystals restored their original fluorescent emissions upon the release of pressure.[45]

The XB interaction was extensively studied in the field of liquid crystals and gels, as an analog to the better studied hydrogen-bonded materials.[46,47] The highly directional XB interactions facilitated unique

supramolecular arrangements in the liquid-crystal material.[48] In addition to the aforementioned areas of research, optoelectronic materials with XB interactions have also been rapidly developed.[35] The XB interaction is a powerful method for tuning the optical properties of solid-state materials by controlling the orientation of the molecular arrangement, and either of the donor or acceptor components of the XB materials can be readily tuned prior to co-crystallization by chemical modifications to improve the optical properties. A study by Duan and co-workers in 2011 took a stilbene derivative 1,4-bis-*p*-cyanostyrylbenzene as the XB acceptor, co-crystallized it with different XB donors. Different XB interactions the XB acceptor formed with different donors led to various solid-state supramolecular arrangements, and ultimately resulted in different emission behaviors, demonstrating the tuning of optical properties through XB interactions.[49] A recent study by Zhao and co-workers used two isomeric XB acceptors *p* and *m*-pyridylvinylanthracene (PVA) and co-crystallized them separately with 1,4-diiodotetrafluorobenzene to investigate their molecular packing modes and optical properties (**Figure 1.8**).[45] The results showed that the isomeric XB acceptors produced vastly different molecular packing modes and different UV-vis absorption and photoluminescent properties, and used these co-crystals as piezofluorochromic materials, which are emissive materials that respond differently upon changes in pressure. Another study by Hu and co-workers investigated the difference in molecular packing modes between the 1,2-bis(4-pyridyl)ethylene/1,4-diiodotetrafluorobenzene and 1,2-bis(4-pyridyl)ethylene/1,3,5-triiodotrifluorobenzene and reported a better molecular orbital overlap observed in the latter co-crystal. The better molecular packing behavior led to a stronger charge-transfer interaction that is supported by theoretical and experimental findings and the latter co-crystal also showed semiconducting behavior in their conductivity measurements whereas the former co-crystal exists as an insulator.[50]

1.4 π-Conjugated Donor-Acceptor Small Molecules

The application of π-conjugated small molecules in the field of materials sciences, including OFETs,[14] OPVs,[46] and OLEDs[47] has been of particular interest due to their ease of synthesis, tunability, and crystallinity. The incorporation of an electron-rich donor and an electron-deficient acceptor into the π-conjugated small molecules, known as donor-acceptor (D-A) systems, also attracts intense attention due to their strong intramolecular charge-transfer effects.[51–53] One of the attractive features of D-A small molecules is their tunability, as there is a large number of donors such as thiophene and carbazole, and acceptors including benzothiadiazole and isoindigo reported in the literature, which could be potentially combined to improve the properties of the optoelectronic materials. The design principle of effective D-A systems is based on molecular orbital (MO) theory, as the intramolecular orbital mixing between the donor and acceptor units lowers the energy level of the LUMO and raises that of the HOMO, thereby narrowing the HOMO-LUMO energy gap of the new molecule (**Figure 1.9**).[54] The reduction of the HOMO-LUMO energy gap facilitates the excitation of the ground-state electron from the HOMO to higher energy levels.

This in turn facilitates broader solar absorption and improves the charge-transfer in organic semiconductors, which is beneficial for the development of organic optoelectronic materials.[55,56] This feature of the D-A systems has motivated numerous research groups to conduct "bandgap engineering" of organic materials in an effort to fine-tune their optoelectronic properties.[57]

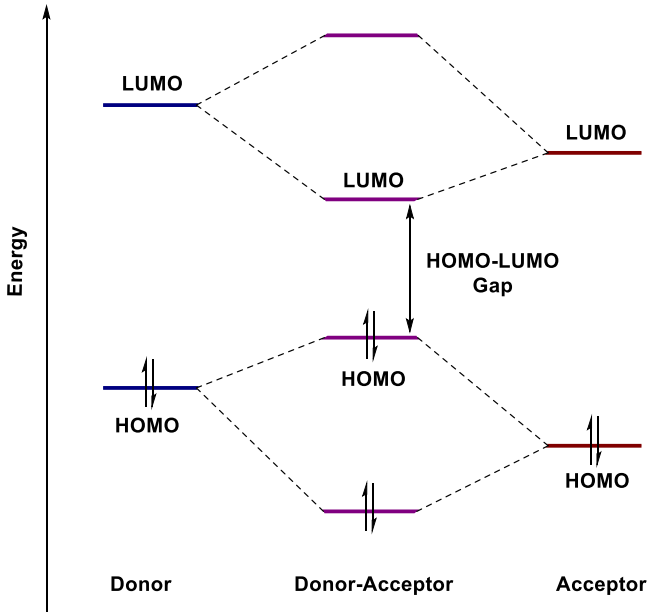

Figure 1.9. The MO diagram of the donor, acceptor, and the resulting donor-acceptor molecules.

1.41 The Triphenylamine Donor

The electron-donating nature of the lone pair of the nitrogen lone pair in the triphenylamine (TPA) moiety makes it an excellent candidate for the design and synthesis of electron-rich π-conjugated donors (**Figure 1.8**). The TPA unit has a low ionization potential (IP), which is a favorable feature for donor molecules as they are oxidized in the optoelectronic devices.[58] The low IP also favors the formation of the radical cation upon excitation,[59] which contributes to the remarkable hole-transporting ability of the TPA unit in organic optoelectronic devices including OFETs, OPVs, and OLEDs.[60–64]

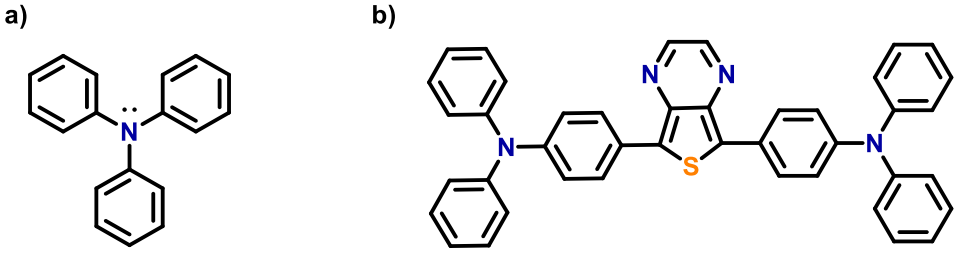

Figure 1.10. a) The structure of TPA, and b) a TPA-containing D-A small molecule.

From a synthetic point of view, the TPA unit is an inexpensive commercially available reagent, and the functionalization of the moiety is convenient. It can be efficiently halogenated in a regioselective

manner prior to metal-catalyzed cross-coupling, which makes TPA a favorable unit for the development of donor molecules. Given by the sp^3 hybridization of the nitrogen atom of the TPA unit, it forms a unique propeller molecular geometry which allows the formation of both linear and star-shaped π-conjugated systems. The star-shaped π-conjugated systems have the conjugation extended in three dimensions,[65] and such an extension in conjugation contribute to the broadening of the absorption of the molecules, which is favorable for optical devices such as OPVs.[65,66]

The incorporation of the TPA group into D-A π-conjugated systems is commonly seen in the literature due to its aforementioned superior electronic properties and ease of functionalization (**Figure 1.10**). The effects of intramolecular orbital interaction of TPA-based D-A molecules is evident from the distribution of the HOMO and LUMO, as the HOMO coefficient is commonly found on the TPA moiety and that of the LUMO resides on the acceptor component.[67,68] The distinct HOMO and LUMO distribution is favorable for tuning the charge-transfer interactions and charge mobilities of organic optoelectronic materials.[14,69]

1.42 The Pentafluorosulfanyl Acceptor

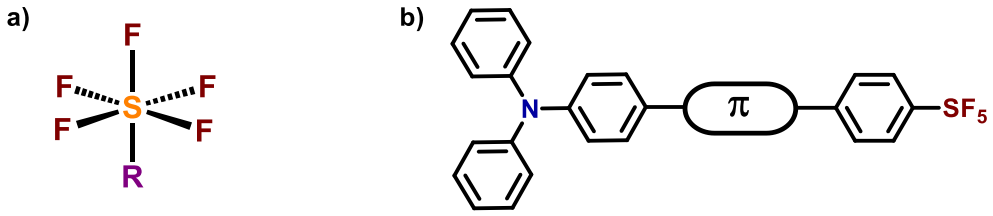

Figure 1.11. a) The structure of the SF_5 functional group, and b) SF_5-containing D-A π-conjugated small molecule.

The highly electronegative pentafluorosulfanyl (SF_5) substituent contains a sulfur in the octahedral geometry, bonded to one axial and four equatorial fluorine atoms (**Figure 1.11a**).[70] The functional group has also shown high steric bulk, lipophilicity, and thermal stability, which is superior to the analogous CF_3 substituent regarding properties.[71] The SF_5 group was first introduced by W. A. Sheppard in 1962,[72] and the subsequent application of the SF_5 was primarily in the field of medicinal chemistry.[73,74] More recently, the SF_5 substituent has been applied in the field of materials chemistry, as Hahn and co-workers studied the effect of a series of SF_5-containing molecules for liquid crystal applications,[75,76] and the incorporation of the SF_5 group in the porphyrin macrocycles and BODIPY was done by Wiehe and co-workers.[77] A study by Mecking and co-workers in 2017 developed a series of SF_5-containing Ni(II) catalysts for the synthesis of ultrahigh-molecular-weight linear polyethylene. Despite the recent efforts in investigating the SF_5 substituent in the context of materials chemistry, the number of studies on the optoelectronic properties of this functional group is scarce. Thus, we were motivated to develop novel D-π-A conjugated small molecules that utilize the SF_5 group as the acceptor, and triphenylamine as the donor, linked covalently by

a π-linker (**Figure 1.11b**), to carry out a systematic study on the solid-state crystal packing, as well as the solution-state, film-state, and solid-state photophysical properties of the SF_5-containing D-A molecules.

1.5 π-Conjugated Donor-Acceptor Polymers

The study of π-conjugated D-A polymers started in 1991 by Yamamoto and co-workers on the electron-rich thiophene and electron-deficient pyridine co-polymer system to narrow the HOMO-LUMO energy gap. The resulting energy gap was found to be slightly smaller than that of polythiophene, which suggested that the effective narrowing of the energy gap requires not only a strong donor but also a strong acceptor.[78] Wynberg and co-workers adopted the D-A concept in 1992 to synthesize low bandgap molecules for intrinsic organic conductors. The presence of strong donor and acceptor in polysquaraine and polycroconaine successfully reduced the HOMO-LUMO energy gap to 0.5 eV, and the polymers showed weak intrinsic electrical conductivity and near-IR absorption.[79] With the development of stronger acceptor moieties, the energy gap of the π-conjugated D-A polymers can be more effectively tailored towards specific organic electronic materials.

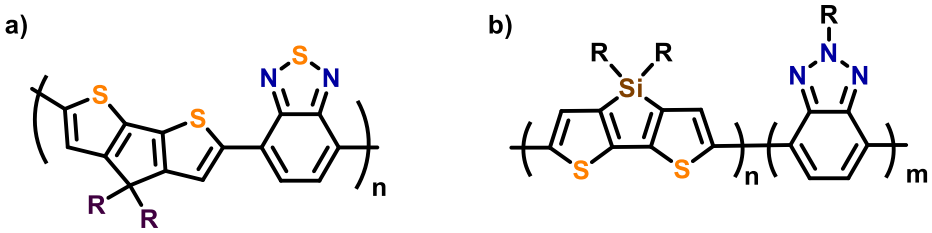

Figure 1.12. a) An alternating D-A copolymer, and b) A block copolymer.

The design of D-A polymers can be of two methods, the D-A alternating co-polymer, which the π-conjugated polymer backbone contains the electron-rich and electron-withdrawing components that are alternatively linked with each other (**Figure 1.12**). The early polymerization technique used to prepare D-A alternating copolymers relied on condensation reactions such as the Knoevenagel polycondensation, and more modern techniques generally utilize Pd-catalyzed reactions such as the Stille and Suzuki polycondensation methods where one monomer contains the organometallic groups, and the other monomer contains the halogen groups. Another type of design is the D-A block copolymer (**Figure 1.12**), where the polymer contains two different repeat units, one being the donor unit, and the other being the acceptor unit. Some reports have shown that the D-A block copolymers have broader optical absorption as compared to their D-A alternating copolymer design, which is similar to the sum of the absorption of the donor homopolymer and the acceptor homopolymer. However, the synthesis of the D-A block copolymer is more challenging than the alternating copolymer counterpart, which is generally done by polymer chain extension and grafting two homopolymers together.

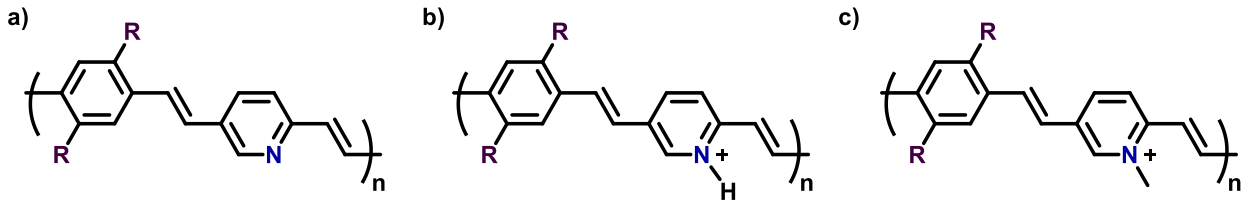

Figure 1.13. a) The structures of PPyPV, b) $PPyPVH^+$, and c) $PPyPVMe^+$.

The incorporation of pyridine units as the acceptor in the D-A polymers allows the protonation and quaternization of the nitrogen to make the more electron-withdrawing pyridinium unit and reduces the HOMO-LUMO energy gap. Poly(pyridylphenylenevinylene) (PPyPV) has been studied for such energy-gap engineering (**Figure 1.13**), as the polymer was protonated by HCl and methylated by methyl triflate to yield the poly(pyridiniumphenylenevinylene) derivatives (**Figure 1.13**), and the pyridinium-polymers showed a significant red-shift in the UV-vis absorption as compared to that of PPyPV, and a drastic increase in the electrical conductivity, indicating a successful reduction in the HOMO-LUMO gap by post-synthetic modifications.[80,81]

1.6 References

(1) Shirakawa, H.; Louis, E. J.; MacDiarmid, A. G.; Chiang, C. K.; Heeger, A. J. *J. Chem. Soc. Chem. Commun.* **1977**, 578-580.

(2) Brédas, J. L.; Silbey, R.; Boudreux, D. S.; Chance, R. R. *J. Am. Chem. Soc.* **1983**, *105*, 6555–6559.

(3) Brédas, J.-L.; Durrant, J. R. *Acc. Chem. Res.* **2009**, *42, 1691-1699*.

(4) Liang, Z.; Tang, Q.; Xu, J.; Miao, Q. *Adv. Mater.* **2011**, *23*, 1535–1539.

(5) Greenham, N. C.; Moratti, S. C.; Bradley, D. D. C.; Friend, R. H.; Holmes, A. B. *Nature* **1993**, *365*, 628–630.

(6) Kelley, T. W.; Baude, P. F.; Gerlach, C.; Ender, D. E.; Muyres, D.; Haase, M. A.; Vogel, D. E.; Theiss, S. D. *Chem. Mater.* **2004**, *16*, 4413–4422.

(7) Pell, L. E.; Schricker, A. D.; Mikulec, F. V.; Korgel, B. A. *Langmuir* **2004**, *20*, 6546–6548.

(8) Meng, D.; Sun, D.; Zhong, C.; Liu, T.; Fan, B.; Huo, L.; Li, Y.; Jiang, W.; Choi, H.; Kim, T. *J. Am. Chem. Soc.* **2016**, *138*, 375–380.

(9) Gibson, G. L.; McCormick, T. M.; Seferos, D. S. *J. Am. Chem. Soc.* **2012**, *134*, 539–547.

(10) Forrest, S. R. *Nature* **2004**, *428*, 911–918.

(11) Facchetti, A. *Chem. Mater.* **2011**, *23*, 733–758.

(12) Facchetti, A.; Yoon, M.-H.; Marks, T. J. *Adv. Mater.* **2005**, *17*, 1705–1725.

(13) Allard, S.; Forster, M.; Souharce, B.; Thiem, H.; Scherf, U. *Angew. Chem., Int. Ed.* **2008**, *47*, 4070–4098.

(14) Wang, C.; Dong, H.; Hu, W.; Liu, Y.; Zhu, D. *Chem. Rev.* **2012**, *112*, 2208–2267.

(15) Carsten, B.; He, F.; Son, H. J.; Xu, T.; Yu, L. *Chem. Rev.* **2011**, *111*, 1493–1528.

(16) Lu, G.; Usta, H.; Risko, C.; Wang, L.; Facchetti, A.; Ratner, M. A.; Marks, T. J. *J. Am. Chem. Soc.* **2008**, *130*, 7670–7685.

(17) Dudnik, A. S.; Aldrich, T. J.; Eastham, N. D.; Chang, R. P. H.; Facchetti, A.; Marks, T. J. *J. Am. Chem. Soc.* **2016**, *138*, 15699–15709.

(18) Meng, Q.; Hu, W. *Phys. Chem. Chem. Phys.* **2012**, *14*, 14152-14164.

(19) Guo, J.; Xu, Y.; Jin, S.; Chen, L.; Kaji, T.; Honsho, Y.; Addicoat, M. A.; Kim, J.; Saeki, A.; Ihee, H.. *Nat. Commun.* **2013**, *4*, 2736.

(20) Cote, A. P.; Benin, A. I.; Ockwig, N. W.; O'Keeffe, M.; Maatzger, A. J.; Yaghi, O. M. *Science* **2005**, *310*, 1166–1170.

(21) Lan, J.; Cao, D.; Wang, W.; Smit, B. *ACS Nano* **2010**, *4*, 4225–4237.

(22) Wan, S.; Guo, J.; Kim, J.; Ihee, H.; Jiang, D. *Angew. Chem., Int. Ed.* **2008**, *47*, 8826–8830.

(23) Wan, S.; Gandara, F.; Asano, A.; Furukawa, H.; Saeki, A.; Dey, S. K.; Liao, L.; Ambrogio, M. W.; Botros, Y. Y.; Duan, X. *Chem. Mater.* **2011**, *23*, 4094–4097.

(24) Chandra, S.; Roy Chowdhury, D.; Addicoat, M.; Heine, T.; Paul, A.; Banerjee, R. *Chem. Mater.* **2017**, *29*, 2074–2080.

(25) He, Y.; Xiang, S.; Chen, B. *J. Am. Chem. Soc.* **2011**, *133*, 14570–14573.

(26) Pantoş, G. D.; Pengo, P.; Sanders, J. K. M. *Angew. Chem., Int. Ed.* **2007**, *46*, 194–197.

(27) Fu, C.; Lin, H. P.; Macleod, J. M.; Krayev, A.; Rosei, F.; Perepichka, D. F. *Chem. Mater.* **2016**, *28*, 951–961.

(28) a) Zheng, Q. N.; Liu, X. H.; Chen, T.; Yan, H. J.; Cook, T.; Wang, D.; Stang, P. J.; Wan, L. J. *J. Am. Chem. Soc.* **2015**, *137*, 6128–6131. b) Tanaka, T.; Tasaki, T.; Aoyama, Y. *J. Am. Chem. Soc.* **2002**, *124*, 12453-12462.

(29) Colin, M. M.; Gaultier de Claubry, H. *Ann. Chim*. **1814**, *90*, 87−100.

(30) Guthrie, F. *J. Chem. Soc*. **1863**, *16*, 239−244.

(31) Rhoussopoulos, *Ber. Dtsch. Chem. Ges*. **1883**, *16*, 202−203.

(32) Hassel, O.; Hvoslef, J. *Acta Chem. Scand*. **1954**, *8*, 873.

(33) Hassel, O.; Romming, C. Q. *Chem. Soc. Rev.* **1962**, *16*, 1−18.

(34) Zingaro, R. A.; Hedges, R. M. *J. Phys. Chem.* **1961**, *65*, 1132–1138.

(35) Cavallo, G.; Metrangolo, P.; Milani, R.; Pilati, T.; Priimagi, A.; Resnati, G.; Terraneo, G. *Chem. Rev*. **2016**, *116*, 2478–2601.

(36) Vartanian, M.; Lucassen, A. C. B.; Shimon, L. J. W.; Van Der Boom, M. E. *Cryst. Growth Des.* **2008**, *8*, 786–790.

(37) Kniep, F.; Jungbauer, S. H.; Zhang, Q.; Walter, S. M.; Schindler, S.; Schnapperelle, I.; Herdtweck, E.; Huber, S. M. *Angew. Chem., Int. Ed.* **2013**, *52*, 7028–7032.

(38) Xu, Z.; Yang, Z.; Liu, Y.; Lu, Y.; Chen, K.; Zhu, W. *J. Chem. Inf. Model.* **2014**, *54*, 69–78.

(39) Christopherson, J.-C.; Topić, F.; Barrett, C. J.; Friščić, T. *Cryst. Growth Des.* **2018**, *18*, 1245-1259.

(40) Desiraju, G. R.; Ho, P. S.; Kloo, L.; Legon, A. C.; Marquardt, R.; Metrangolo, P.; Politzer, P.; Resnati, G.; Rissanen, K. *Pure Appl. Chem.* **2013**, *85*, 1711-1713.

(41) Brinck, T.; Murray, J. S.; Politzer, P. *Int. J. Quantum Chem.* **1992**, *44*, 57–64.

(42) Präsang, C.; Whitwood, A. C.; Bruce, D. W. *Cryst. Growth Des.* **2009**, *9*, 5319-5326.

(43) Cinčić, D.; Friščić, T.; Jones, W. *Chem. Eur. J.* **2008**, *14*, 747–753.

(44) Shen, Q. J.; Pang, X.; Zhao, X. R.; Gao, H. Y.; Sun, H. L.; Jin, W. J. *CrystEngComm* **2012**, *14*, 5027-5034.

(45) Bai, L.; Bose, P.; Gao, Q.; Li, Y.; Ganguly, R.; Zhao, Y. *J. Am. Chem. Soc.* **2017**, *139*, 436–441.

(46) Metrangolo, P.; Präsang, C.; Resnati, G.; Liantonio, R.; Whitwood, A. C.; Bruce, D. W. *Chem. Commun.* **2006**, *0*, 3290–3292.

(47) Nguyen, H. L.; Horton, P. N.; Hursthouse, M. B.; Legon, A. C.; Bruce, D. W. *J. Am. Chem. Soc.* **2004**, *126*, 16–17.

(48) Xu, J.; Liu, X.; Ng, J. K.-P.; Lin, T.; He, C. *J. Mater. Chem.* **2006**, *16*, 3540–3545.

(49) Yan, D.; Delori, A.; Lloyd, G. O.; Friščić, T.; Day, G. M.; Jones, W.; Lu, J.; Wei, M.; Evans, D. G.; Duan, X. *Angew. Chem., Int. Ed.* **2011**, *50*, 12483–12486.

(50) Zhu, W.; Zheng, R.; Zhen, Y.; Yu, Z.; Dong, H.; Fu, H.; Shi, Q.; Hu, W. *J. Am. Chem. Soc.* **2015**, *137*, 11038–11046.

(51) Zhang, Q. T.; Tour, J. M. *J. Am. Chem. Soc.* **1998**, *120*, 5355-5362.

(52) Veldman, D.; Meskers, S. C. J.; Janssen, R. A. J. *Adv. Funct. Mater.* **2009**, *19*, 1939–1948.

(53) Zhao, G. J.; Chen, R. K.; Sun, M. T.; Liu, J. Y.; Li, G. Y.; Gao, Y. L.; Han, K. L.; Yang, X. C.; Sun, L. *Chem. Eur. J.* **2008**, *14*, 6935–6947.

(54) Brocks, G.; Tol, A. *J. Phys. Chem.* **1996**, *100*, 1838–1846.

(55) Chang, Y. Te; Hsu, S. L.; Su, M. H.; Wei, K. H. *Adv. Mater.* **2009**, *21*, 2093–2097.

(56) Phan, H.; Wang, M.; Bazan, G. C.; Nguyen, T. Q. *Adv. Mater.* **2015**, *27*, 7004–7009.

(57) Beaujuge, P. M.; Amb, C. M.; Reynolds, J. R. *Acc. Chem. Res.* **2010**, *43*, 1396–1407.

(58) Agarwala, P.; Kabra, D. *J. Mater. Chem. A* **2017**, *5*, 1348–1373.

(59) Thelakkat, M. *Macromol. Mater. Eng.* **2002**, *287*, 442–461.

(60) Song, Y.; Di, C.; Yang, X.; Li, S.; Xu, W.; Liu, Y.; Yang, L.; Shuai, Z.; Zhang, D.; Zhu, D. *J. Am. Chem. Soc.* **2006**, *128*, 15940–15941.

(61) Cravino, A.; Roquet, S.; Aleveque, O.; Leriche, P.; Frere, P.; Roncali, J. *Chem. Mater.* **2006**, *18*, 2584–2590.

(62) Roquet, S.; Cravino, A.; Leriche, P.; Alévêque, O.; Frère, P.; Roncali, J. *J. Am. Chem. Soc.* **2006**, *128*, 3459–3466.

(63) Shirota, Y. *J. Mater. Chem.* **2005**, *15*, 75–93.

(64) Tao, Y.; Wang, Q.; Yang, C.; Zhong, C.; Qin, J.; Ma, D. *Adv. Funct. Mater.* **2010**, *20*, 2923–2929.

(65) Cravino, A.; Leriche, P.; Alévêque, O.; Roquet, S.; Roncali, J. *Adv. Mater.* **2006**, *18*, 3033–3037.

(66) Zhang, J.; Deng, D.; He, C.; He, Y.; Zhang, M.; Zhang, Z. G.; Zhang, Z.; Li, Y. *Chem. Mater.* **2011**, *23*, 817–822.

(67) Li, Z.; Zhu, Z.; Chueh, C. C.; Jo, S. B.; Luo, J.; Jang, S. H.; Jen, A. K. Y. *J. Am. Chem. Soc.* **2016**, *138*, 11833–11839.

(68) Gudeika, D.; Grazulevicius, J. V.; Volyniuk, D.; Juska, G.; Jankauskas, V.; Sini, G. *J. Phys. Chem. C* **2015**, *119*, 28335–28346.

(69) Lin, Y.; Zhan, X. *Acc. Chem. Res.* **2016**, *49*, 175–183.

(70) Hua, G.; Du, J.; Slawin, A. M. Z.; Woollins, J. D. *J. Org. Chem.* **2014**, *79*, 3876–3886.

(71) Matsuzaki, K.; Okuyama, K.; Tokunaga, E.; Saito, N.; Shiro, M.; Shibata, N. *Org. Lett.* **2015**, *17*, 3038–3041.

(72) Sheppard, W. A. *J. Am. Chem. Soc.* **1962**, *84*, 3064–3072.

(73) Ilardi, E. A.; Vitaku, E.; Njardarson, J. T. *J. Med. Chem.* **2014**, *57*, 2832–2842.

(74) Zhang, Y.; Wang, Y.; He, C.; Liu, X.; Lu, Y.; Chen, T.; Pan, Q.; Xiong, J.; She, M.; Tu, Z. *J. Med. Chem.* **2017**, *60*, 4135–4146.

(75) Kirsch, P.; Hahn, A. *Eur. J. Org. Chem.* **2005**, 3095–3100.

(76) Kirsch, P.; Hahn, A. *Eur. J. Org. Chem.* **2006**, 1125–1131.

(77) Golf, H. R. A.; Reissig, H. U.; Wiehe, A. *J. Org. Chem.* **2015**, *80*, 5133–5143.

(78) Zhou, Z.-H.; Maruyama, T.; Kanbara, T.; Ikeda, T.; Ichimura, K.; Yamamoto, T.; Tokuda, K.. *J. Chem. Soc. Chem. Commun.* **1991**, 1210-1212.

(79) Havinga, E. E.; ten Hoeve, W.; Wynberg, H. *Polym. Bull.* **1992**, *29*, 119–126.

(80) Marsella, M. J.; Fu, D. K; Swager, T. M. *Adv. Mater.* **1995**, *7*, 145–147.

(81) Fu, D. K.; Xu, B.; Swager, T. M. *Tetrahedron* **1997**, *53*, 15487–15494.

Chapter 2. π-Conjugated Halogen-bonded Networks

2.1 Introduction

The formation of structurally defined and organized molecular assemblies through non-covalent interactions has been an intense area of research in materials chemistry. Interactions such as van der Waals, π-π stackings are known to be essential to the performance of organic optoelectronic devices including OPVs and OFETs.[1,2] Moreover, organic co-crystals involving hydrogen-bonding (HB) have been developed for optoelectronic applications due to its role in promoting well-defined supramolecular assemblies and intermolecular charge-transfer between the HB donor and acceptor.[3] In addition to HB, organic co-crystals with the analogous halogen-bonding (XB) interactions have demonstrated highly organized supramolecular assemblies due to the highly anisotropic interactions.[4] Some of the XB co-crystals have shown extremely high phosphorescent quantum yield up to 55% resulting from the "heavy atom effect".[5] More recently, fluorescent and electrically conductive XB materials have been studied, which expanded their applications in the field of optoelectronic materials.[6,7] More fundamental studies on the charge-transfer of XB co-crystals have also been performed by Hu and co-workers through theoretical and experimental investigations to understand the photophysical properties of XB materials.[8] However, the structural design of the XB donor and acceptors have remained simple, as many of them are commercially available reagents. Such approach is limiting our design of novel XB supramolecular assemblies and the possibility of the development of high-performance XB materials.

For my current project, we initially planned to synthesize 2D halogen-bonded networks that resemble COF structures for OFET applications. However, after several attempts, we realized that 2D networks may not be achieved by simple solution-grown crystallization techniques.[9] Thus, we turned our focus on 1D halogen-bonded chains and their potential OFET properties. The co-crystals were sent to our collaborator and no meaningful OFET properties were observed. In this work, we sought to design XB co-crystals using π-conjugated molecules XB acceptors such as pyrazine, 1,4-BPB, 1,4-BPEB, 2,5-BPET, *N,N'*-PNDI (**Figure 2.1**) and co-crystallize these acceptors with the XB donors TFDIB and TFTIB, individually to obtain novel supramolecular structures, and investigate their solid-state photophysical properties. Inspired by the recent work of Zhao and coworkers on the red-shifted photophysical spectra of the organic co-crystals upon halogen-bonding formations,[6] we were also interested to study the potential effect of halogen bonding interactions in the photophysical properties of these organic crystals. These 1D halogen-bonded and π-stacked conjugated chains may exhibit interesting inter-chain charge-transfer properties. By varying the structures of the XB acceptor units, potential tuning of the photophysical properties may be achieved. DFT calculations on the co-crystal systems were performed to elucidate the molecular orbital distributions and the energy levels of the co-crystal. Thermogravimetric analysis (TGA), and differential scanning analysis (DSC) were employed to study the thermal stability of selected co-crystals.

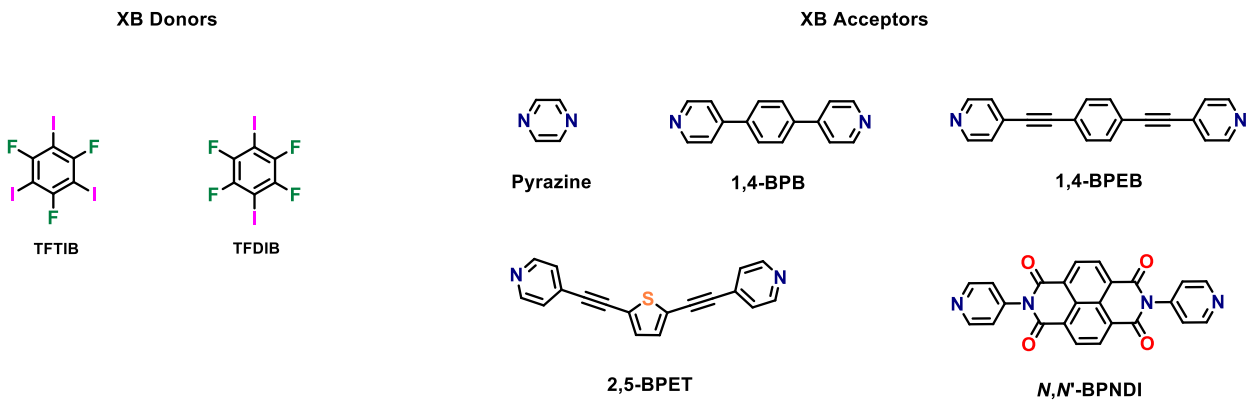

Figure 2.1. Structures the XB donors and acceptors in this study.

2.2 Results and Discussion

2.21. Synthesis of XB Donors and Acceptors

The synthetic routes for the two XB donors TFTIB and TFDIB were based on a modified procedure in the literature (**Scheme 2.1**).[10] TFDIB and TFTIB cost $44.9/g and $110.2/g, respectively on Sigma Aldrich. In comparison, their starting materials compound **1** and **2** cost $25.7/g and $18.0/g, respectively. The significant price differences motivated us to synthesize the XB donors in the laboratory. The iodination of **1** with 4.5 equivalents of KI gave TFDIB in 61% yield, and TFDIB was synthesized from **2** with the similar synthetic method with 3.5 equivalents of KI, which resulted in 63% yield. Both XB donors were separately crystallized in *n*-hexanes before co-crystallizations. Both synthesized XB donors were characterized by ^{19}F and ^{13}C NMR.

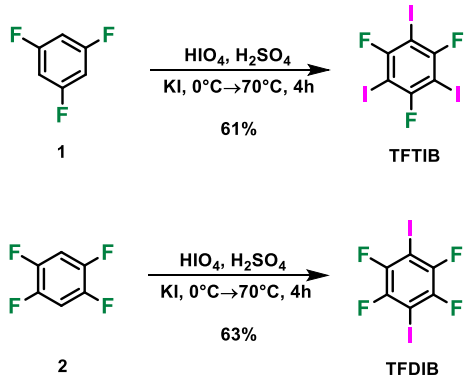

Scheme 2.1. Synthesis of the XB donors TFTIB and TFDIB.

The synthetic routes for 1,4-BPEB,[11] 1,4-BPB,[12] 2,5-BPET,[13] and *N*,*N*'-BPNDI[14] are shown in **Scheme 2.2**. The synthesis of 1,4-BPEB started from the Sonogashira cross-coupling between **3** and **4** at room temperature to give intermediate **5**. The deprotection of the TMS group was done by KOH in MeOH/THF at room temperature, followed by a Sonogashira cross-coupling with 2.1 equivalents of **7** to afford 1,4-BPEB in 60% yield. 1,4-BPB was synthesized from the Suzuki cross-coupling between **7** and **8**

at reflux to give 1,4-BPB in 55% yield. The intermediates of the 2,5-BPET were synthesized from two reaction sequences. Intermediate **10** was synthesized from the Sonogashira cross-coupling between **7** and **4** at room temperature, followed by the removal of the TMS group with KOH in MeOH/THF at room temperature under N_2. The thiophene moiety was synthesized from the bromination of **11** to give intermediate **12**, and 2,5-BPET was afforded by the Sonogashira reaction between two equivalents of **10** and **12**, which resulted in 54% yield. Another acceptor *N*,*N*'-BPNDI was synthesized from the condensation of the commercially available compound **13** and 2 equivalents of **14** to give the desired compound in 50% yield. The XB acceptors were synthesized following modified literature procedures and were characterized by ^{1}H NMR.

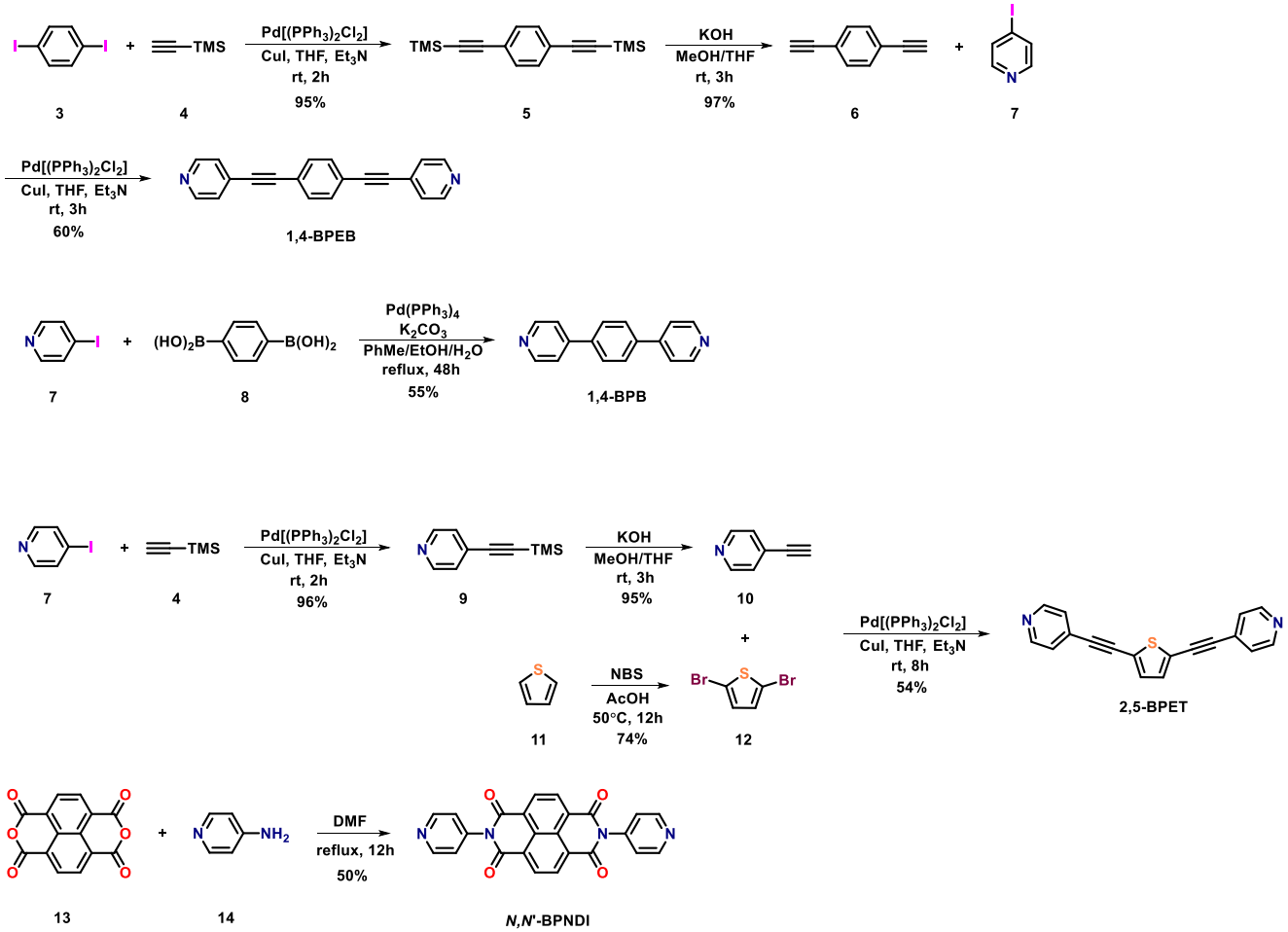

Scheme 2.2. Synthesis of the XB acceptors 1,4-BPEB, 1,4-BPB, 2,5-BPET, and *N*,*N*'-BPNDI.

2.22 Co-crystallization

From XB donors TFDIB and TFTIB, two co-crystal series were designed. Series I contains the co-crystallizations of TFDIB and the XB acceptors (**Scheme 2.3a**), and series II contains the co-crystallization of TFTIB and the XB acceptors (**Scheme 2.3b**). All the co-crystals were grown by the slow-diffusion

method, where the XB donor and the acceptor were first dissolved in a minimum quantity of chloroform, and a layer of methanol was then carefully layered on top. Good quality co-crystals were formed within a week. Owing to the low solubility of *N*,*N*'-BPNDI, it was first dissolved in hot DMF, then hot chloroform containing TFDIB was carefully layered on top of the hot DMF. The layered solutions were kept on the hot plate overnight before gradually cooling to room temperature. X-ray quality co-crystals were formed within two weeks.

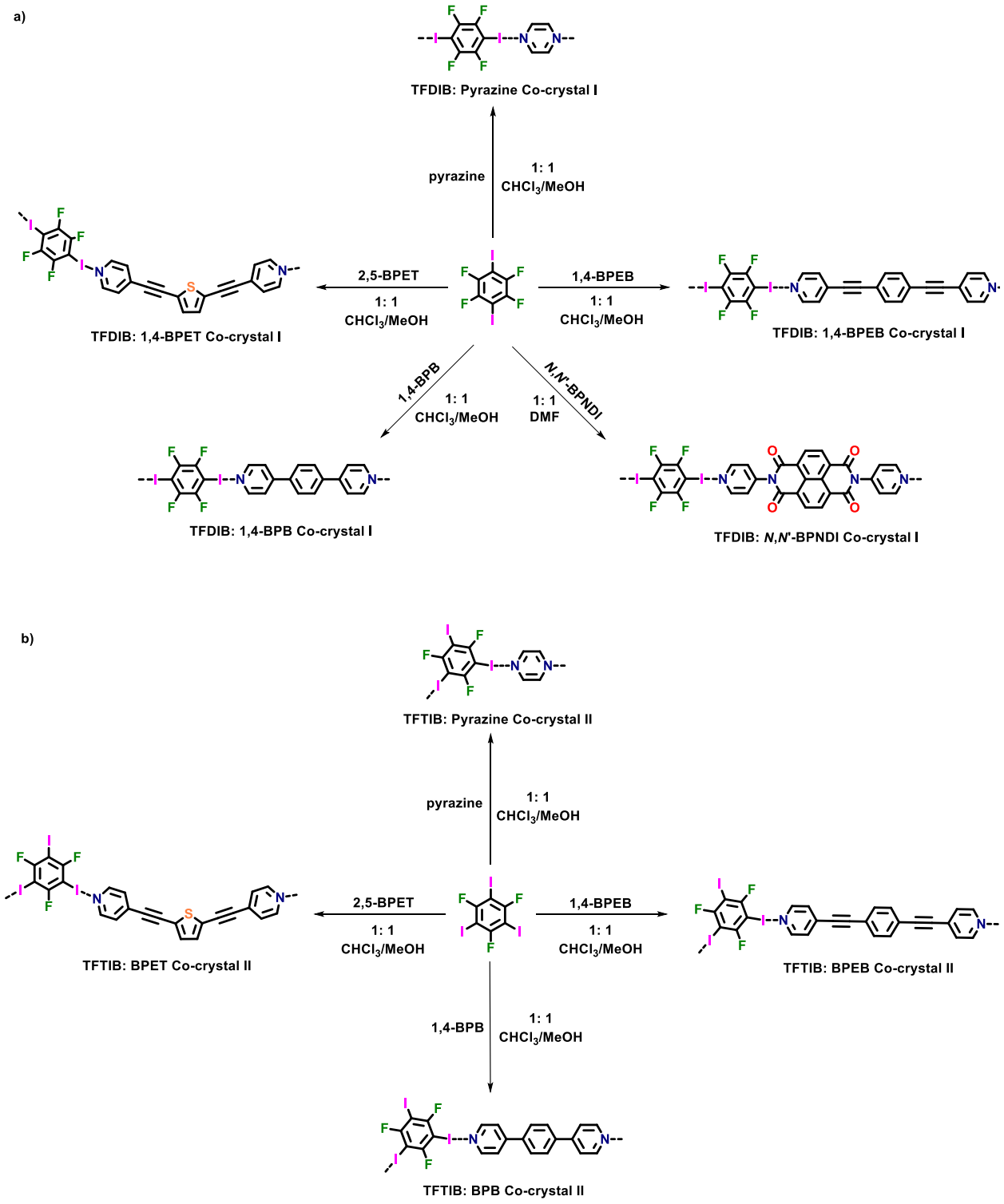

Scheme 2.3. The co-crystallizations of TFDIB/TFTIB and the N-containing halogen-bond acceptors.

3.23 X-ray Crystallography

The supramolecular structures of the halogen-bonded co-crystals were characterized by single-crystal X-ray diffraction (SCXRD), and the complete crystallographic data of the co-crystals were reported in Table 2.1.

Table 2.1. Details of the crystallographic data of the XB co-crystals.

crystal	**TFDIB: Pyrazine Co-crystal I**	**TFTIB: Pyrazine Co-crystal II**	**TFDIB: 1,4-BPB Co-crystal I**	**TFTIB: 1,4-BPB Co-crystal II**	**TFDIB: 1,4-BPEB Co-crystal I**	**TFTIB: 1,4-BPEB Co-crystal II**	**TFDIB: 2,5-BPET Co-crystal I**	**TFDIB: 2,5-BPET Co-crystal II**	**TFDIB: *N,N*'-BPNDI Co-crystal I**
formula	$C_{10}H_4F_4I_2N_2$	$C_8H_2F_3I_3N$	$C_{22}H_{12}F_4I_2N_2$	$C_{22}H_{12}F_3I_3N_2$	$C_{26}H_{12}F_4I_2N_2$	$C_{26}H_{12}F_3I_3N_2$	$C_{24}H_{10}F_4I_2N_2S$	$C_{24}H_{10}F_3I_3N_2S$	$C_{30}H_{12}F_4I_2N_4O_4$
temperature/K	296	200(2)	296	200(2)	296	200	200	200	200
crystal size/mm^3	0.591 x 0.396 x 0.352	0.362 x 0.352 x 0.236	0.501 x 0.315 x 0.090	0.980 x 0.340 x 0.170	0.885 x 0.202 x 0.044	0.362 x 0.222 x 0.120	0.371 x 0.184 x 0.070	0.458 x 0.347 x 0.214	0.268 x 0.196 x 0.179
crystal system	Triclinic	Monoclinic	Monoclinic	Triclinic	Monoclinic	Orthorhombic	Monoclinic	Monoclinic	Triclinic
space group	*P -1*	*P 21/c*	*P 21/c*	*P -1*	*P 21/c*	*P b c n*	*P 21*	*P 21/c*	*P -1*
***a*/Å**	5.8052(6)	9.1958(9)	12.5254(11)	7.0869(19)	12.383(5)	4.9189(2)	11.5075(6)	11.8349(6)	9.7578(5)
***b*/Å**	8.7287(8)	.8485(7)	6.9427(6)	8.828(2)	5.1345(19)	17.9387(8)	5.0225(3)	8.8655(5)	10.7173(5)
***c*/Å**	13.5068(13)	16.8600(16)	13.5296(12)	19.383(5)	18.587(7)	28.5111(13)	20.2677(11)	23.0913(12)	13.5710(7)
***α*/deg**	72.5930(10)	90	90	94.811(3)	90	90	90	90	84.0060(10)
***β*/deg**	79.7690(10)	99.3250(10)	117.4280(10)	99.388(3)	99.122(4)	90	102.4510(10)	92.6270(10)	85.6620(10)
γ/deg	85.4870(10)	90	90	110.000(3)	90	90	90	90	78.3500(10)
***V*/ Å^3**	642.45(11)	1200.8(2)	1044.28(16)	1111.5(5)	1166.8(7)	2515.78(19)	1143.85(11)	2420.2(2)	1380.21(12)
Z	2	4	2	2	2	4	2	4	2
***ρ* (calcd)/Mgm^{-3}**	2.491	3.041	2.017	2.217	1.942	2.086	1.998	2.185	1.978
***θ* range for data**	1.601 to 28.244°	2.244 to 28.317	1.832 to 28.237°	2.154 to 29.236°	1.666 to 28.696°	1.428 to 27.823°	1.029 to 27.934°	1.722 to 32.287°	1.511 to 28.270°
collection/° F(000)	440	972	600	688	648	1472	652	1480	788
ref collected/unique	7844/3084	13874	12062/2537	14081/5547	13467/2922	28133/2999	13675/5350	49015/8197	16794/6602
R1, *w*R$_2$ (I > 2*σ*(I))	13.5068(13)	16.8600(16)	13.5296(12)	19.383(5)	18.587(7)	28.5111(13)	20.2677(11)	23.0913(12)	13.5710(7)
R1, *w*R$_2$ (all data)	0.0257, 0.0622	0.0192, 0.0423	0.0212, 0.0535	0.0304, 0.0652	0.0323, 0.0736	0.0235, 0.0587	0.0427, 0.0797	0.0240, 0.0509	0.0266, 0.0553
goodness-of-fit, *S*	0.0328, 0.0655	0.0223, 0.0432	0.0250, 0.0559	0.0393, 0.0690	0.0437, 0.0781	0.0250, 0.0594	0.0862, 0.1054	0.0319, 0.0555	0.0359, 0.0596

The TFDIB: Pyrazine Co-crystal I system crystallized in the triclinic space group *P*-1 (**Figure 2.2a**). The N···I distance was found to be 2.937(4) for I(1)···N(1) and 2.941(4) Å for I(2)···N(2), which is a typical XB length (XB distances range from 2.6 to 3.6 Å),[4] and the angle between the donor and the acceptor was found to be 176.54(13)˚ for C(6)-I(2)···N(2) and 174.42(12)˚ for C(3)-I(1)···N(1), indicating the formation of highly anisotropic 1D chains through halogen-bonding interactions. The 1D supramolecular assembly was also reinforced by multiple parallel-displaced π-stacking interactions between TFDIB and pyrazine molecules (Table S1), demonstrating efficient packing in the solid-state.

The TFTIB: Pyrazine Co-crystal II system crystallized in the monoclinic space group *P 21/c* (**Figure 2.2b**). TFTIB formed monotopic halogen-bonding interaction with the pyrazine despite having three iodine groups available, and the pyrazine formed ditopic halogen-bonding interactions with two TFTIB molecules. The N···I distance between N(1) and I(1) was found to be 2.910 Å, at an angle of 173.56˚. The dihedral angle between the N(1),…,C(8) and C(1),…,C(4) planes were 40.01˚, showing non-planar halogen-bonded chains.

1,4-BPB and TFDIB co-crystallized in the monoclinic space group *P* 2_1/c (**Figure 2.2c**). The N···I distance was found to be 2.851(2) Å. Owing to the twisted nature of the central ring, with the dihedral angle between N(1),…,C(8) and C(9),…,C(11) ring planes being 29.35(13)˚, the XB angle was measured to be 176.15(9)˚, and formed 1D chains via halogen-bonding interactions. In addition to the halogen-bonding interactions, the 1D halogen-bonded chains were crosslinked by C···I interactions with a distance of 3.661(2) Å, and both F(2) of TFDIB formed bifurcated F···C and F···H interactions with distances of 3.081(3) Å and 2.63 Å, respectively, at an angle of 56.57˚.

1,4-BPB and TFTIB formed the co-crystal in the triclinic space group *P -1* (**Figure 2.2d**). Each 1,4-BPB molecule formed ditopic halogen-bonding interactions with I(2) and I(3) of TFTIB, which resulted in a two-dimensional (2D) zig-zag structure. The N···I distance between N(1) and I(2), and N(2) and I(3) were 2.853 Å and 2.846 Å, and at bond angles of 169.06˚, 168.80˚, respectively. A weak interaction between I(1) and F(2) with a distance of 3.090 Å was observed, thus extending the zig-zag chains along the plane.

1,4-BPEB and TFDIB co-crystallized in the monoclinic space group *P* 2_1/c. Increased strength of halogen-bonding interactions was observed, as the N···I distance was found to be 2.790(3) Å. The planar geometry of BPEB (the dihedral angle between C(11),…,C(13) and N(1),…,C(8) ring planes is 3.13(18)˚) gave rise to highly anisotropic 1D halogen-bonding interactions between BPEB and TFDIB, at an angle of 178.03(12)˚. The supramolecular solid-state structure of TFDIB: 1,4-BPEB involved with orthogonal 1D chain arrangement, held by weak face-to-face π–stacking (Table S3), and weak interchain C···F and F···H

interactions with distances of 3.080 Å and 2.612 Å, respectively forming a three-dimensional (3D) staggered lamellar structure (**Figure 2.2e**).

The TFTIB and 1,4-BPEB co-crystal formed in the orthorhombic space group *Pbcn*. The geometry of BPEB is almost planar (the dihedral angle between C(12),…,C(14) and N(1),…,C(9) ring planes is 10.51(12)˚). Unlike the TFDIB: 1,4-BPEB Co-crystal I which formed highly planar 1D chains, the 1,4-BPEB nitrogen atoms formed halogen-bonding interactions with I(2) and I(3) of TFTIB with a distance of 2.885(2) Å and gave rise to the zig-zag chains where 1,4-BPEB and TFTIB were out-out-plane. Even though I(1) of TFTIB did not participate in halogen-bonding interactions, it formed bifurcated weak hydrogen bonds with H(9) of 1,4-BPEB at an angle of 144.05˚. Both 1,4-BPEB and TFTIB formed weak face-to-face π-π stackings with itself, and the 3D supramolecular assembly was also assisted by strong F⋯H interactions between F(1) and H(8) with 2.443 Å (**Figure 2.2f**).

2,5-BPET and TFDIB co-crystallized in the monoclinic space group $P2_1$. The molecule of 2,5-BPET is almost planar with dihedral angles of 9.3(6)˚ and 8.1(6)˚ between N(1),…,C(5) and N(2),…,C(18) ring planes and the central S(1),…,C(11) ring plane. The bent geometry of 2,5-BPET formed a quasi-1D chain with TFDIB via halogen-bonding interactions where the N⋯I distance was 2.789(11) Å for N(1) ⋯I(1) and 2.944(10) Å for N(2) ⋯I(2) with 177.0(5) and 173.6(4) bond angles respectively. Both 2,5-BPET and TFDIB formed weak face-to-face π-π stackings along the *b*-axis, in which the 1D chains were staggered. The supramolecular co-crystal assembly was reinforced by four additional interactions at the thiophene S, where it formed bifurcated S⋯C interactions with the C(6) alkyne at an angle of 180˚, and bifurcated S⋯F interactions with the F(3) (3.232(10) Å) and F(4) (3.104(10) Å) of TFDIB at 75.88˚ angle (**Figure 2.2g**)

2,5-BPET: TFTIB co-crystal II crystallized in the monoclinic space group $P2_1c$. Unlike 2,5-BPET in the co-crystal I system, BPET in the current system was found to be non-planar, where the pyridine unit at the 5 position of the thiophene was rotated out of plane by 60.34(12)˚, the other pyridine unit is almost coplanar with the central ring (2.92(12)˚). The non-linear halogen-bonding interaction with TFTIB where the XB angle was found to be 167.74(7) for N(1)⋯I(2) and 172.90(8) for N(2) ⋯I(1), and the N⋯I distance 2.883(2) and 2.874(3) Å respectively. The supramolecular assembly of the current co-crystal II was found to be less ordered than that of co-crystal I, the pyridine group of 2,5-BPET exhibited weak parallel-displaced π-π stacking with TFTIB, F⋯H were observed between F(3) and H(16) of the thiophene moiety, and F(3) and H(23) of the pyridine moiety at an angle of 89.22˚ and with distances of 2.509 Å and 2.634 Å respectively (**Figure 2.2h**).

N,N'-BPNDI and TFDIB co-crystallized in the triclinic space group *P* -1. The NDI core and the pyridine unit formed a torsional angle of 62.13˚ to avoid steric interactions. *N,N*'-BPNDI and TFDIB formed highly anisotropic 1D halogen-bonding interaction at a 177.60˚ angle and the N···I distance of 2.874 Å. The NDI units formed weak face-to-face π-π stacking with a distance of 3.302 Å, hydrogen bonding interaction with 2.483 Å was observed between O2 and the neighboring H23 of the pyridine to reinforce the interchain packing. The supramolecular assembly of the co-crystal exhibited a lamellar motif, which was further assisted by F···H interactions on the same plane between F3 and H10, and F4 and H9 with distances of 2.431 Å and 2.516 Å, respectively. The interactions found in this co-crystal system gave rise to well-packed 1D chains formed via halogen-bonding interaction (**Figure 2.2i**).

All co-crystal systems exhibited halogen-bonding interactions of different strengths measured by bond lengths due to their difference in geometry and electronic natures. Additional non-covalent interactions such as hydrogen bonding and π-π stackings were observed in almost all co-crystals system to give their 3D supramolecular complexes. Varying XB donors of the co-crystal systems led to entirely different crystal structures. In the case of the pyrazine co-crystals, Co-crystal I system resulted in continuous halogen-bonding interactions and linear 1D chains with parallel-displaced interchain π-stackings. Co-crystal II did not show the continuous halogen-bonding interactions that were observed in Co-crystal I. Instead, TFTIB only formed monotopic halogen-bonding interactions with pyrazine, thus resulting in short chains with three units. Co-crystal I formed more anisotropic XB than Co-crystal II, but Co-crystal II resulted in slightly shorter halogen-bonding interactions than Co-crystal I.

The TFDIB: 1,4-BPB Co-crystal I formed highly ordered linear 1D chains through halogen-bonding interactions as compared to Co-crystal II, and the XB lengths in Co-crystal I were shorter than that of Co-Crystal II, and the linear XB formation could have contributed to the shortening of the XB interactions. For Co-crystal II, the major non-covalent interaction other than the XB was the H···π interaction between H(10) and C(4), with a distance of 2.835 Å, and this interaction reinforced the interchain packing along the *c*-axis. For Co-crystal I, the halogen-bonded network appeared to be a pseudo-2D sheet, which drastically differs from the crystal structure of Co-crystal II.

The co-crystallization of 1,4-BPEB and TFDIB gave rise to the 3D supramolecular structure with perpendicular 1D linear chains held by halogen-bonding interactions, whereas Co-crystal II showed stacking of the zig-zag chains formed by XB. The linear halogen-bonding interaction observed in Co-crystal I allowed the formation of shorter XB length than that of Co-crystal II. The perpendicular 1D linear chains were also observed in 2,5-BPET: TFDIB Co-crystal I, and its crystal structure was found to be more organized than that of Co-crystal II. Both co-crystal systems showed π-π stackings that reinforced the 3D

supramolecular structure, and Co-crystal II demonstrated stronger π-π interactions than that of Co-crystal I.

The strongest halogen-bonding interaction of 2.790 Å was observed in TFDIB: 1,4-BPEB Co-crystal I, as the highly planar and linear geometry of 1,4-BPEB assisted in forming a linear and strong contact with the XB donor. Comparing the result of TFDIB: 1,4-BPEB Co-crystal I with TFTIB: 1,4-BPEB Co-crystal II, the Co-crystal II system formed slightly shorter halogen-bonding interaction of 2.885(2) Å. Another highly conjugated 2,5-BPET with an electron-donating thiophene core did not show such strong halogen-bonding interactions compared to TFDIB: 1,4-BPEB Co-crystal I, due to its bent structure, however, the S atom of the thiophene enabled multiple non-covalent short contacts with C, F, and H to reinforce the supramolecular assembly. TFDIB: *N*,*N*'-BPNDI Co-crystal I formed highly anisotropic 1D halogen-bonding interactions of 2.874 Å, but it was found to be weaker than that of TFDIB: 1,4-BPEB Co-crystal I, due to the electron-withdrawing property of the NDI core.

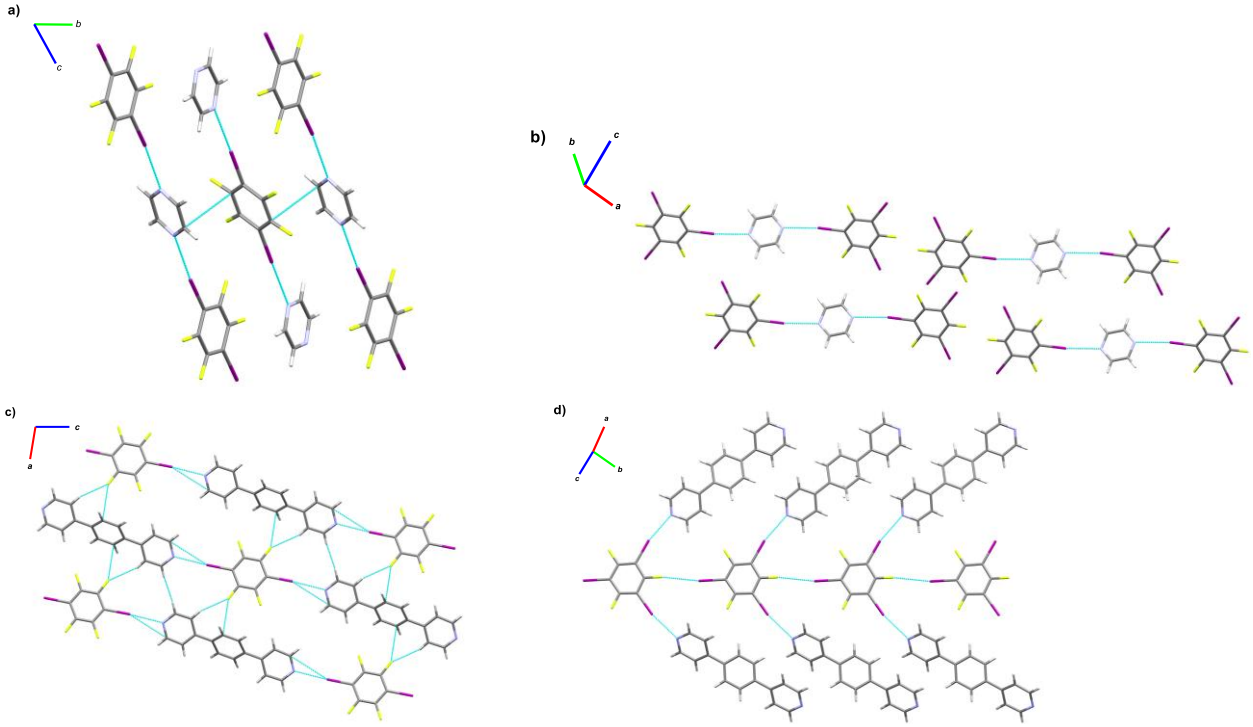

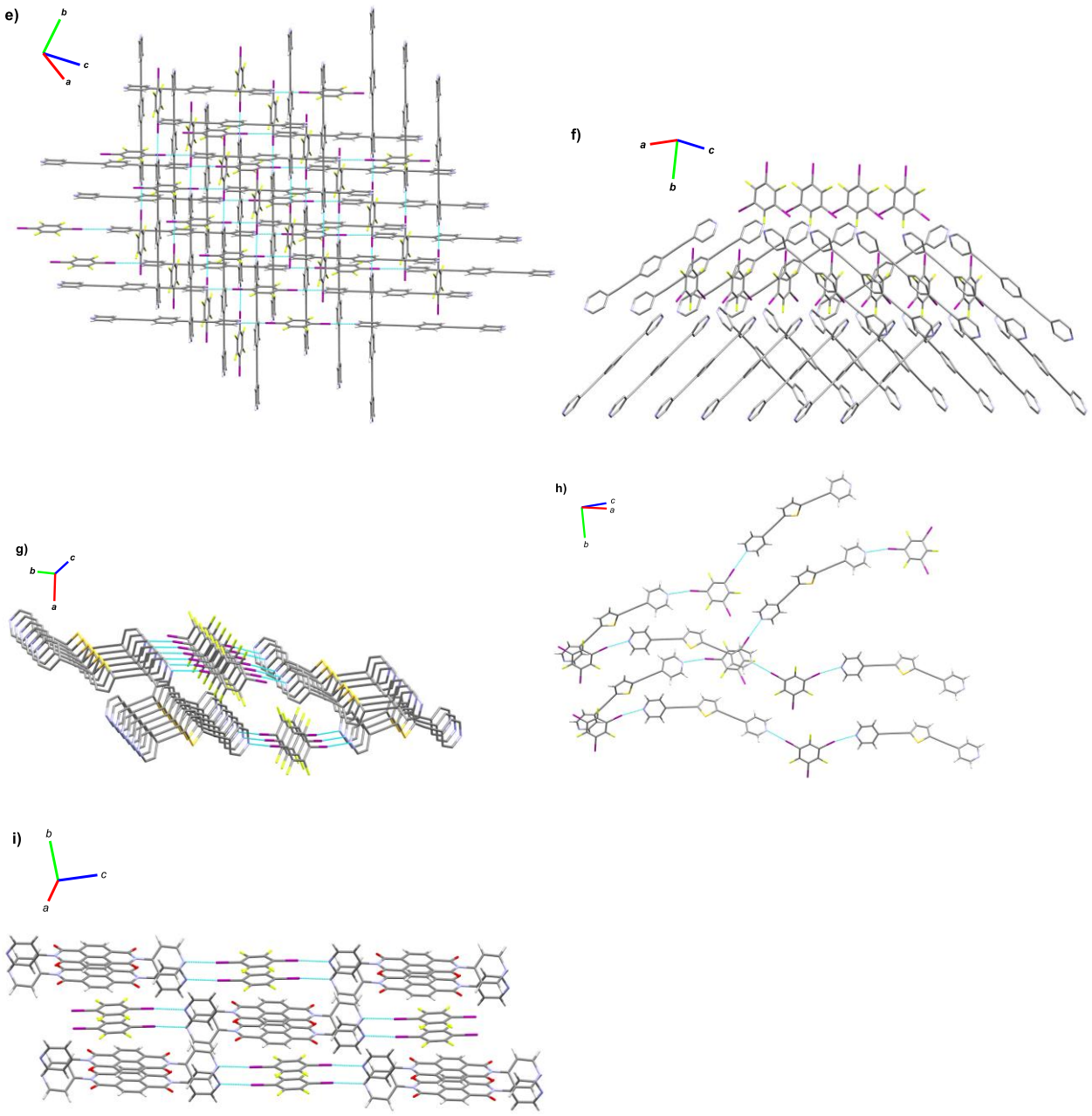

Figure 2.2. The crystal packing diagrams of a) TFDIB: Pyrazine Co-crystal I, b) TFTIB: Pyrazine Co-crystal II, c) 1,4-BPB: TFDIB Co-crystal I, d) 1,4-BPB: TFTIB Co-crystal II, e) 1,4-BPEB: TFDIB Co-crystal I, f) 1,4-BPEB: TFTIB Co-crystal II, g) 2,5-BPET: TFDIB Co-crystal I, h) 2,5-BPET: TFTIB Co-crystal II, and i) *N*,*N*'-BPNDI: TFDIB co-crystal I.

2.24 DFT Studies

DFT calculations were employed to understand the molecular orbital interactions in XB complexes. The XB networks were simplified into the donor-acceptor-donor (D-A-D) triad complex for the sake of reducing the computational cost. The D-A-D complexes were constructed according to the single-crystal structures, regarding the XB distances, angles, and dihedral angles. The calculations were done at the

B3LYP level of theory with split-valence basis sets of LANL2DZ for the I atom and 6-31G+(d,p) for all other atoms. The localization of the highest occupied molecular orbital (HOMO) and the lowest unoccupied molecular orbital (LUMO) and the corresponding energy levels of the XB donor, acceptor, and co-crystals were calculated.

For TFDIB: pyrazine co-crystal I and TFDI: 1,4-BPB co-crystal I, the localization of the HOMO and LUMO is completely distinct, where the HOMO resides on the XB donor TFDIB, and the LUMO localized on the XB acceptors (**Figure 2.4**). The complete separation of the frontier molecular orbitals is indicative of effective donor-acceptor interactions, which could potentially improve the charge-transfer property of the systems. However, for the 1,4-BPEB and 2,5-BPET co-crystal series, both the HOMO and LUMO were found on the XB acceptors, which indicates weaker halogen-bonded D-A systems. The energy levels of the XB donor, acceptors, and co-crystals were calculated separately, and all of the XB systems have shown a reduction in the HOMO-LUMO energy gap to some extent, which is likely due to the molecular orbital interactions between the XB donor and the acceptor (**Figure 2.4**). The most notable change observed is the lowering of the LUMO energy level in the co-crystal systems, which is likely due to the introduction of the electron-deficient TFDIB component. The current DFT calculation only accounts for the effect of XB interactions in the localization of the frontier orbitals and energy levels, and it does not include the effect of π-π interactions, which could potentially affect the distribution of the molecular orbitals as well.

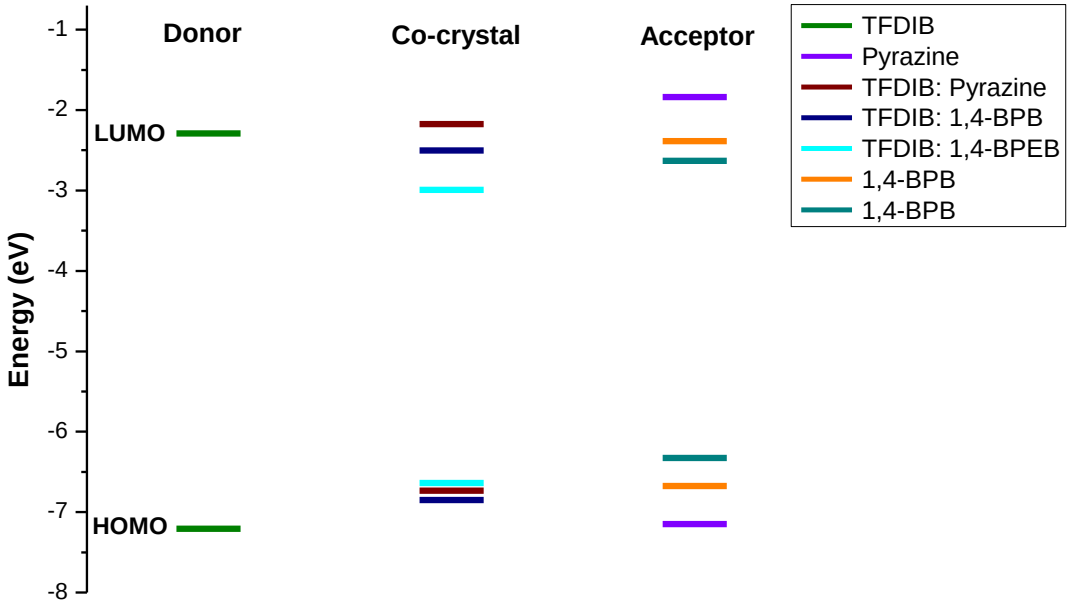

Figure 2.4. The energy levels of the frontier molecular orbitals of the XB donor, acceptors, and the co-crystals.

2.25 Photophysical Properties

The effect of the halogen-bonding on the optical properties of the co-crystals was investigated by solid-state UV-vis and fluorescence spectroscopy, and the properties of co-crystals I was compared with the co-crystals II series. The absorption spectra of the co-crystals showed minor red-shifts relative to their corresponding chromophoric XB acceptors, and such changes could result from the halogen-bonding interactions. An overall red-shift in λ_{max} of the co-crystals was observed as the degree of conjugation of the chromophoric XB acceptors was increased (**Figure 2.5**).

In the case of TFDIB: Pyrazine Co-crystal I, the λ_{max} was found at 323 nm, with a shoulder at 229 nm. TFTIB: Pyrazine Co-crystal II exhibited a distinct broad absorption peak as compared to Co-crystal I, with the λ_{max} at 330 nm. The λ_{onset} of the Co-crystal II was 10 nm red-shifted relative to Co-crystal I, indicating a narrowing of the HOMO-LUMO energy gap from 3.18 eV to 3.09 eV. The difference in the absorption profile of the two co-crystals could be attributed to their different crystal packings, with Co-crystal II being more closely packed than Co-crystal I (**Figure 2.5a**).

The co-crystals TFDIB: 1,4-BPB and TFTIB: 1,4-BPB showed λ_{max} at 399 nm and 397 nm, respectively. The two co-crystal systems exhibited distinct absorption profiles, possibly resulting from their different crystal packings. The λ_{onset} of TFDIB: 1,4-BPB was found at 421 nm, and it was red-shifted to 451 nm for TFTIB: 1,4-BPB, thus, the HOMO-LUMO energy gap of TFDIB: 1,4-BPB and TFTIB: 1,4-BPB were calculated to be 2.95 eV and 2.75 eV, respectively (**Figure 2.5b**).

The λ_{max} of TFDIB: 1,4-BPEB Co-crystal I and TFTIB: 1,4-BPEB Co-crystal II were both found at 399 nm. The λ_{onset} of TFDIB: 1,4-BPEB Co-crystal I and TFTIB: 1,4-BPEB Co-crystal II were found to be at 533 nm and 550 nm, which indicated a narrowing of the HOMO-LUMO gap from 2.33 eV and 2.25 eV, respectively (**Figure 2.5c**). TFTIB: 1,4-BPEB Co-crystal II showed a further reduction in the HOMO-LUMO energy gap compared to that of TFDIB: 1,4-BPEB Co-crystal I, potentially due to better molecular orbital interactions resulted from its more efficient crystal packing.

The TFDIB: 2,5-BPET Co-crystal I and TFTIB: 2,5-BPET Co-crystal II showed distinct absorption spectra. Co-crystal I exhibited three sharp absorption peaks at 313 nm, 400 nm, and 429 nm, whereas Co-crystal II resulted in a broader absorption peak compared to Co-crystal I with λ_{max} at 347 nm (**Figure 2.5d**). Despite their completely different absorption pattern, the λ_{onset} values of both co-crystals were found at 545 nm, which corresponds to a HOMO-LUMO energy gap of 2.27 eV.

Changes in the absorption spectra from *N,N*'-BPNDI to TFDIB: *N,N*'-BPNDI Co-crystal I, where the λ_{max} of *N,N*'-BPNDI was found at 350 nm, and it was red-shifted to 369 nm upon co-crystallization. The λ_{onset} of 427 nm for *N,N*'-BPNDI was red-shifted to 462 nm for TFDIB: *N,N*'-BPNDI Co-crystal I (**Figure**

2.5e), the change in the λ_{onset} indicated the narrowing of the HOMO-LUMO energy gap from 2.90 eV to 2.68 eV.

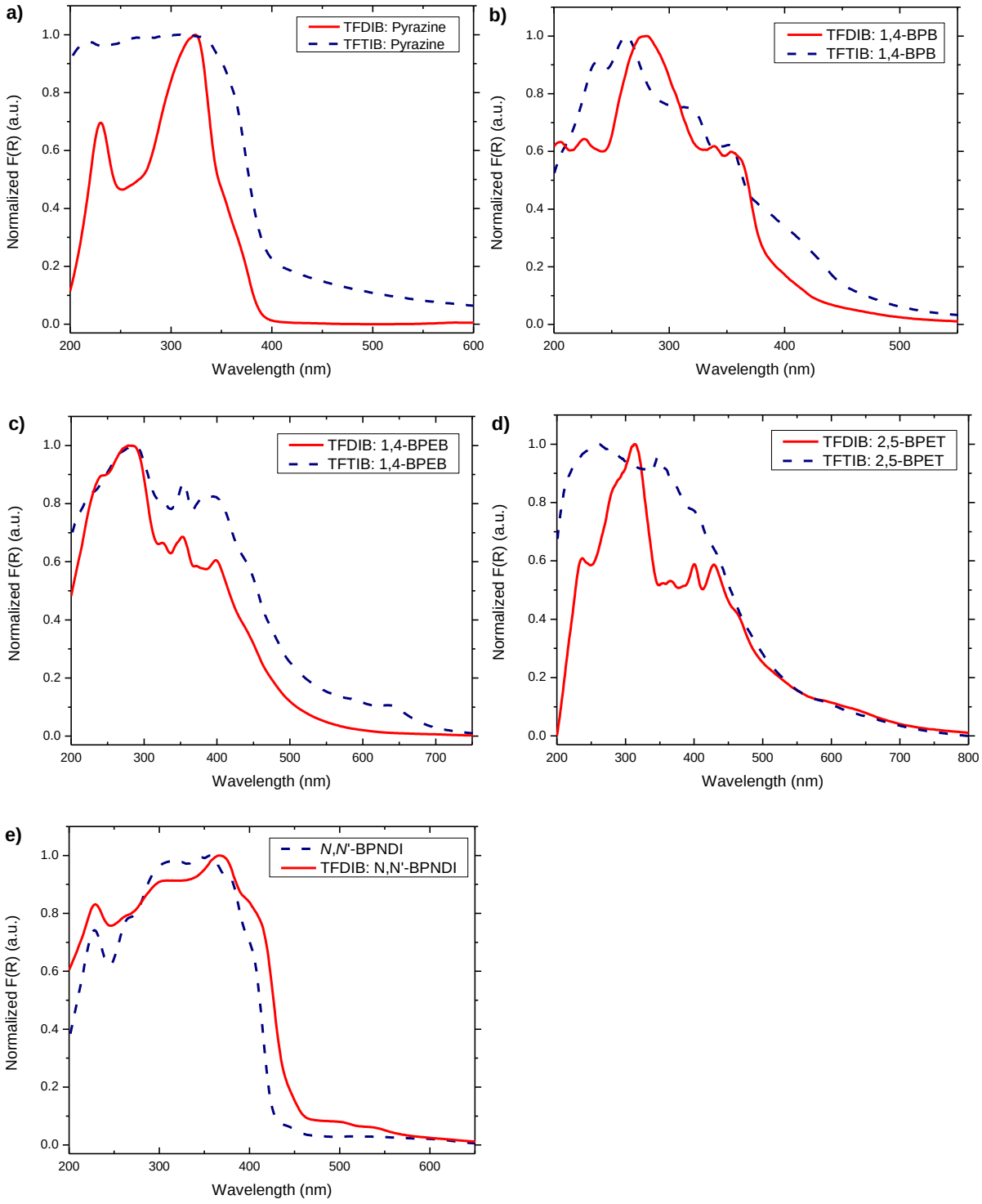

Figure 2.5. Normalized UV-vis absorption profiles of the starting materials (dash line) and co-crystal I (solid line) and II series (dash line).

The solid-state emission of the co-crystals was investigated, and the co-crystals with 1,4-BPEB, 1,4-BPB, and 2,5-BPET appeared to be fluorophores. 1,4-BPEB: TFDIB Co-crystal I had the λ_{em} at 497 nm, and it was red-shifted to 505 nm in the case of 1,4-BPEB: TFTIB Co-crystal II. In the case of 1,4-BPB: TFDIB Co-crystal I, the λ_{em} was observed at 500 nm, and it was red-shifted to 511 nm for 1,4-BPB: TFTIB Co-crystal II. A similar phenomenon was found for the 2,5-BPET co-crystals, the λ_{em} of Co-crystal II was red-shifted to 506 nm from 496 nm for the Co-crystal I (**Figure 2.5c**). The different emissions exhibited by the co-crystals demonstrated that the emission of the same fluorophore acceptor could be considerably altered by varying the XB donor and different crystal packings.

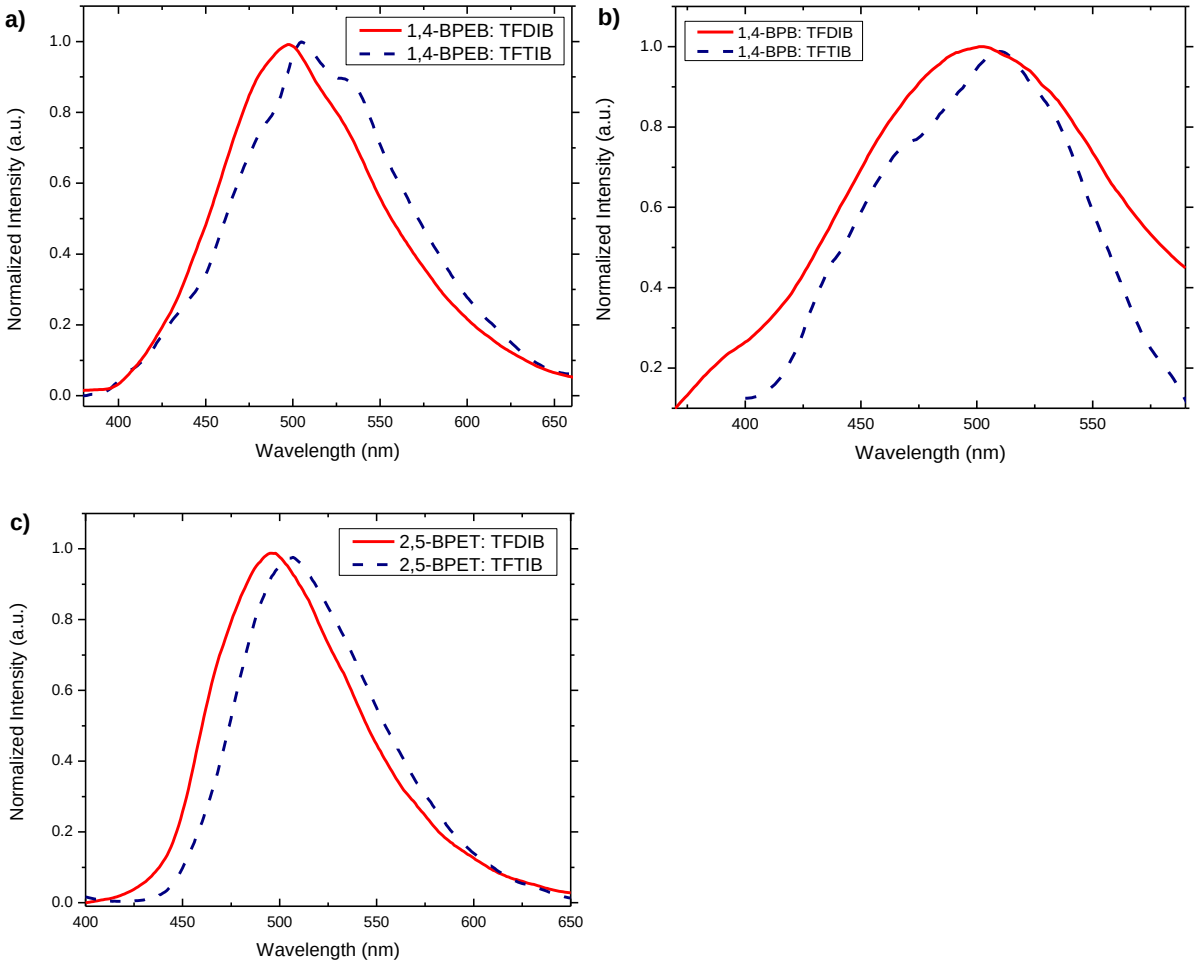

Figure 2.5. Normalized solid-state photoluminescence of the Co-crystals I (solid line) and Co-crystal II series (dash line).

The 1,4-BPEB Co-crystal series showed changes in emission upon mechanical grinding. TFDIB: 1,4-BPEB Co-crystal I system showed a 16 nm blue-shift from 491 nm to 475 nm upon grinding, a similar change in emission was also observed in TFTIB: 1,4-BPEB Co-crystal II system, where a 25 nm blue-shift from 505 nm to 480 nm occurred upon grinding (**Figure 2.6**). When the ground co-crystals were heated to

60 ˚C for 30 min, further blue-shifts of 12 nm and 24 nm were observed in TFDIB: 1,4-BPEB Co-crystal I and TFTIB: 1,4-BPEB Co-crystal II, respectively.

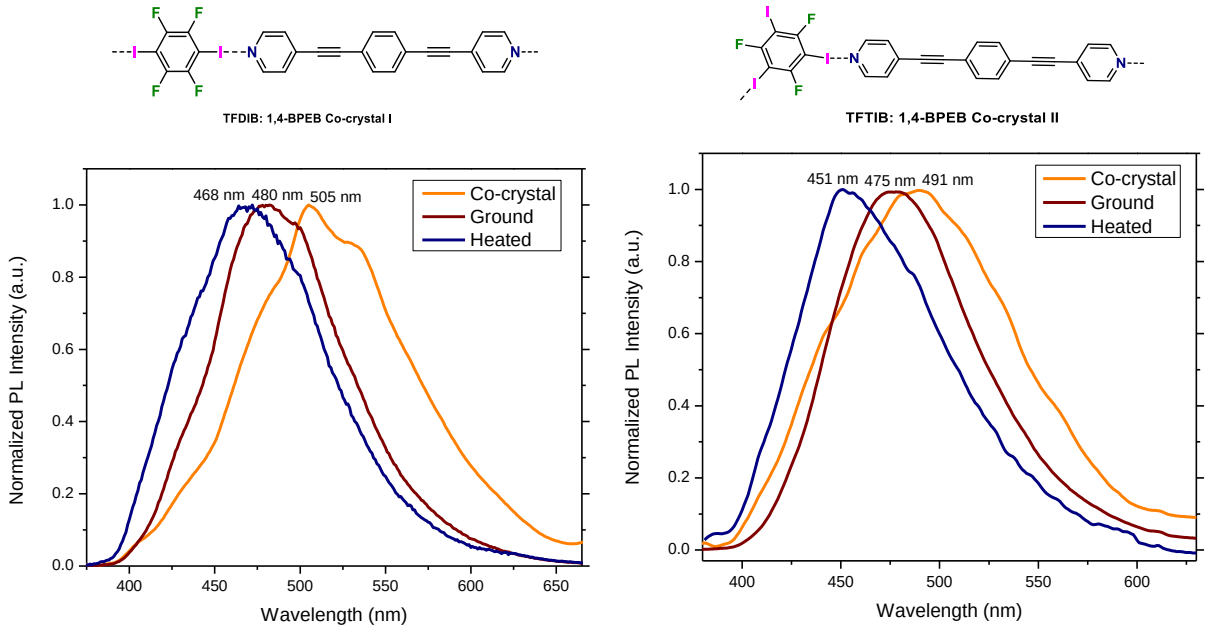

Figure 2.6. Normalized photoluminescent spectra of the 1,4-BPEB co-crystal series before and after grinding.

2.26 Thermal properties

To probe the change in emission in response to heat of the 1,4-BPEB co-crystal series, thermal properties of the co-crystals were studied by TGA and DSC. The XB acceptor 1,4-BPEB was first studied by TGA to measure its % weight loss as a function of temperature and compared to the results of the co-crystals (**Figure 2.7**). The TGA curve of 1,4-BPEB was distinct from the two co-crystals, where the onset point temperature was at 251˚C, followed by a steady weight loss up to 322 ˚C. TFDIB: 1,4-BPEB Co-crystal I showed an onset temperature at 186 ˚C, and the depression of the onset temperature as compared to that of 1,4-BPEB was likely resulting from the weight loss of the less thermally stable TFDIB molecules. Unlike the steady weight loss that was observed in the case of 1,4-BPEB, TFDIB: 1,4-BPEB Co-crystal I exhibited another onset at 270 ˚C, which could be indicative of the disruption of the π-π stacking and the weight loss of 1,4-BPEB molecules. Similar to the TGA result of TFDIB: 1,4-BPEB Co-crystal I, TFTIB: 1,4-BPEB Co-crystal II showed the first onset temperature at 166 ˚C, and a second onset temperature at 248 ˚C. The TGA results suggested that the XB co-crystals thermally decompose as separate units, where the more unstable component decomposes first, followed by the more stable component. Owing to the low melting point of the XB donors, TFDIB and TFTIB, the TGA onset temperatures of the co-crystals were depressed compared to that of 1,4-BPEB.

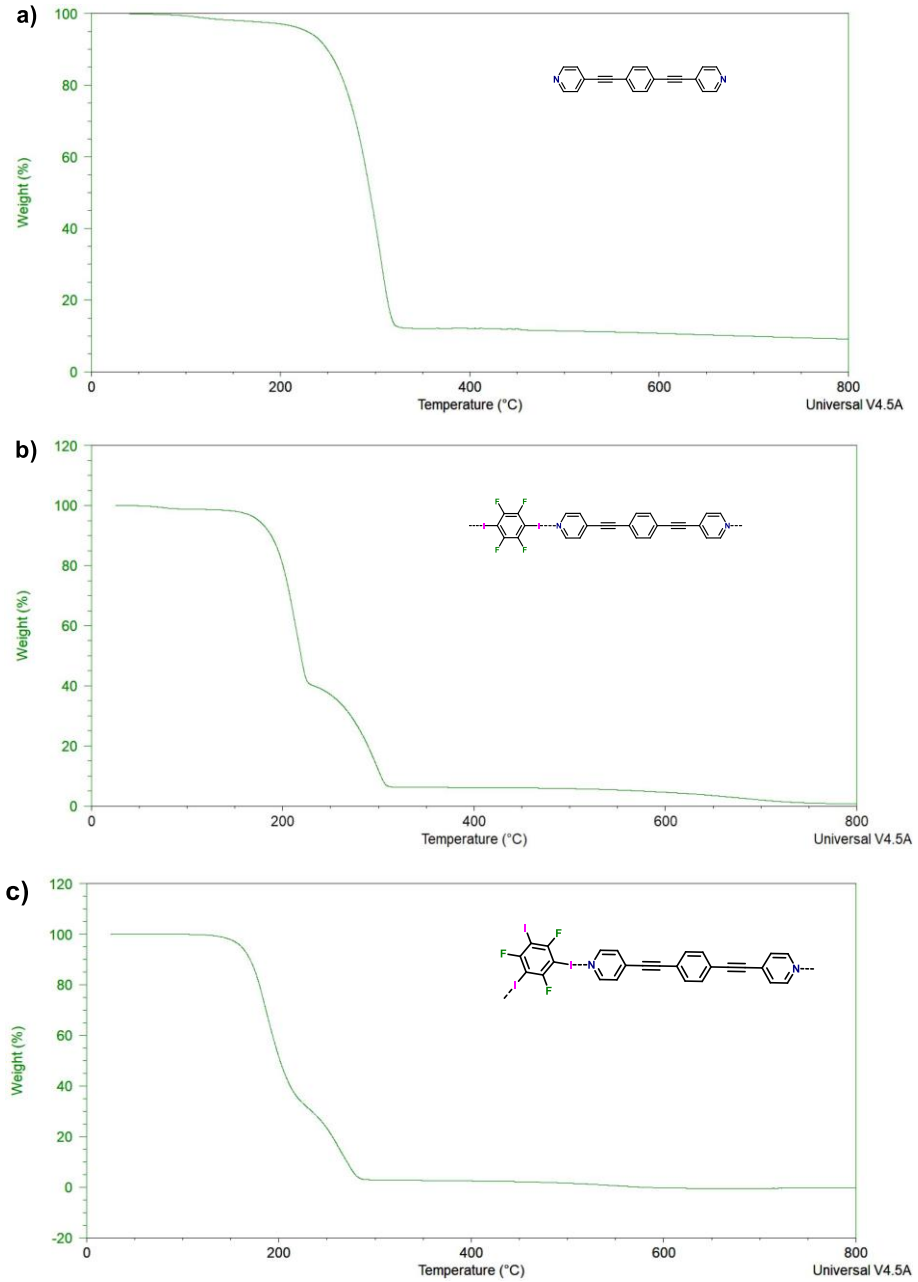

Figure 2.7. The TGA plots of 1,4-BPEB, TFDIB: 1,4-BPEB Co-crystal I, and TFTIB: 1,4-BPEB Co-crystal II.

As an attempt to explain the blue-shift in the emission of the co-crystals upon heating, DSC was employed to examine the phase change of the crystals as a function of the temperature (**Figure 2.8**). The measurement was done from 23 ˚C to 170˚C, and both co-crystals showed no phase transition within the temperature range, which failed to account the change in emission upon heating at 60 ˚C.

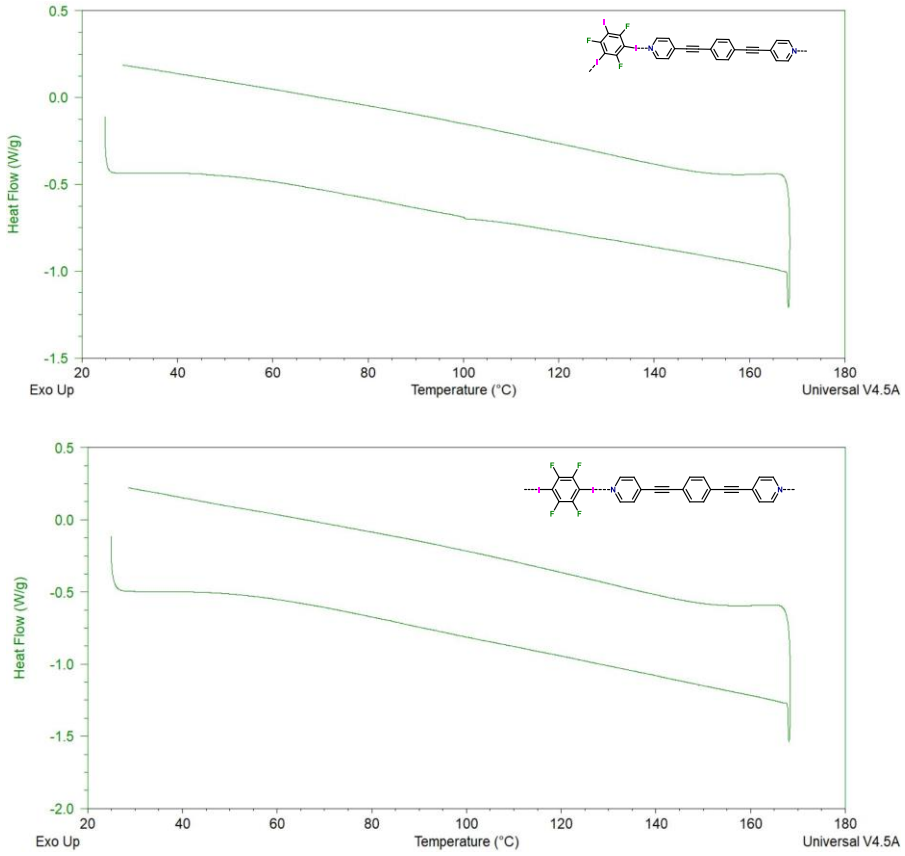

Figure 2.8. The DSC plots of 1,4-BPEB, TFDIB: 1,4-BPEB Co-crystal I, and TFTIB: 1,4-BPEB Co-crystal II.

2.27 Powder X-ray Diffraction

Powder X-ray diffraction (PXRD) method was employed on the ground 1,4-BPEB co-crystal series to study the potential changes in crystallinity upon mechanical grinding. The data were compared to the simulated PXRD from the SCXRD results of the crystalline co-crystals.

By comparing the PXRD results of the ground TFDIB: 1,4-BPEB Co-crystal I to the simulated PXRD pattern of its crystalline state (**Figure 2.9a**), the ground sample showed a dramatic decrease in peak intensity, which was likely caused by the disruption of its crystallinity upon mechanical grinding. The ground TFTIB: 1,4-BPEB Co-crystal II also showed a drastic decrease in the peak intensity comparing to its simulated PXRD pattern at the crystalline state, which indicated its amorphous nature after grinding. The result was possibly due to the disruption of the halogen-bonding interactions and π-π stackings of the co-crystal upon mechanical grinding. Tying in PXRD results with the observed change in emission, it is indicative that the halogen-bonding interactions and π-π stackings are responsible for intermolecular communications and charge-transfer interactions, and by breaking the interactions, the co-crystals exhibited up to a 25 nm blue-shift upon mechanical grinding.

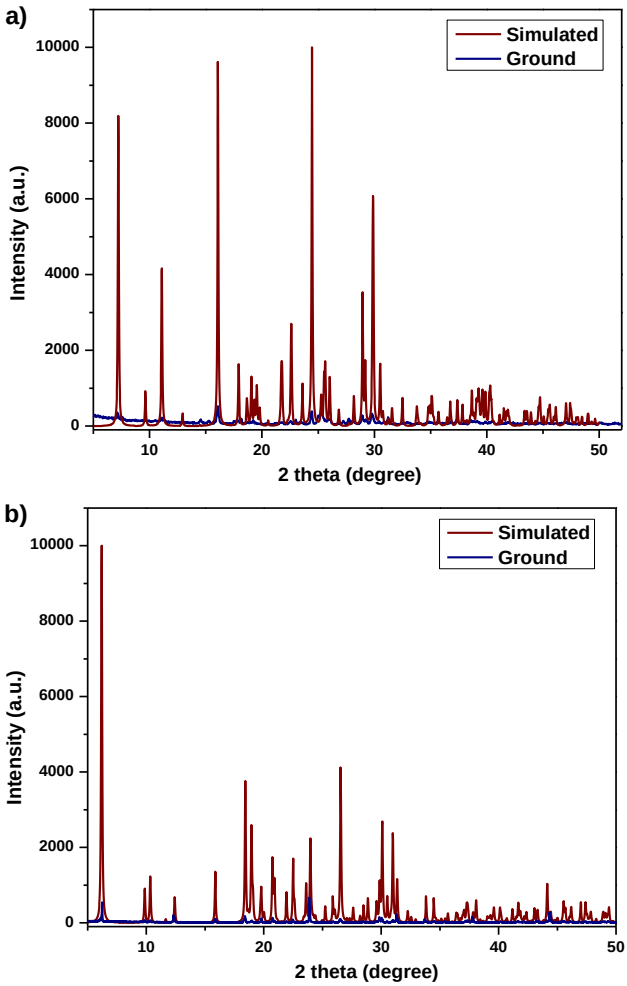

Figure 2.9. a) The simulated PXRD data of TFDIB: 1,4-BPEB Co-crystal I. b) The PXRD data of TFTIB: 1,4-BPEB Co-crystal II.

2.3 Conclusion

The current new π-conjugated XB systems formed from wither TFDIB and TFTIB as donors resulted in distinctive supramolecular networks due to the difference in topicity. We were not able to form 2D halogen-bonded networks this might suggest that its formation process may not be thermodynamically favorable using the solution-grown technique, and energy may be required to induce its formation. All co-crystal exhibited medium to strong XB interactions which enabled the formation of continuous networks, along with π-π, C-H$\cdots$ π, and heteroatom$\cdots\pi$ interactions that reinforced the 3D network assembly. The difference in the solid-state crystal structures of the co-crystal series I and II resulted in different optical absorption and emission behaviors. Both 1,4-BPEB co-crystal series have shown blue-shifts in emission upon mechanical grinding, and further blue-shifts were observed upon heating. Their response to these external pressures could be attributed to the change in solid-state molecular packing from highly crystalline to amorphous states, which was supported by the PXRD data. The solid-state XB and π-π interactions of the co-crystals brought unique molecular arrangements as well as molecular orbital interactions, which

resulted in lowering of the LUMO energy level and reductions in the HOMO-LUMO energy gaps. Our halogen-bonded crystals did not exhibit any meaning properties in OFET studies, as suggested by our collaborator. This might be caused by the relatively low thermal stability of the crystals, and the intermolecular interactions might not be strong enough to facilitate strong charge-transport. Comparing our current study with Zhao's,[6] we did not observe such a significant red-shift in absorption and emission of the halogen-bonded crystal relative to those of the starting materials. Our results raise questions about the degree of contribution of halogen bonding interactions to the photophysical properties, and further studies which involve better crystal design and fundamental investigation might be needed.

2.4 Experimental Section

Synthesis of TFTIB. The compound was synthesized according to the reported procedure with minor modifications.[10] To 22 mL of H_2SO_4 was charged HIO_4 (3.29 g, 14.4 mmol), and the suspension was subsequently added KI (7.25 g, 43.7 mmol) over a period of 5 min at 0 ˚C. Subsequently, **1** (1.28 g, 9.69 mmol) was added to the reaction mixture via a syringe over 15 min at 0 ˚C, and the mixture was heated to 70 ˚C and stirred for 4 hours. The mixture was cooled to room temperature and poured onto ice then extracted with ether. The organic layer was washed with 1.0M NaOH, brine and dried with Na_2SO_4. After removing the solvent in vacuo, the product was purified by recrystallization in hexanes to afford **TFTIB** as a white crystalline solid (3.01 g, 61% yield). ^{19}F NMR (282 MHz, $CDCl_3$) δ -68.9 (s, 3F). ^{13}C NMR (75.4 MHz, $CDCl_3$) δ 162.25 (dt), 63.74 (td).[10]

Synthesis of TFDIB. The compound was synthesized according to the reported procedure with minor modifications.[10] To 20 mL of H_2SO_4 was added HIO_4 (3.04 g, 13.3 mmol), and KI (5.22 g, 31.4 mmol) was added to the suspension over a period of 5 min at 0 ˚C. Subsequently, **2** (1.34 g, 8.96 mmol) was added to the reaction mixture via a syringe over 15 min at 0 ˚C, and the mixture was heated to 70 ˚C and stirred for 4 hours. The mixture was cooled to room temperature and poured onto ice then extracted with ether. The organic layer was washed with 1.0M NaOH, brine and dried with Na_2SO_4. After removing the solvent in vacuo, the product was purified by recrystallization in hexanes to afford **TFDIB** as a white crystalline solid (2.27 g, 63% yield). ^{19}F NMR (282 MHz, $CDCl_3$) δ -118.0 (s, 4F). ^{13}C NMR (75.4 MHz, $CDCl_3$) δ 147.86-145.38 (m), 72.89 (m).[10]

Synthesis of 1,4-BPB. The compound was synthesized following a reported procedure.[12] To a deoxygenated mixture of **8** (0.14 g, 0.82 mmol), **7** (0.500 g, 2.45 mmol), K_2CO_3 (0.680 g, 4.89 mmol), and of $Pd(PPh_3)_4$ (0.0900 g, 0.0100 mmol) was added a 2:1:1 mixture of degassed PhMe/H_2O/EtOH, and the mixture was stirred at reflux for 48 hours. The organic compound was extracted with DCM and concentrated HCl was added dropwise to the organic layer to bring the pH to 2. The resulted precipitate was collected and dissolved in distilled H_2O and concentrated NaOH solution was added dropwise to bring

the pH to 10, which resulted in the precipitation of the pure product as a white solid (1.04 g, 55% yield). ^{1}H NMR (400 MHz, $CDCl_3$): δ 8.69 (d, 4H), 7.76 (s, 4H), 7.55 (dd, 2H).

Synthesis of 5. The compound was synthesized according to the reported procedure with minor modifications.[11] To a deoxygenated mixture of **3** (0.5 g, 1.52 mmol), **4** (0.33 g, 3.33 mmol), $Pd(PPh_3)_2Cl_2$ (0.042 g, 4 mol %) in 5 mL of THF and 5 mL of Et_3N, was added CuI (0.0055 g, 2 mol%), and the reaction mixture was stirred under an atmosphere of N_2 at room temperature for 2 hours. The mixture was filtered through a pad of celite and poured into deionized H_2O and extracted with DCM. The organic layer was dried over anhydrous Na_2SO_4, and the solvent was evaporated in vacuo. The crude was purified by silica gel column chromatography using hexanes and ethyl acetate (9:1 v/v) as eluent to give the product as a yellow powder (0.39 g, 95% yield). ^{1}H NMR (400 MHz, $CDCl_3$): δ 7.37 (s, 4H), 0.23 (s, 18H).

Synthesis of 6. The compound was synthesized according to the reported procedure with minor modifications.[11] To a deoxygenated 2:1 mixture of THF/MeOH (15 mL) and **5** (0.390 g, 1.43 mmol) was added KOH (0.240 g, 4.30 mmol), and the mixture was stirred at room temperature for 3 hours under an atmosphere of N_2 and then poured into a saturated aqueous solution of NH_4Cl. The product was extracted by DCM and dried over Na_2SO_4 and purified by silica gel column chromatography using hexanes and DCM (5:1 v/v) as eluent to give the product as a light-yellow solid (0.12 g, 97% yield). ^{1}H NMR (400 MHz, $CDCl_3$): δ 7.42 (s, 4H), 3.15 (s, 2H).

Synthesis of 1,4-BPEB. The compound was synthesized according to the reported procedure with minor modifications.[15] To a deoxygenated mixture of **7** (0.049 g, 0.85 mmol), **6** (0.170 g, 0.380 mmol), and $Pd(PPh_3)_2Cl_2$ (0.0200 g, 0.0390 mmol) in 5 mL of THF and 1 mL of Et_3N, was added CuI (0.0074 g, 0.039 mmol), and the reaction mixture was stirred under an atmosphere of N_2 at room temperature for 3 hours. The mixture was filtered through a pad of celite and poured into deionized H_2O and extracted with DCM. The organic layer was dried over anhydrous Na_2SO_4, and the solvent was evaporated in vacuo. The crude was purified by a short pad of silica gel column chromatography using hexanes and ethyl acetate (3:1 v/v) as eluent to give **1,4-BPEB** as a yellow product (0.065 g, 60% yield). ^{1}H NMR (400 MHz, $CDCl_3$): δ 8.63 (m, 4H), 7.56 (s, 4H), 7.39 (dd, 4H).

Synthesis of 9. The compound was synthesized according to the reported procedure with minor modifications.[16] To a deoxygenated mixture of **7** (0.500 g, 2.44 mmol), **4** (0.290 g, 2.93 mmol), $Pd(PPh_3)_2Cl_2$ (0.086 g, 5 mol %) in 5 mL of THF and 5 mL of Et_3N, was added CuI (0.023 g, 5 mol%), and the reaction mixture was stirred under an atmosphere of N_2 at room temperature for 2 hours. The mixture was filtered through a pad of celite and poured into deionized H_2O and extracted with DCM. The organic layer was dried over anhydrous Na_2SO_4, and the solvent was evaporated in vacuo. The crude was purified

by silica gel column chromatography using hexanes and ethyl acetate (9:1 v/v) as eluent to give the product as a yellow oil (0.41 g, 96% yield). The ^{1}H NMR spectrum was in agreement with the literature.

Synthesis of 10. The compound was synthesized according to the reported procedure with minor modifications.[17] To a deoxygenated 1:1 mixture of THF/MeOH (10 mL) and **9** (0.200 g, 1.14 mmol) was added KOH (0.130 g, 2.28 mmol), and the mixture was stirred at room temperature for 3 hours under an atmosphere of N_2 and then poured into a saturated aqueous solution of NH_4Cl. The product was extracted with DCM and dried over anhydrous Na_2SO_4 and purified by silica gel column chromatography using hexanes and DCM (3:1 v/v) as eluent to give the product as an off-white solid (0.11 g, 95% yield). ^{1}H NMR (400 MHz, $CDCl_3$): δ 8.55 (d, 2H), 7.29 (d, 2H), 3.26 (s, 1H).

Synthesis of 12. The compound was synthesized following a reported procedure.[18] To 125 mL of AcOH was added **11** (5.25 g, 62.4 mmol) and NBS (22.2 g, 125 mmol), and the reaction mixture was stirred at 50 ℃ for 12 hours. After cooling to room temperature, the mixture was poured into 125 mL of cold saturated aqueous NaOH solution and extracted with hexanes. The crude was purified by silica gel column chromatography using pure hexanes as eluent to give the product as a colorless oil (11.0 g, 74%). ^{1}H NMR (400 MHz, $CDCl_3$): δ 6.82 (s, 2H).

Synthesis of 2,5-BPET. The compound was synthesized according to the reported procedure with minor modifications.[13] To a deoxygenated mixture of **12** (0.672 g, 2.00 mmol), **10** (0.43 g, 4.2 mmol), $Pd(PPh_3)_2Cl_2$ (0.007 g, 0.005 mmol) in 20 mL of THF and 5 mL of Et_3N, was added CuI (0.002 g, 0.005 mmol), and the reaction mixture was stirred under an atmosphere of N_2 at room temperature for 8 hours. The mixture was filtered through a pad of celite and poured into deionized H_2O and extracted with DCM. The organic layer was dried over anhydrous Na_2SO_4, and the solvent was evaporated in vacuo. The crude was purified by a short pad of silica gel column chromatography using hexanes and ethyl acetate (3:1 v/v) as eluent to give **1,4-BPEB** as a dark yellow product (0.43 g, 54% yield). ^{1}H NMR (400 MHz, $CDCl_3$): δ 7.67-7.65 (m, 4H), 7.56-7.55 (m, 4H), 7.13-7.10 (m, 2H).

Synthesis of *N,N*'-BPNDI. The compound was synthesized following a reported procedure.[14] To 20 mL of anhydrous DMF was added **13** (0.800 g, 2.98 mmol) and **14** (0.560 g, 6.00 mmol). The mixture was heated at reflux for 12 hours under an atmosphere of N_2, and it was subsequently poured into ice H_2O. The precipitate was collected and washed with DCM and acetone, and the product was recrystallized in DMF to afford a brown solid (0.63 g, 50% yield). The compound was characterized by single-crystal X-ray diffraction.

2.5 References

(1) Ajayaghosh, A.; Praveen, V. K. *Acc. Chem. Res.* **2007**, *40*, 644–656.

(2) Menard, E.; Podzorov, V.; Hur, S. H.; Gaur, A.; Gershenson, M. E.; Rogers, J. A. *Adv. Mater.* **2004**, *16*, 2097–2101.

(3) Fu, C.; Lin, H. P.; Macleod, J. M.; Krayev, A.; Rosei, F.; Perepichka, D. F. *Chem. Mater.* **2016**, *28*, 951–961.

(4) Cavallo, G.; Metrangolo, P.; Milani, R.; Pilati, T.; Priimagi, A.; Resnati, G.; Terraneo, G. *Chem. Rev.* **2016**, *116*, 2478–2601.

(5) Bolton, O.; Lee, K.; Kim, H. J.; Lin, K. Y.; Kim, J. *Nat. Chem.* **2011**, *3*, 205–210.

(6) Bai, L.; Bose, P.; Gao, Q.; Li, Y.; Ganguly, R.; Zhao, Y. *J. Am. Chem. Soc.* **2017**, *139*, 436–441.

(7) Yan, D.; Delori, A.; Lloyd, G. O.; Friščić, T.; Day, G. M.; Jones, W.; Lu, J.; Wei, M.; Evans, D. G.; Duan, X. *Angew. Chem., Int. Ed.* **2011**, *50*, 12483–12486.

(8) Zhu, W.; Zheng, R.; Zhen, Y.; Yu, Z.; Dong, H.; Fu, H.; Shi, Q.; Hu, W. *J. Am. Chem. Soc.* **2015**, *137*, 11038–11046.

(9) Zheng, Q. N.; Liu, X. H.; Chen, T.; Yan, H. J.; Cook, T.; Wang, D.; Stang, P. J.; Wan, L. J. *J. Am. Chem. Soc.* **2015**, *137*, 6128–6131.

(10) a) Hellmann, M.; Bilbo, A. J.; Pummer, W. J. *J. Am. Chem. Soc.* **1955**, *77*, 3650–3651. b) Chambers, R. D.; Skinner, C. J.; Atherton, M. J.; Moilliet, J. S. *J. Chem. Soc., Perkin Trans. I*, **1996**, 1659-1664.

(11) Yoosaf, K.; Llanes-Pallas, A.; Marangoni, T.; Belbakra, A.; Marega, R.; Botek, E.; Champagne, B.; Bonifazi, D.; Armaroli, N. *Chem. Eur. J.* **2011**, *17*, 3262–3273.

(12) Sen, S.; Neogi, S.; Aijaz, A.; Xu, Q.; Bharadwaj, P. K. *Dalton Trans.* **2014**, *43*, 6100–6107.

(13) Sokolov, A. N.; Friščić, T.; MacGillivray, L. R. *J. Am. Chem. Soc.* **2006**, *128*, 2806–2807.

(14) Koshkakaryan, G.; Klivansky, L. M.; Cao, D.; Snauko, M.; Teat, S. J.; Struppe, J. O.; Liu, Y. *J. Am. Chem. Soc.* **2009**, *131*, 2078–2079.

(15) Grunder, S.; Huber, R.; Horhoiu, V.; González, M. T.; Schönenberger, C.; Calame, M.; Mayor, M. *J. Org. Chem.* **2007**, *72*, 8337–8344.

(16) Moreno-García, P.; Gulcur, M.; Manrique, D. Z.; Pope, T.; Hong, W.; Kaliginedi, V.; Huang, C.; Batsanov, A. S.; Bryce, M. R.; Lambert, C. *J. Am. Chem. Soc.* **2013**, *135*, 12228–12240.

(17) Xu, D.; Zhu, W.; An, Q.; Li, W.; Li, X.; Yang, H.; Yin, J.; Li, G. *Chem. Commun.* **2012**, *48*, 3494-3496.

(18) Yu, J.; Shen, T. L.; Weng, W. H.; Huang, Y. C.; Huang, C. I.; Su, W. F.; Rwei, S. P.; Ho, K. C.; Wang, L. *Adv. Energy Mater.* **2012**, *2*, 245–252.

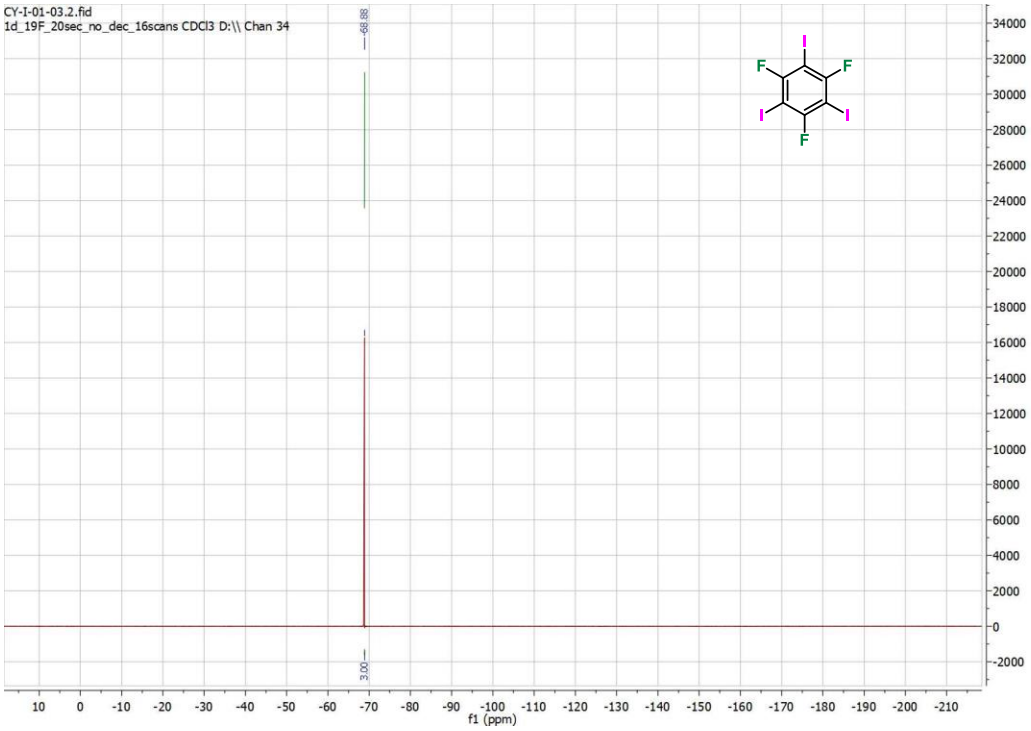

Figure 2.10. ^{19}F NMR of TFTIB.

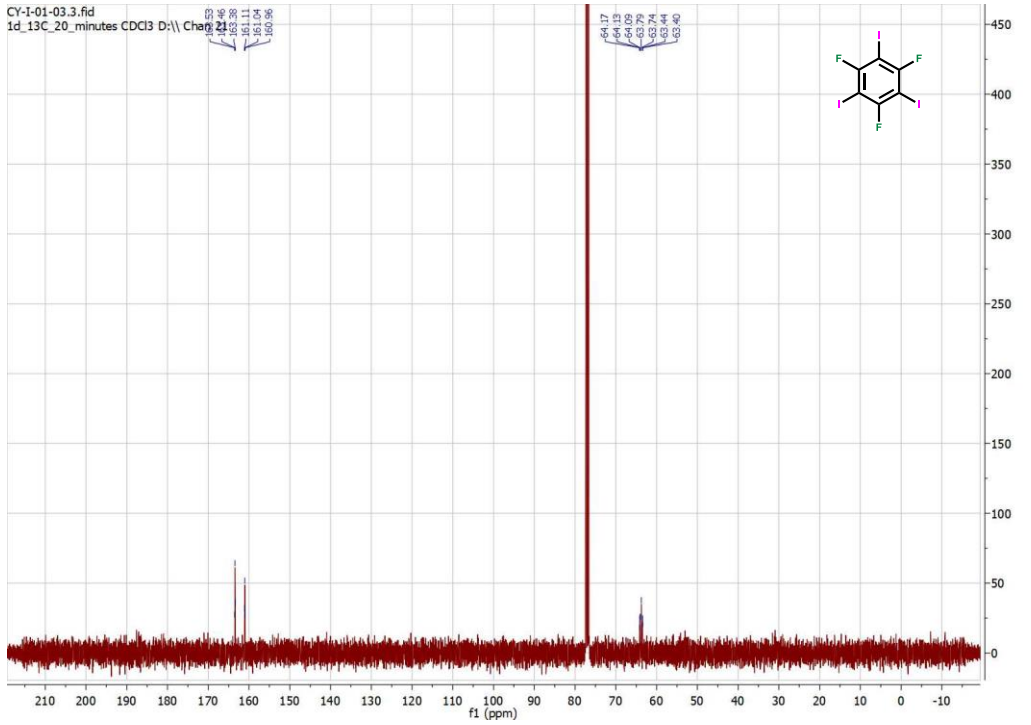

Figure 2.11. ^{13}C NMR of TFTIB.

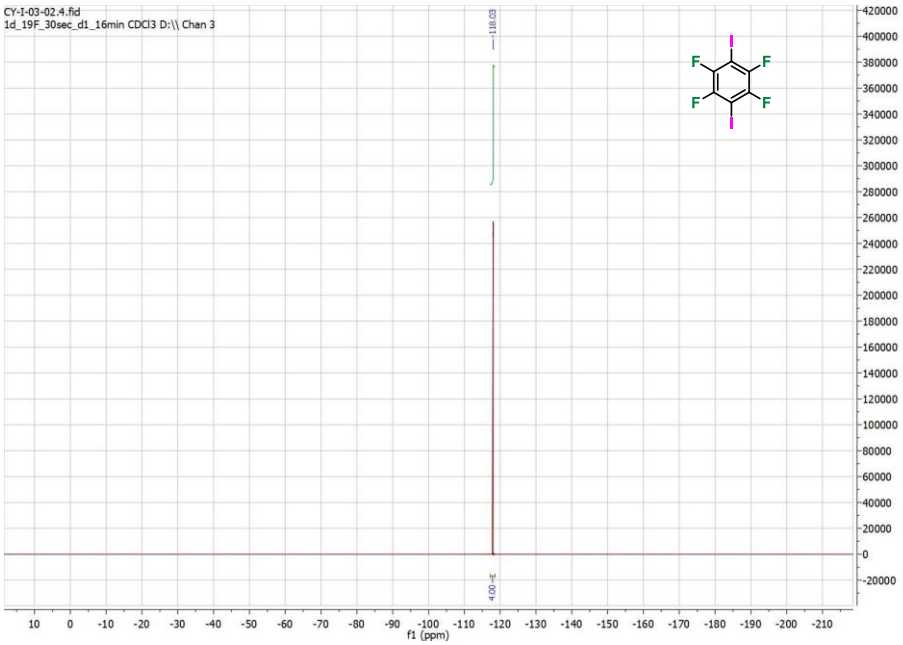

Figure 2.12. ^{19}F NMR of TFDIB.

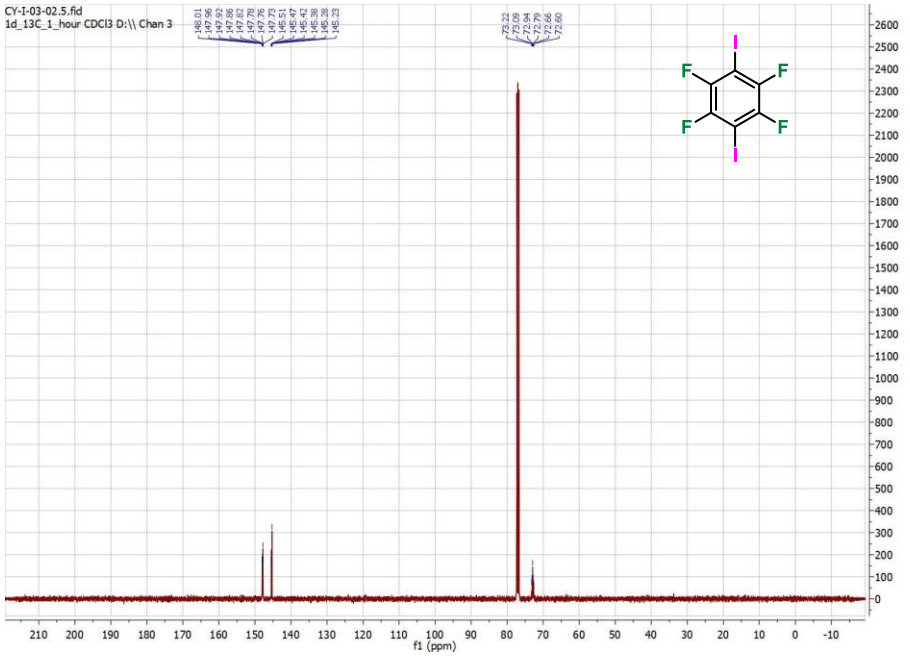

Figure 2.13. ^{13}C NMR of TFDIB.

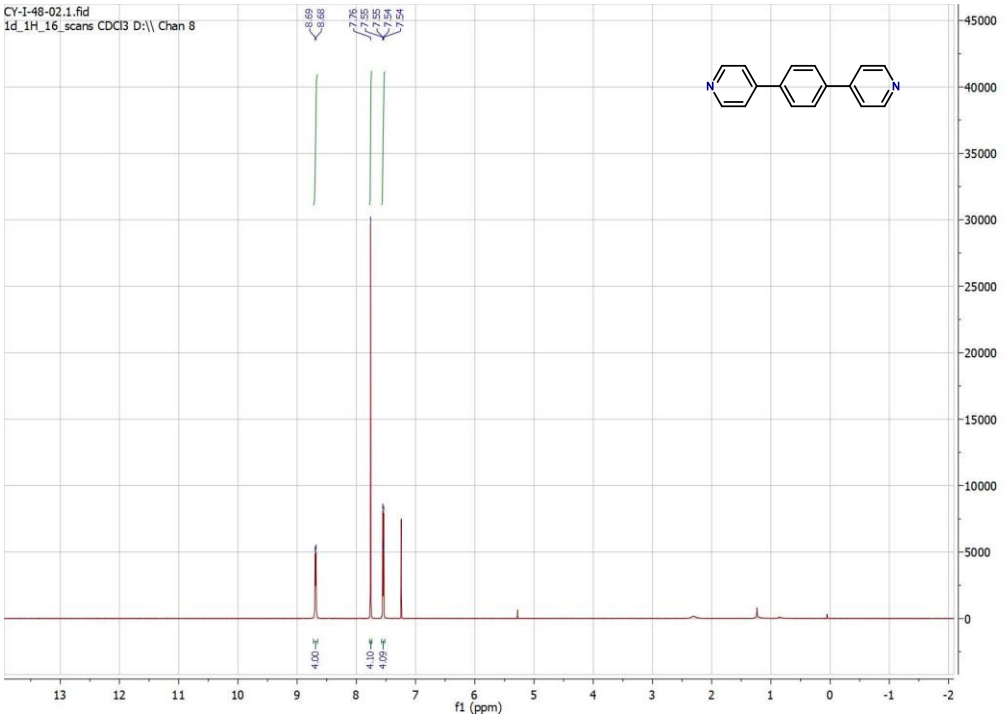

Figure 2.14. ^{1}H NMR of 1,4-BPB.

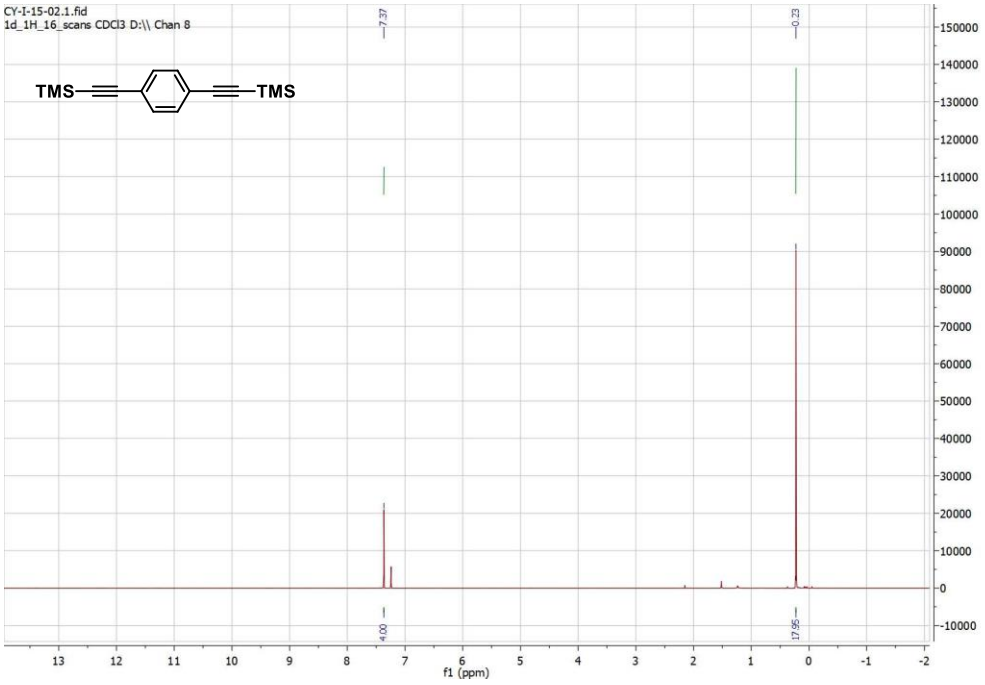

Figure 2.15. ^{1}H NMR of compound 5.

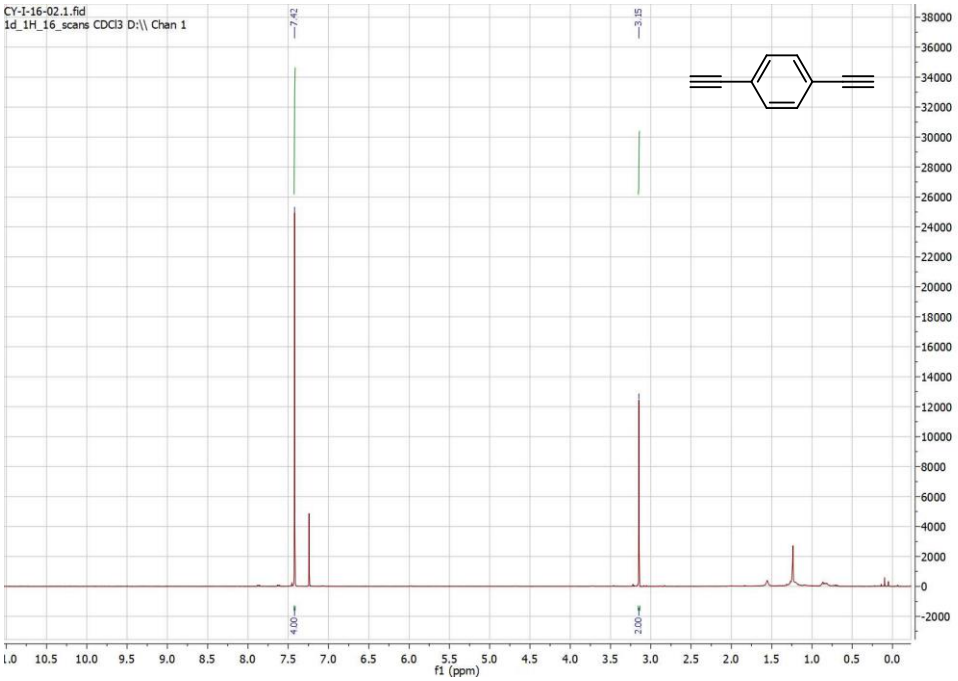

Figure 2.16. ^{1}H NMR of compound 6.

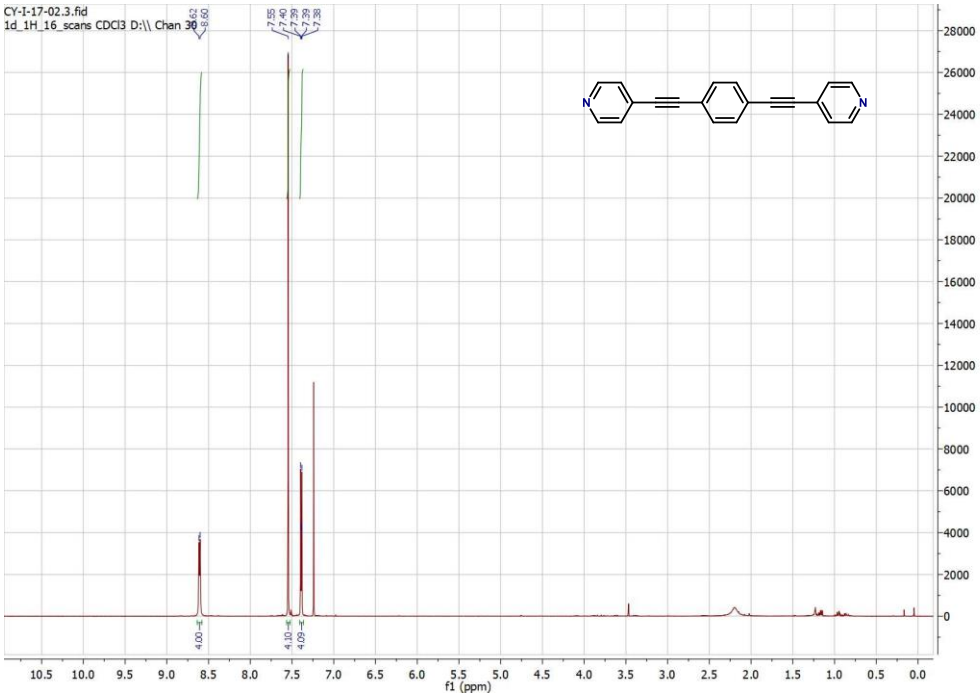

Figure 2.17. ^{1}H NMR of 1,4-BPEB.

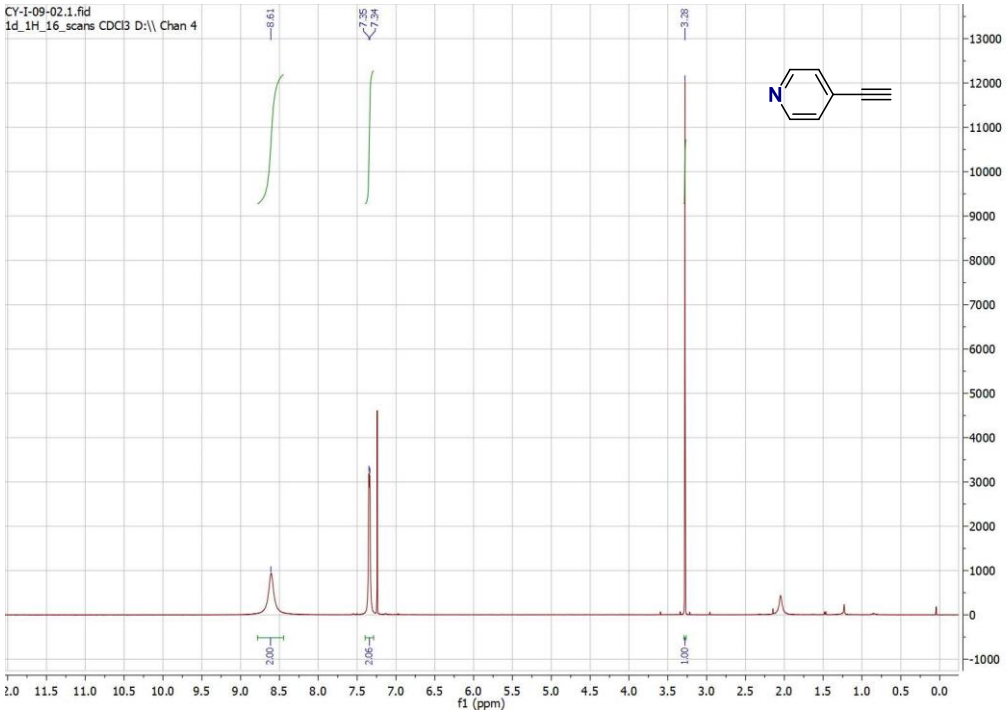

Figure 2.18. ^{1}H NMR of compound 10.

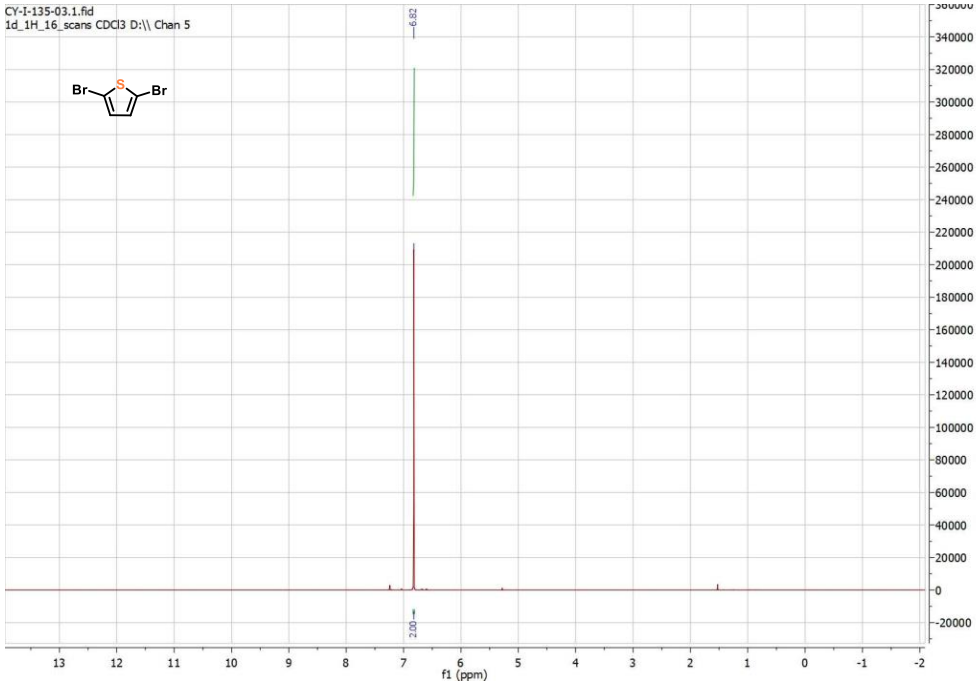

Figure 2.19. ^{1}H NMR of compound 12.

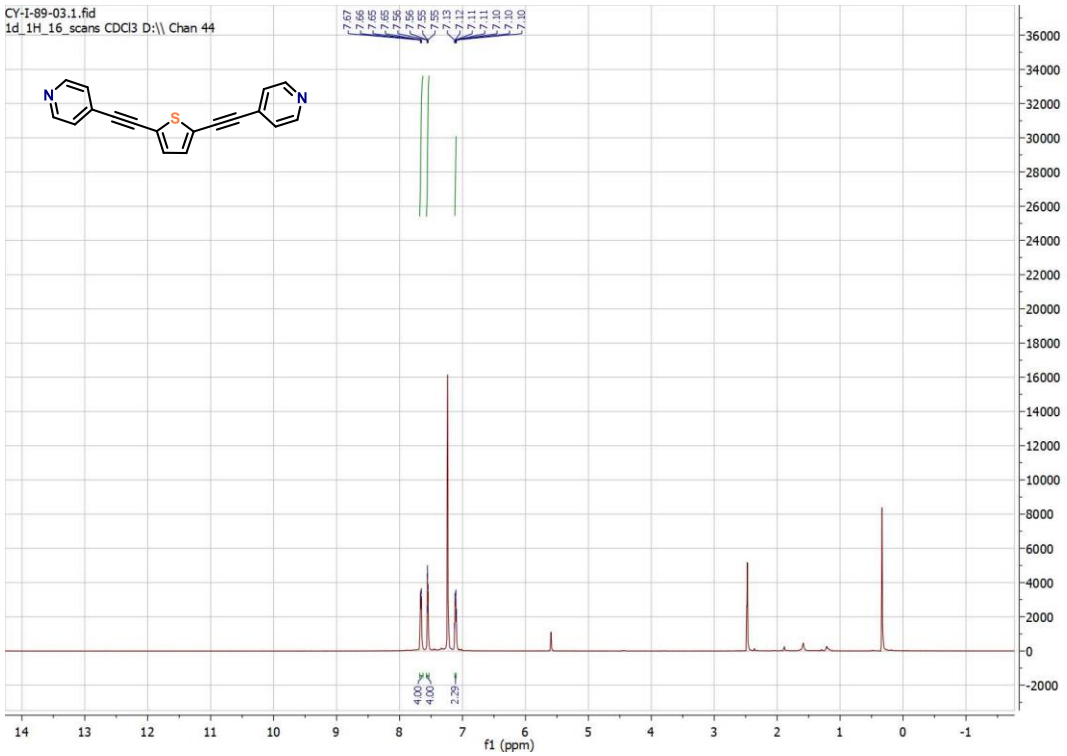

Figure 2.20. ^{1}H NMR of 2,5-BPET.

Chapter 3. Pentafluorosulfanyl-Based π-Conjugated Small Molecules as Optoelectronic Materials

3.1 Introduction

In the previous chapter, intermolecular D-A systems held by halogen-bonding interactions were discussed, and intramolecular D-A π-conjugated molecules are studied in this chapter. The application of π-conjugated small molecules in the field of materials science, including organic field-effect transistors (OFETs), organic photovoltaics (OPVs), and organic light-emitting diodes (OLEDs) has been of particular interest due to their ease of synthesis, tunability, and crystallinity.[1–3] The incorporation of an electron-rich donor and an electron-deficient acceptor into the π-conjugated small molecules, known as the donor-acceptor (D-A) small molecule systems also attracted intensive research attention due to their strong intramolecular charge-transfer induced by intramolecular orbital interactions.[4–6] Through strong intramolecular orbital interactions, the energy gap between the highest occupied molecular orbital (HOMO) and the lowest unoccupied molecular orbital (LUMO) can be reduced, thus potentially leads to the broadening of the optical absorption in the visible region and improvements in the charge-transport properties of the semiconductors.[7]

The optoelectronic properties of the D-A systems can be readily tuned through a rational combination of different electron-rich and electron-deficient π-conjugated moieties.[8] Compared to the highly utilized CF_3 group, the analogous SF_5 is seldom studied in the context of materials chemistry.[9] The SF_5 group possesses higher electronegativity (3.65) than that of the CF_3 group (3.36), which suggests it to be a stronger acceptor. The steric bulk of the SF_5 group created by the five fluorine atoms potentially minimizes aggregation-caused quenching and improves the solubility of the π-conjugated molecules. This is a favourable characteristic in materials chemistry since the electron-withdrawing unit can act as both an acceptor and a solubilizing unit, which omits the need of installing additional alkly chains for solubilization. The triphenylamine (TPA) group, on the other hand, is an excellent electron-rich group that has been utilized in various D-A systems as a donor.[10]

The goal of our current project is to investigate the SF_5 group as an acceptor moiety in a conjugated D-A system, and by employing different π-linkers, we hope to successfully tune the photophysical properties of the D-A compounds. Herein, we report the synthesis of two π-conjugated molecules that contains TPA as the donor and phenyl-SF_5 as the acceptor, bridged by two different π-linkers. The photophysical properties of the SF_5 containing molecules were investigated in the solution-, film-, and solid-states, and the experimental studies were further supported by theoretical calculations. The crystal structures of these two SF_5-containing molecules were determined by SCXRD to elucidate their molecular packing in the solid-state.

3.2 Results and Discussion

3.21 Synthesis

The previously prepared compound **1** was reacted with trimethylsilylacetylene via a Sonogashira cross-coupling reaction to afford compound **2** in 91%, and the TMS protecting group was then removed by K_2CO_3 in a mixture of MeOH and THF to give compound **3** in excellent yield. Compound **4** was synthesized by treating thiophene with NBS in acetic acid, and compound **5** was afforded in 45% yield from a Sonogashira cross-coupling reaction between compound **4** and one equivalent of trimethylsilylacetylene. Compound **3** and **5** were coupled via a Sonogashira cross-coupling reaction to give compound **6** in 50% yield. The TMS deprotection was done by K_2CO_3 in a mixture of MeOH/THF to afford compound **7** in 95% yield. The target compound **3f** was obtained via a Sonogashira cross-coupling between compound **7** and 4-bromophenylsulfurpentafluoride in 80% yield (**Scheme 3.1a**).

Another SF_5-containing compound **3e** was synthesized from a four-step reaction sequence. An olefination was done on the previously prepared compound **11** via a Wittig reaction to give compound **12** in 67% yield. Compound **12** was then reacted with 4-bromobenzaldehyde via a Heck cross-coupling reaction to afford intermediate **13** in 86% yield. An olefination was later done on **13** through a Wittig reaction to give intermediate **14** in 50% yield. Compound **14** was subsequently reacted with 4-bromophenylsulfurpentafluoride via a Heck cross-coupling reaction to obtain the target compound **3e** in 68% yield (**Scheme 3.1b**).

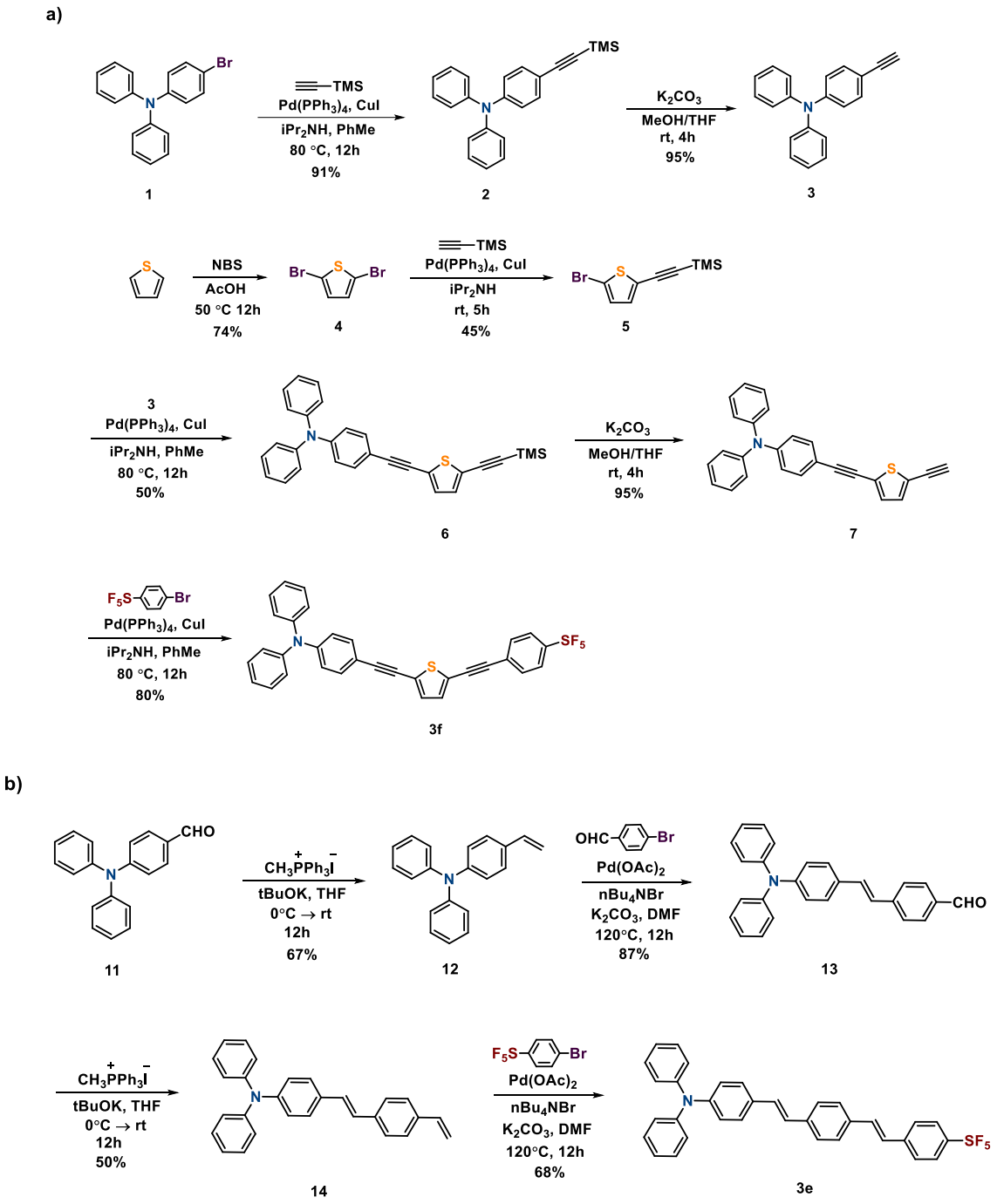

Scheme 3.1. a) The synthesis of compound **3f**, and b) The synthesis of compound **3e**.

3.22 Crystallization

The crystals of compound **3e** and **3f** were both grown by the slow-diffusion method; compound **3f** was dissolved in minimum amount of hot chloroform and a layer of ethanol was carefully layered on top of it. Compound **3e** was also dissolved in hot chloroform and acetonitrile was layered on top of it since the

addition of ethanol would facilitate immediate precipitation of the compound. X-ray quality crystals were grown within one week for both compounds.

3.23 Single-Crystal X-ray Structures

The crystal structures of compounds **3f** and **3e** were determined by single-crystal X-ray diffraction (**Figure 3.1**), and the complete crystallographic data were reported in **Table 3.1**.

Table 3.1. Details of the crystallographic data of compounds **3f** and **3e**.

crystal	3f	3e
formula	$C_{32}H_{20}F_5NS_2$	$C_{34}H_{26}F_5NS$
temperature/K	200(2)	200(2)
crystal size/mm^3	0.356 x 0.199 x 0.088	0.910 x 0.230 x 0.030
crystal system	Triclinic	Monoclinic
space group	P *-1*	*Cc*
***a*/Å**	9.7623(16)	51.849(9)
***b*/Å**	12.653(2)	10.9446(18)
***c*/Å**	13.845(2)	9.8186(15)
***α*/deg**	69.164(2)	90
***β*/deg**	78.669(2)	91.81
***γ*/deg**	84.175(2)	90
***V*/ Å^3**	1566.3(4)	5569.0(16)
Z	2	8
***ρ* (calcd)/Mgm^{-3}**	1.225	1.373
***θ* range for data**	1598 to 25.249	0.786 to 25.245
collection/° F(000)	592	2384
ref collected/unique	15990	15997
R1, *w*R$_2$ (I > 2*σ*(I))	0.0532, 0.1177	0.1000, 0.2630

R1, wR_2 (all data)	0.1114, 0.1437	0.1762, 0.3137
goodness-of-fit, *S*	1.009	1.041

Compound **3f** crystallized in the triclinic space group P *-1*, and compound **3e** crystallized in the monoclinic space group *Cc*. Both crystal structures exhibited extensive intermolecular interactions that reinforce the supramolecular assemblies. Compound **3f** showed strong C-H$\cdots\pi$ interactions between C(3)-H(3)$\cdots$C(16) and C(22)-H(22)$\cdots$C(19) with 2.69 Å and 2.81 Å, respectively. The SF_5 group of compound **3f** also participated in strong intermolecular H-bonding interactions, where the distances between C(10)-H(10)$\cdots$F(5), and C(31)-H(31)$\cdots$F(1) were measured to be 2.60 Å and 2.50 Å, respectively (**Figure 3.2**). The short distance between the electron-rich triphenylamine group and the electron-deficient phenyl SF_5 group could be indicative of a strong intermolecular D-A interaction.

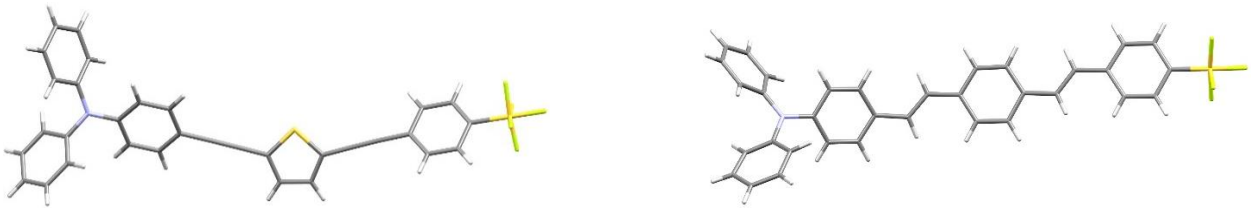

Figure 3.1. The single-crystal X-ray structures of compounds **3f** (left) and **3e** (right).

Compound **3e** demonstrated a herringbone packing motif with strong edge-to-face interactions, assisted by multiple intermolecular interactions in the crystal packing, such as π-π interactions ranging from 3.27- 3.38 Å, and C-H$\cdots\pi$ interactions with distances from 2.57-2.86 Å. The SF_5 group was found to form strong H-bonds between C(24)-H(24)$\cdots$F(8), and C(40)-H(40))$\cdots$F(10), with distances of 2.56 Å and 3.05 Å, respectively. In addition, F$\cdots\pi$ interaction was also observed between F(9) and C(18), with a distance of 3.15 Å (**Figure 3.2**).

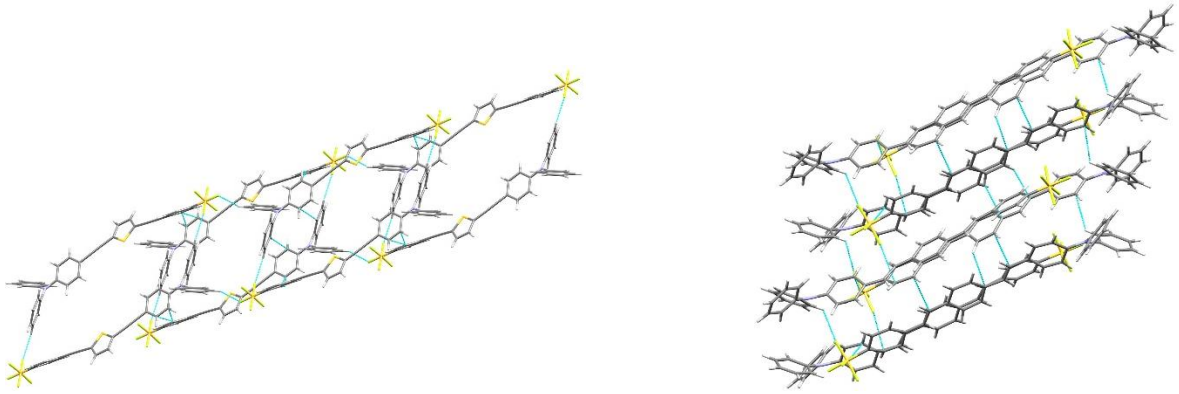

Figure 3.2. The molecular packing diagrams of compounds **3f** (left) and **3e** (right) along the *b*-axis.

3.24 Photophysical Properties

The photophysical properties of compound **3e** and **3f** were characterized in solution, thin-film, and solid-states. The solution-state UV-vis absorption of the two compounds was first studied in dichloromethane (DCM) solution, and the λ_{abs} of compound **3e** showed a 9 nm red-shift relative to **3f**. The two compounds also showed different solution-state emissive behaviors in DCM, where the λ_{em} of **3e** showed a 23 nm red-shift as compared to **3f**. Compound **3e** and **3f** have shown large Stokes shifts of 125 nm and 111 nm, respectively. The observed large Stoke shifts in these two compounds could be promising for potential bioimaging applications[11]. Compound **3e** and **3f** were co-dissolved with poly(methyl methacrylate) individually and spin-coated on glass substrates to obtain solution-processed thin-films. The film-state photophysical properties are shown in **Figure 3.3**, compounds **3e** and **3f** showed Stoke shifts of 88 nm and 85 nm, respectively. The λ_{em} of compound **3e** was found at 562 nm, which is significantly red-shifted relative to compound **3f** at 496 nm.

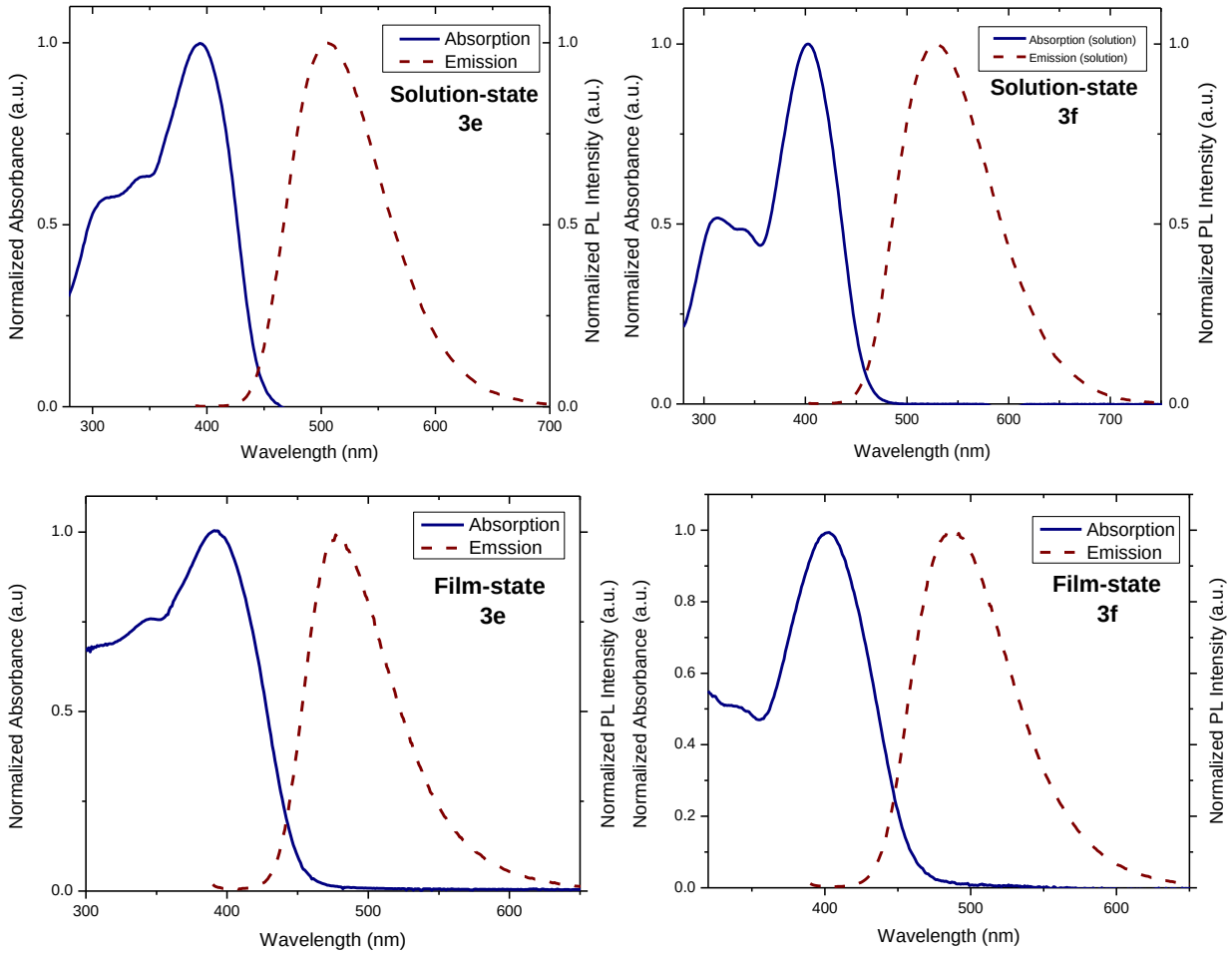

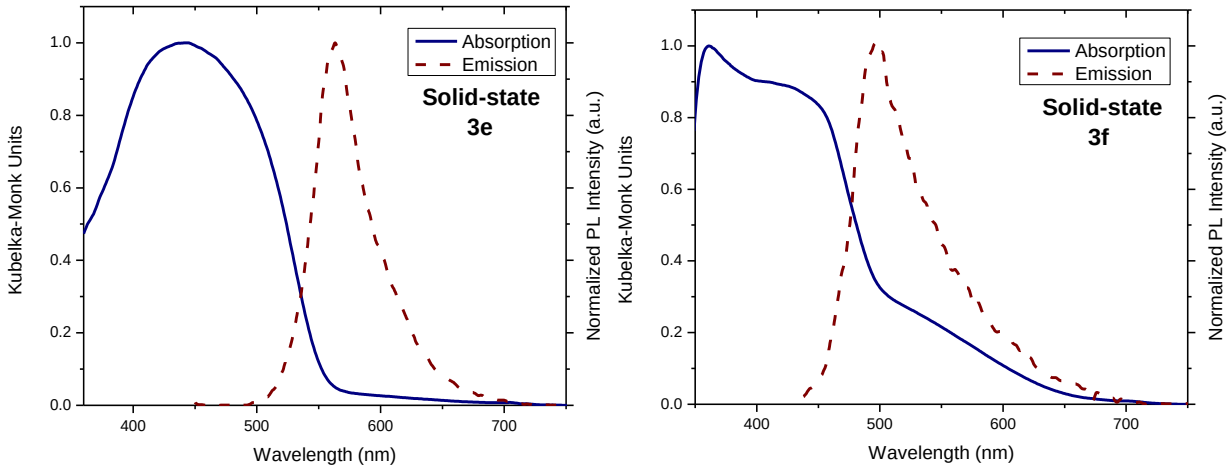

Figure 3.3. The absorption and emission spectra of compounds **3e** and **3f** in the solution-state, film-state, and solid-state.

3.24 Density Functional Theory Calculations

To study the frontier molecular orbital distributions and the photophysical properties of the SF_5-containing D-A π-conjugated systems with a theoretical approach, density functional theory (DFT) and time-dependent DFT (TD-DFT) calculations were employed on a series of SF_5-containing molecules **3a-h** (**Figure 3.4**), where compounds **3a-d** and **3g-h** were synthesized by Dr. Gautam in our group.[12] The geometries of the compounds were first optimized at the B3LYP/6-31G(d) level of theory, and the HOMO-LUMO distribution was subsequently obtained. A certain degree of delocalization of the HOMO-LUMO distribution was observed in compounds **3a-h**, which indicates typical π-conjugated D-A systems. The HOMO coefficients were mainly concentrated on the triphenylamine moiety, which acts as the electronic donor, and the LUMO coefficients were mainly localized in the region proximal to the SF_5 group, which acts as the electronic acceptor. It was shown that the delocalization of the HOMO-LUMO distribution became more apparent as the conjugation length was increased. In the case of **3a-c**, where the phenyl-SF_5 group is directly attached to the triphenylamine donor, some HOMO lobes could be found on the phenyl-SF_5 group. When the π-linker was incorporated into the molecular systems, either a phenyl or a thiophene group, the electronic communication between the triphenylamine donor and the SF_5 acceptor was likely weakened. Less HOMO and LUMO characteristic were found on the triphenylamine and the phenyl-SF_5, respectively, which indicates the formation of better D-A systems. The incorporation of the TCNE and TCNQ moieties into the systems dramatically changed the molecular orbital distributions, as they are stronger electronic acceptors compared to the SF_5 group, which pull the LUMO distribution away from the SF_5 region.[13]

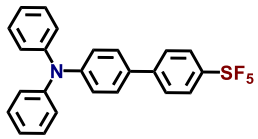

3a

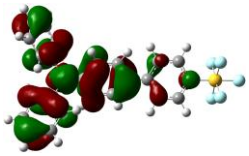

HOMO

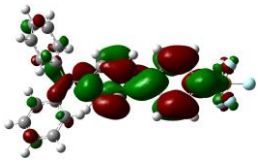

LUMO

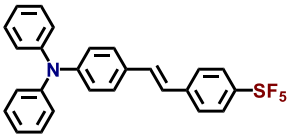

3b

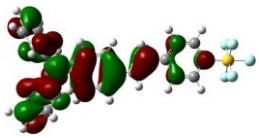

HOMO

LUMO

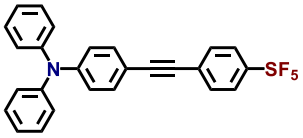

3c

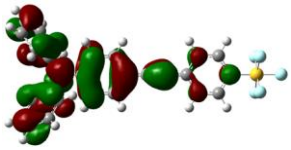

HOMO

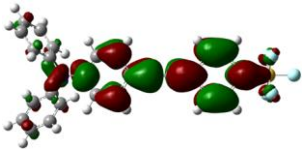

LUMO

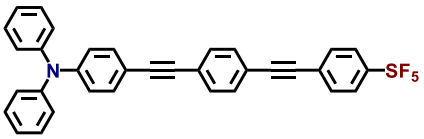

3d

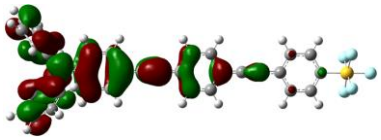

HOMO

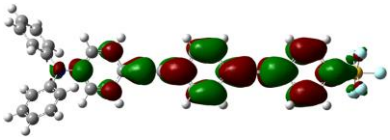

LUMO

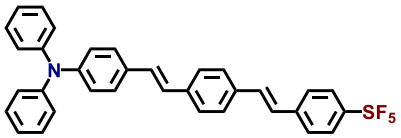

3e

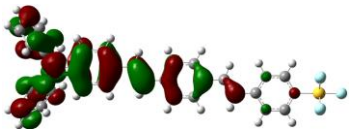

HOMO

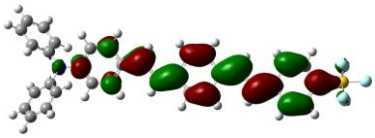

LUMO

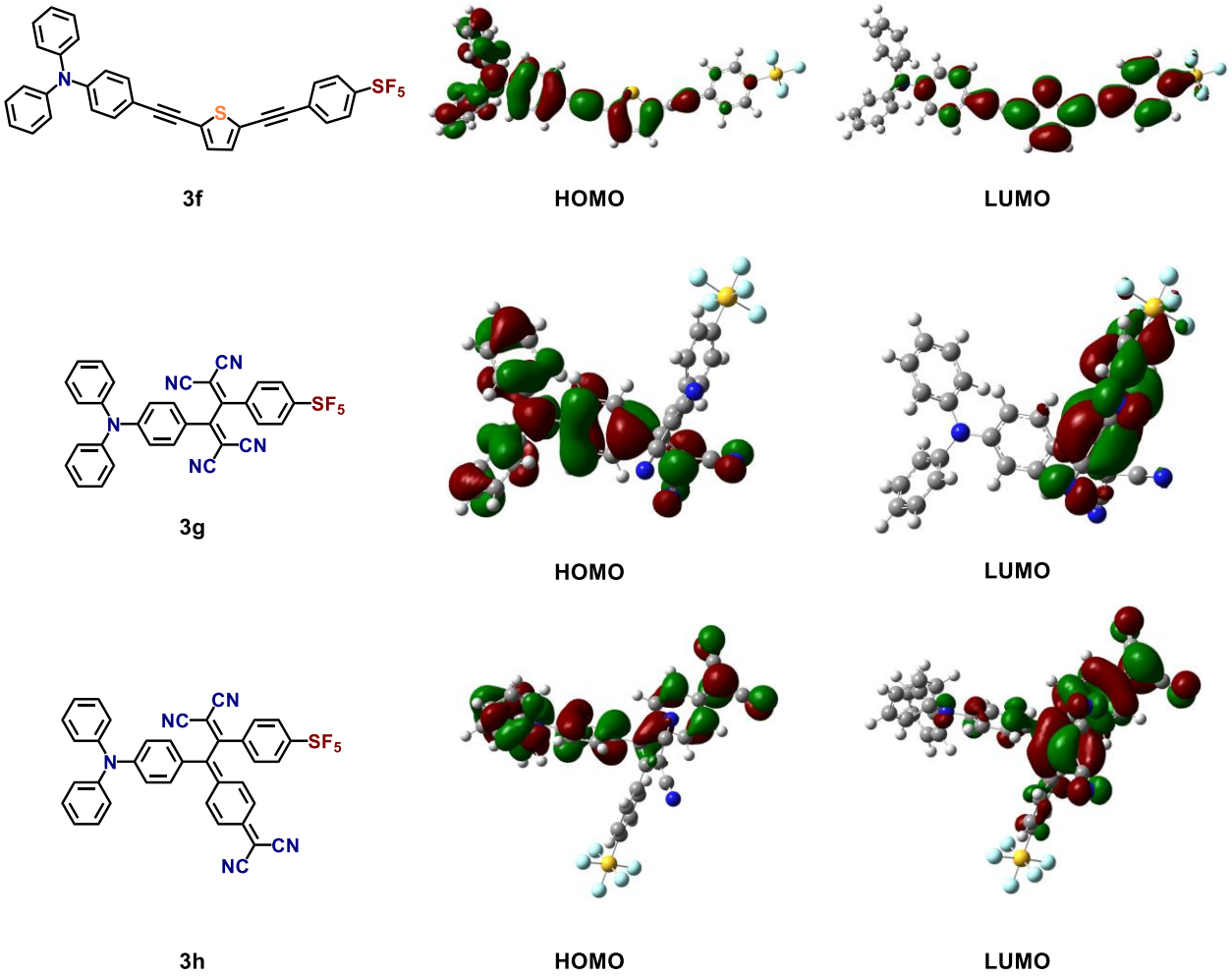

Figure 3.4. The structures of compounds **3a-h**, and their frontier molecular orbital distributions at the B3LYP/6-31G(d) level of theory.

The energy levels of compounds **3a-f** were also calculated at the same level of theory, and a trend of narrowing HOMO-LUMO energy gaps was observed going from compound **3a** to **f**. When comparing compounds **3e** and **3f**, compound **3f** showed a lowering of both the HOMO and LUMO energy levels relative to **3e**, thus resulted in a slightly narrower HOMO-LUMO energy gap as compared to **3e** (**Figure 3.5**). The introduction of the electron-deficient TCNE and TCNQ moieties considerably lowered the HOMO and LUMO energy levels and brought narrowing of the HOMO-LUMO energy gap. Compound **3h** showed the HOMO level at -5.92 eV and the LUMO level at -3.40 eV, which is drastically lowered as compared to its precursor compound **3c**. Compound **3g** contains a stronger electronic acceptor TCNQ compared to TCNE in compound **3h**, and the resulting HOMO and LUMO energy levels were lowered to -5.74 eV and -3.87 eV, respectively (**Figure 4.5**). The UV-vis absorption profiles of the SF_5-containing dyes from the TD-DFT calculations showed good agreement between the theoretical and experimental data. The TD-DFT calculation also revealed that the HOMO to LUMO electron transition was associated with

the largest oscillator strength, which suggests that the major charge-transfer effect within of the SF_5-containing molecules was the HOMO to LUMO transition.

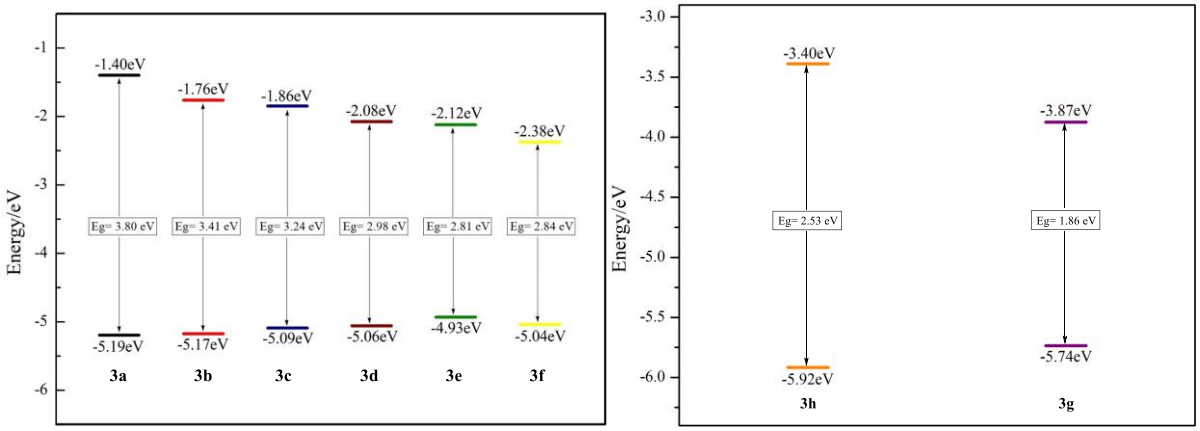

Figure 3.5. Left: The HOMO-LUMO energy levels of compound **3a-f**. Right: The HOMO-LUMO energy levels of compound **3h-f** at the B3LYP/6-31G(d) level of theory.

3.3 Conclusion

The electron-deficient SF_5 group has been incorporated and demonstrated as an effective electron acceptor in the D-A systems. From the DFT calculations, the HOMO and LUMO coefficients are found to be localized on the electron-rich triphenylamine group and the electron-deficient phenyl-SF_5 groups, respectively. Therefore, a series of D-A π-conjugated SF_5-containing molecules have been designed. The TD-DFT calculations revealed HOMO to LUMO electronic excitations as the dominant transition type in these SF_5 compounds, indicating strong intermolecular charge-transfer interactions. Compounds **3**e and **3f** were further studied by solution-state UV-vis absorption and fluorescence emission experiments, whereby large Stokes shifts were observed in both compounds, which are promising for bioimaging applications. Single-crystal X-ray diffraction studies elucidated the crystal packing mode of the two compounds in the solid-state, and multiple strong intermolecular interactions were observed in compounds **3e** and **3f**, including C-H$\cdots\pi$ and $\pi\cdots\pi$ interactions. In addition, the SF_5 groups participated in C-H$\cdots$F and F$\cdots\pi$ interactions, which further assisted in the supramolecular assemblies in the solid-state. The heteroatom interactions displayed herein may be useful as a tool for crystal engineering. Compound **3e** crystallized in an organized herringbone packing motif with edge-to-face interactions, which is absent in the crystal structure of compound **3f**. The difference between the supramolecular packing mode of the two compounds potentially led to their distinctive solid-state absorptions and emissions. As a result of the current study, we concluded that the SF_5 group can behave as an excellent electron acceptor in D-A systems. By varying the π-linker between the TPA and SF_5 moieties, we were able to successfully tune the absorption and emission properties of the molecules. We hope that the current study can serve as a rudimentary understanding on SF_5 in the context of materials chemistry, and more organic optoelectronic materials can be designed using

the SF_5 functional group. Our group has also successfully reported these results in the *Journal of Organic Chemistry*.[12]

3.4 Experimental Section

Synthesis of 2. The compound was synthesized according to the reported procedure with minor modifications.[13] To a deoxygenated mixture of **1** (1.00 g, 3.00 mmol), trimethylsilylacetylene (0.190 g, 3.72 mmol), and $Pd(PPh_3)_4$ (0.029 g, 2.5 mol%) in 10 mL of toluene and 5 mL of *i*Pr_2NH, was added CuI (0.005 g, 2.5 mol%), and the reaction mixture was stirred under an atmosphere of N_2 at 80 ℃ for 12 hours. The mixture was filtered through a pad of celite and poured into deionized H_2O and extracted with DCM. The organic layer was dried over Na_2SO_4, and the solvent was evaporated in vacuo. The crude was purified by silica gel column chromatography using hexanes and DCM (5:1 v/v) as eluent to give **2** as a yellow oil in 91% yield. ^{1}H NMR (400 MHz, $CDCl_3$): δ 7.29 (d, 2H), 7.24 (t, 4H), 7.06 (d, 4H), 7.03 (t, 2H), 6.95 (d, 2H), 0.24 (s, 9H).

Synthesis of 3. The compound was synthesized according to the reported procedure with minor modifications.[13] To a deoxygenated mixture of **2** (1.00 g, 2.93 mmol), 10 mL of THF and 10 mL of MeOH was added K_2CO_3 (2.02 g, 14.6 mmol), and the mixture was stirred at room temperature for 4 hours under an atmosphere of N_2 and then poured into a saturated solution of aqueous NH_4Cl. The product was extracted by DCM and dried over Na_2SO_4 and purified by silica gel column chromatography using hexanes and DCM (5:1 v/v) as eluent to give **3** as an off-white solid (0.75 g, 95% yield). ^{1}H NMR (400 MHz, $CDCl_3$): δ 7.35-7.25 (m, 6H), 7.12-7.04 (m, 6H), 6.97 (d, 2H), 3.02 (s, 1H).

Synthesis of 4. The compound was synthesized following a reported procedure.[14] To 125 mL of AcOH was added thiophene (5.25g, 62.4 mmol) and NBS (22.2 g, 125 mmol), and the reaction mixture was stirred at 50 ℃ for 12 hours. After cooling to room temperature, the mixture was poured into 125 mL of cold saturated NaOH solution and extracted with hexanes. The crude was purified by silica gel column chromatography using pure hexanes as eluent to give **4** as a colorless oil (11.0g, 74%). ^{1}H NMR (400 MHz, $CDCl_3$): δ 6.82 (s, 2H).

Synthesis of 5. The compound was synthesized following a reported procedure.[15] To a deoxygenated mixture of *i*Pr_2NH (55 mL), **4** (2.15 g, 8.87 mmol), trimethylsilylacetylene (0.870 g, 8.87 mmol), $Pd[(PPh_3)_2]Cl_2$ (0.15 g, 25 mol%) was added CuI (0.041g, 25 mol%), and the mixture was stirred under an atmosphere of N_2 for 5 hours. The mixture was filtered through a pad of celite and poured into deionized H_2O and extracted with DCM. The organic layer was dried over anhydrous Na_2SO_4, and the solvent was evaporated in vacuo. The crude product was purified by silica gel column chromatography using hexanes and DCM (5:1 v/v) as eluent to give **2** (1.01g, 45% yield). ^{1}H NMR (400 MHz, $CDCl_3$): δ 7.29 (d, 2H),

7.24 (t, 4H), 7.06 (d, 4H), 7.03 (t, 2H), 6.95 (d, 2H), 0.24 (s, 9H). ^{1}H NMR (400 MHz, $CDCl_3$): δ 6.95 (d, 1H), 6.88 (d, 1H), 0.23 (s, 9H).

Synthesis of 6. To a deoxygenated mixture of **4** (0.230 g, 1.11 mmol), **5** (0.240 g, 1.11 mmol), and $Pd(PPh_3)_4$ (0.0560 g, 5 mol%) in 10 mL of toluene and 10 mL of *i*Pr_2NH, was added CuI (0.028 g, 5 mol%), and the reaction mixture was stirred under an atmosphere of N_2 at 80 ℃ for 12 hours. The mixture was filtered through a pad of celite and poured into deionized H_2O and extracted with DCM. The organic layer was dried over anhydrous Na_2SO_4, and the solvent was evaporated in vacuo. The crude product was purified by silica gel column chromatography using hexanes and DCM (8:2 v/v) as eluent to give **6** as a yellow solid in 50% yield. ^{1}H NMR (400 MHz, $CDCl_3$): δ 7.33 (m, 2H), 7.27 (t, 4H), 7.08 (m, 8H), 6.98 (d, 2H), 0.25 (s, 9H). ^{13}C NMR (75.4 MHz, $CDCl_3$): δ 148.32, 147.05, 132.48, 131.07, 129.46, 125.17, 123.77, 121.95, 115.04, 99.90, 97.13, 94.37, 81.49, 34.71, 31.62, 25.32, 22.69, 20.75, 14.17, 0.14.

Synthesis of 7. To a deoxygenated mixture of **6** (0.20 g, 0.45 mmol), THF (10 mL) and MeOH (5 mL) was added K_2CO_3 (0.310 g, 2.23 mmol), and the mixture was stirred at room temperature for 4 hours under an atmosphere of N_2 and then poured into a saturated solution of aqueous NH_4Cl. The product was extracted with DCM and dried over anhydrous Na_2SO_4 and purified by silica gel column chromatography using hexanes and DCM (5:1 v/v) as eluent to give **7** as a dark yellow solid (0.18 g, 95% yield). ^{1}H NMR (400 MHz, acetone-d_6) δ 7.41-7.32 (m, 6H), 7.26-7.25 (d, 1H), 7.20-7.19 (d 1H), 7.15-7.10 (m, 6H), 6.97-6.94 (m, 2H), 4.08 (s, 1H). HRMS (EI) *m/z* cald for $C_{26}H_{17}NS$ 375.1082; found 375.1080.

Synthesis of 3f. To a 1:1 mixture of deoxygenated toluene/*i*Pr_2NH (20 mL) was charged **7** (102 mg, 0.270 mmol), 4-bromophenylsulfurpentafluoride (80.0 mg, 0.280 mmol), $Pd(PPh_3)_4$ (16 mg, 5 mol%), and CuI (1.3 mg, 5 mol%), and the reaction mixture was stirred under nitrogen atmosphere at 80˚C for 12 hours. The cooled mixture was diluted with DCM and filtered through a pad of celite, and the solvent was removed under reduced pressure. The crude product was purified by silica gel column chromatography using hexanes and DCM (9:1 v/v) as eluent to give compound **3f** as an orange solid (0.13 mg, 80% yield). Mp: 178.5−179.5 °C. ^{1}H NMR (400 MHz, acetone-d_6) δ 7.96-7.93 (d, 2H), 7.79-7.76 (d, 2H), 7.43-7.28 (m, 8H), 7.16-7.12 (m, 6H), 6.98-6.96 (d, 2H). ^{13}C NMR (75.4 MHz, $CDCl_3$) δ 153.1, 148.4, 147.0, 132.8, 132.5, 131.4, 131.34, 129.4, 126.4, 126.38, 126.09, 125.2, 123.8, 122.78, 121.8, 114.7, 95.2, 91.8, 85.5, 81.3. ^{19}F NMR (282 MHz, $CDCl_3$): δ 83.75, 62.09. HRMS (EI) *m/z* cald for $C_{32}H_{20}F_5NS_2$: 577.0957; found 577.0958.

Synthesis of 12. The compound was synthesized according to the reported procedure with minor modifications.[16] To a suspension of methyl triphenylphosphonium iodide in 20 mL of anhydrous THF was added *t*-BuOK (0.930 g, 8.23 mmol) at 0 ℃ and the suspension was slowly brought to room temperature over a period of 30 min. Subsequently, **11** (1.50 g, 5.49 mmol) was added to the suspension, and it was

stirred at room temperature for 12 hours under an atmosphere of N_2. The reaction was quenched by H_2O and extracted with DCM and dried over anhydrous Na_2SO_4. After the evaporation of the solvent, the crude was purified by silica gel column chromatography using hexanes and DCM (8:2 v/v) to afford **12** as a white solid (1.0 g, 67% yield). ^{1}H NMR (400 MHz, DMSO-*d*): δ 7.35-7.33 (dd, 2H), 7.28-7.24 (m, 4H), 7.03-6.96 (m, 6H), 6.96-6.88 (m, 2H), 6.62 (dd, 1H), 5.65 (dd, 1H), 5.12 (dd, 1H).

Synthesis of 13. To 8 mL of deoxygenated DMF was added **12** (0.34 g, 1.26 mmol), 4-bromobenzaldehyde (0.230 g, 1.26 mmol), K_2CO_3 (1.71 g, 12.6 mmol), tetrabutylammonium bromide (0.810 g, 2.52 mmol), and $Pd(OAc)_2$ (0.0850 g, 3 mol%), and the reaction mixture was heated at 120 ℃ under an atmosphere of N_2 for 12 hours. After dilution with diethyl ether, the mixture was filtered through a pad of celite, washed with H_2O, and dried over anhydrous Na_2SO_4. The crude was purified by silica gel column chromatography using hexanes and DCM (9:1 v/v) as eluent to give compound **13** as a yellow solid (0.41 g, 87%). ^{1}H NMR (400 MHz, $CDCl_3$): δ 9.69 (s, 1H), 7.83 (d, 2H), 7.60 (d, 2H), 7.39 (d, 2H), 7.28-6.98 (m, 16H).

Synthesis of 14. To a suspension of methyl triphenylphosphonium iodide in 12 mL of anhydrous THF was added *t*-BuOK (0.180 g, 1.63 mmol) at 0 ℃ and the suspension was slowly brought to room temperature over a period of 30 min. Subsequently, **13** (0.410 g, 1.08 mmol) was added to the suspension, and it was stirred at room temperature for 12 hours under an atmosphere of N_2. The reaction was quenched by H_2O and extracted by DCM and dried over anhydrous Na_2SO_4. After the evaporation of the solvent, the crude was purified by silica gel column chromatography using hexanes and DCM (8:2 v/v) to afford **14** as a yellow solid (0.20 g, 50% yield). ^{1}H NMR (400 MHz, $CDCl_3$): δ 7.45-7.36 (m, 5H), 7.26-7.22 (m, 5H), 7.11-6.94 (m, 8H), 6.69 (dd, 1H), 5.74 (d, 1H), 5.24 (dd, 1H).

Synthesis of 3e. To 5 mL of deoxygenated DMF was added **14** (0.086 g, 0.23 mmol), 4-bromophenylsulfur pentafluoride (0.065 g, 0.23 mmol), K_2CO_3 (0.320 g, 2.30 mmol), tetrabutylammonium bromide (0.15 g, 0.46 mmol), and $Pd(OAc)_2$ (0.015 g, 3 mol%), and the reaction mixture was heated at 120 ℃ under an atmosphere of N_2 for 12 hours. After a dilution with DCM, the mixture was filtered through a pad of celite, washed with H_2O, and dried over anhydrous Na_2SO_4. The crude was purified by silica gel column chromatography using hexanes and DCM (9:1 v/v) as eluent to give compound **3e** as a yellow solid (0.090 g, 68%). Mp: 232.0−233.0 °C. ^{1}H NMR (400 MHz, acetone-d_6): δ 7.88−7.81 (m, 4H), 7.67−7.61 (m, 4H), 7.54 (d, 2H, J = 8 Hz), 7.46 (d, 1H, J = 16 Hz), 7.38−7.27 (m, 6H), 7.17 (d, 1H, J = 16 Hz), 7.10−7.06 (m, 6H), 7.02 (d, 2H). ^{13}C NMR (75.4 MHz, $CDCl_3$): δ 152.5, 147.6, 147.5, 140.7, 137.9, 135.3, 131.6, 131.2, 129.3, 128.7, 127.4, 127.2, 126.7, 126.4, 126.3, 126.25, 125.9, 124.6, 123.4, 123.1. ^{19}F NMR (282 MHz, CDCl3): δ 85.05, 63.1 (d, 4F). HRMS (EI-magnetic sector) m/z: [M]+ calcd for C34H26F5NS 575.1706, found, 575.1689.

3.5 References

(1) Wang, C.; Dong, H.; Hu, W.; Liu, Y.; Zhu, D. *Chem. Rev*. **2012**, *112*, 2208–2267.

(2) Lin, L. Y.; Chen, Y. H.; Huang, Z. Y.; Lin, H. W.; Chou, S. H.; Lin, F.; Chen, C. W.; Liu, Y. H.; Wong, K. T. *J. Am. Chem. Soc.* **2011**, *133*, 15822–15825.

(3) Leung, L. M.; Lo, W. Y.; So, S. K.; Lee, K. M.; Choi, W. K. *J. Am. Chem. Soc.* **2000**, *122*, 5640–5641.

(4) Zhang, Q. T.; Tour, J. M. *J. Am. Chem. Soc.* **1998**, *120*, 5355-5362.

(5) Veldman, D.; Meskers, S. C. J.; Janssen, R. A. J. *Adv. Funct. Mater.* **2009**, *19*, 1939–1948.

(6) Zhao, G. J.; Chen, R. K.; Sun, M. T.; Liu, J. Y.; Li, G. Y.; Gao, Y. L.; Han, K. L.; Yang, X. C.; Sun, L. *Chem. Eur. J.* **2008**, *14*, 6935–6947.

(7) Beaujuge, P. M.; Amb, C. M.; Reynolds, J. R. *Acc. Chem. Res.* **2010**, *43*, 1396–1407.

(8) van Mullekom, H. A. M.; Vekemans, J. A. J. M.; Meijer, E. W. *Chem. Eur. J.* **1998**, *4*, 1235–1243.

(9) Golf, H. R. A.; Reissig, H. U.; Wiehe, A. *J. Org. Chem.* **2015**, *80*, 5133–5143.

(10) Gudeika, D.; Grazulevicius, J. V.; Volyniuk, D.; Juska, G.; Jankauskas, V.; Sini, G. *J. Phys. Chem. C* **2015**, *119*, 28335–28346.

(11) Guo, Z.; Park, S.; Yoon, J.; Shin, I. *Chem. Soc. Rev.* **2014**, *43*, 16–29.

(12) Gautam, P.; Yu, C. P.; Zhang, G.; Hillier, V. E.; Chan, J. M. W. *J. Org. Chem.* **2017**, *82*, 11008–11020.

(13) Kivala, M.; Diederich, F. *Acc. Chem. Res.* **2009**, *42*, 235–248.

(14) Xu, F.; Peng, L.; Orita, A.; Otera, J. *Org. Lett.* **2012**, *14*, 3970–3973.

(15) Yu, J.; Shen, T. L.; Weng, W. H.; Huang, Y. C.; Huang, C. I.; Su, W. F.; Rwei, S. P.; Ho, K. C.; Wang, L. *Adv. Energy Mater.* **2012**, *2*, 245–252.

(16) Huang, C.; Zhen, C. G.; Siew, P. S.; Kian, P. L.; Chen, Z. K. *Org. Lett.* **2005**, *7*, 391–394.

(17) Harlé, J. B.; Mine, S.; Kamegawa, T.; Nguyen, V. T.; Maeda, T.; Nakazumi, H.; Fujiwara, H. *J. Phys. Chem. C* **2017**, *121*, 15049–15062.

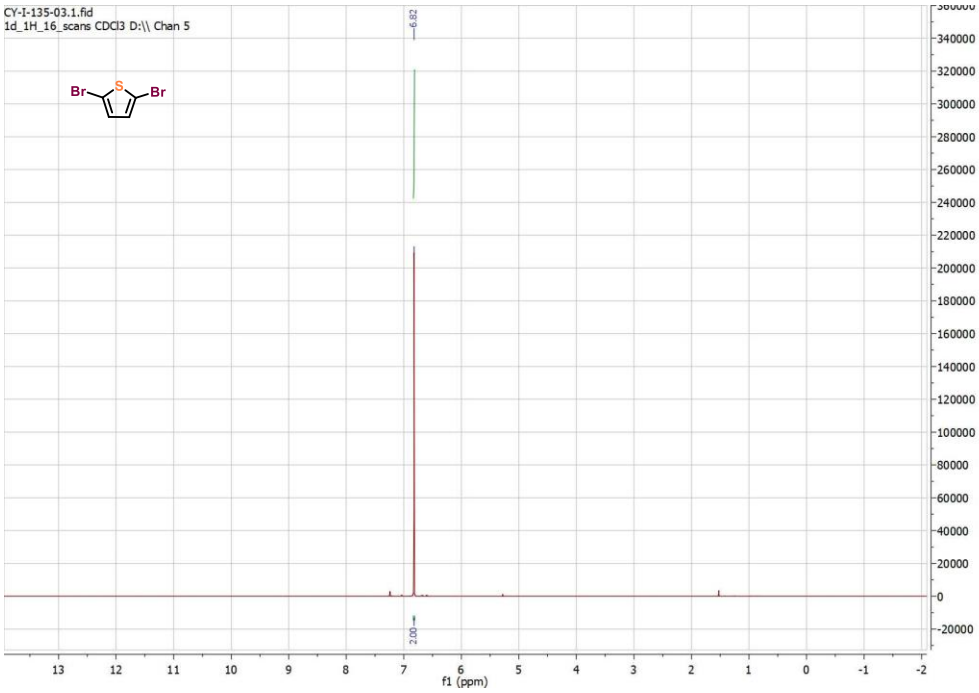

Figure 3.6. ^{1}H NMR of compound 4.

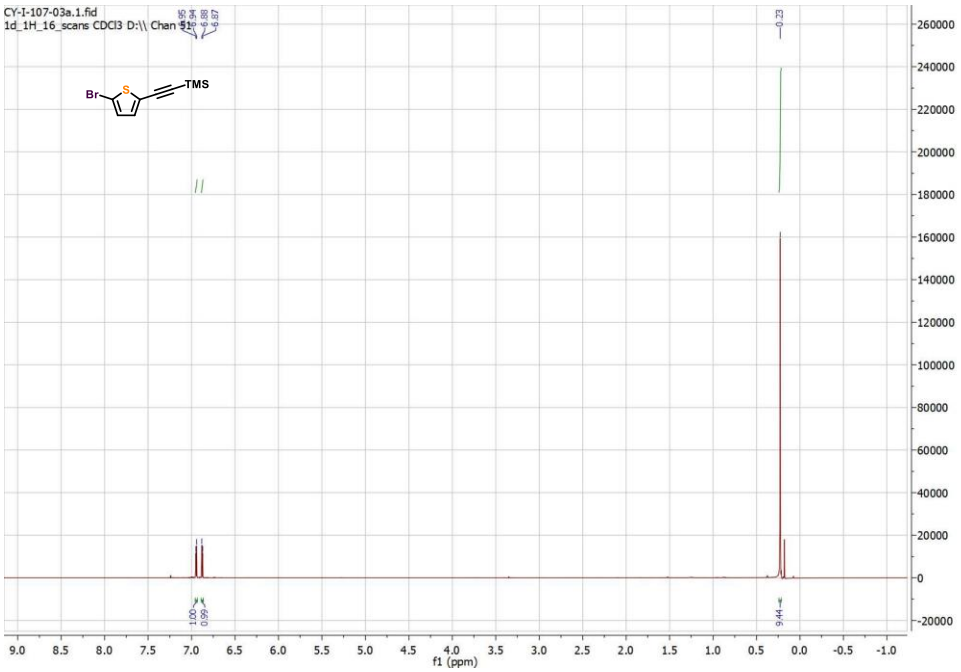

Figure 3.7. ^{1}H NMR of compound 5.

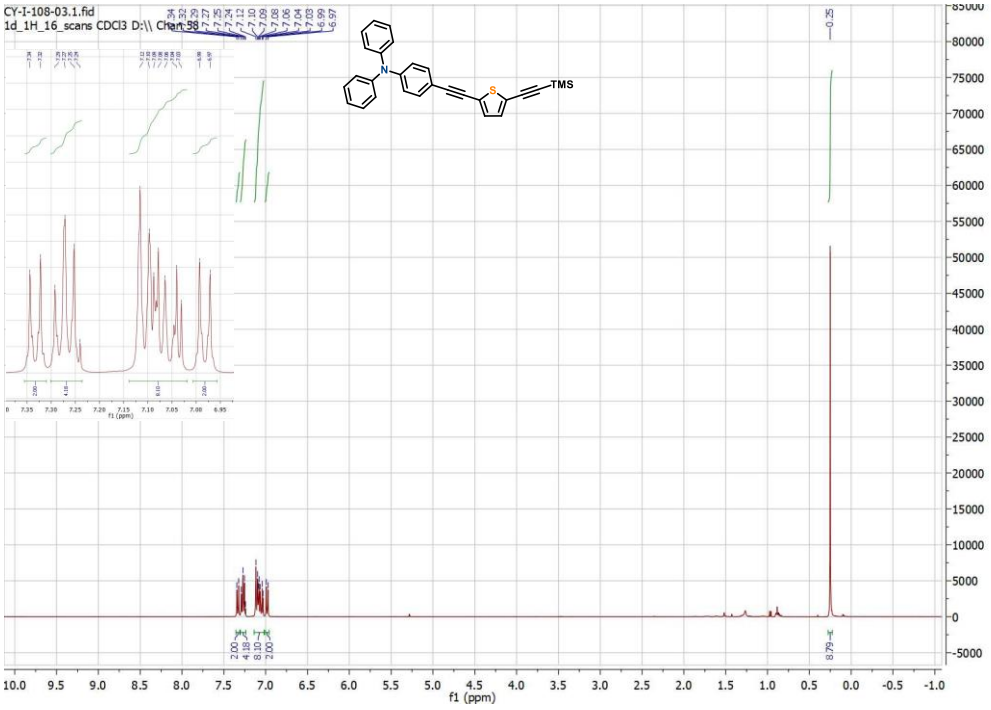

Figure 3.8. ^{1}H NMR of compound 6.

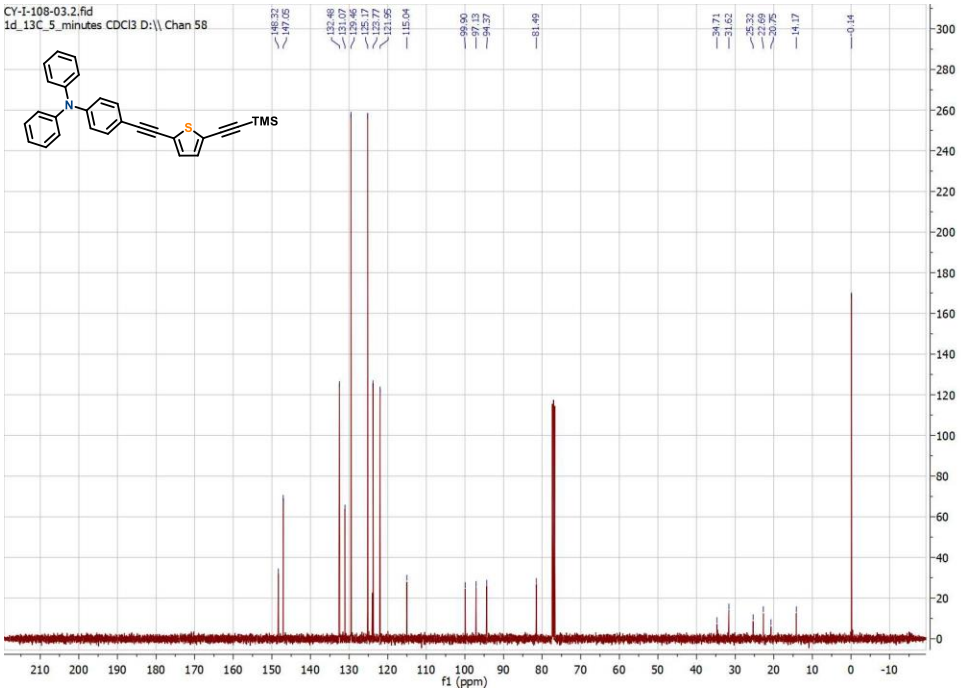

Figure 3.9. ^{13}C NMR of compound 6.

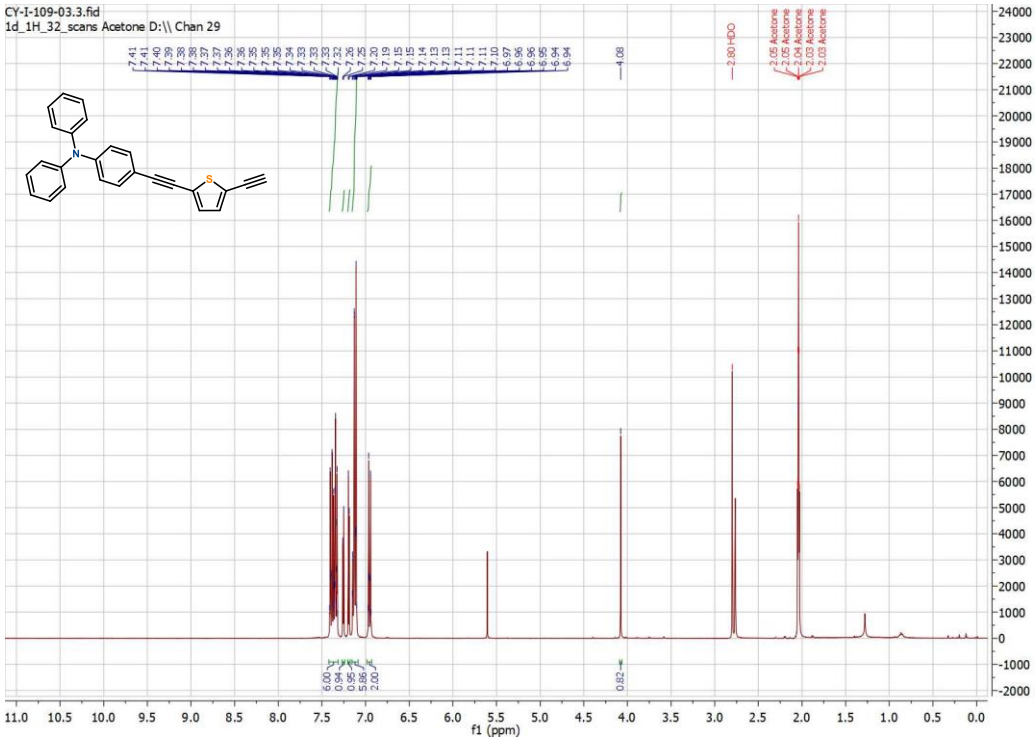

Figure 3.10. ^{1}H NMR of compound 7.

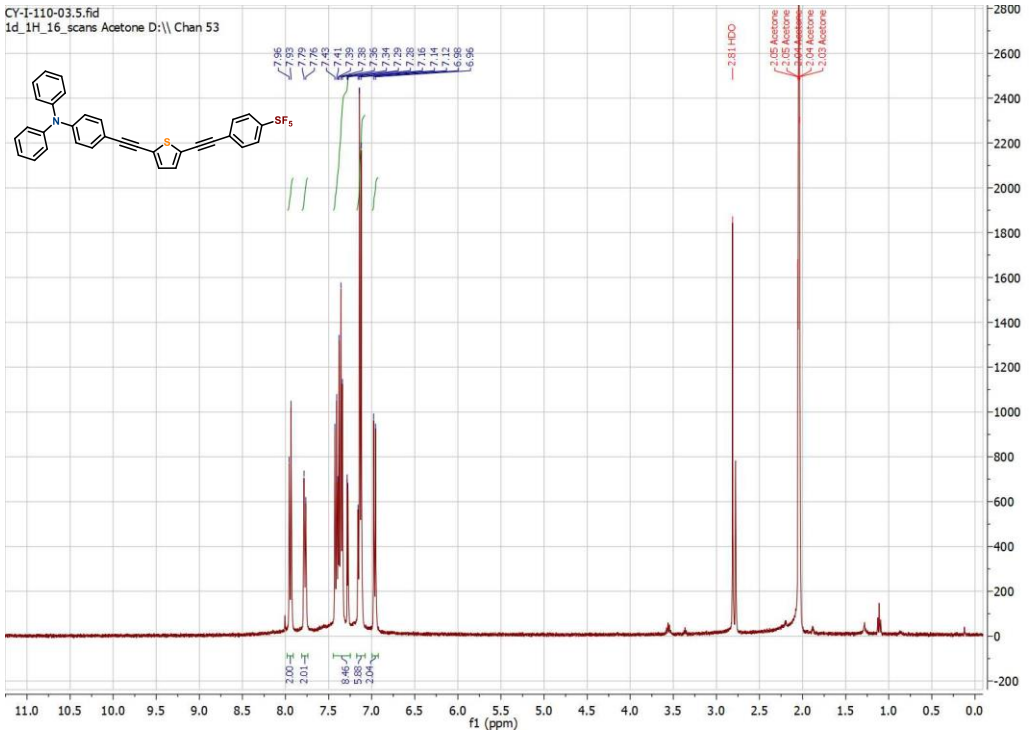

Figure 3.11. ^{13}C NMR of compound 7.

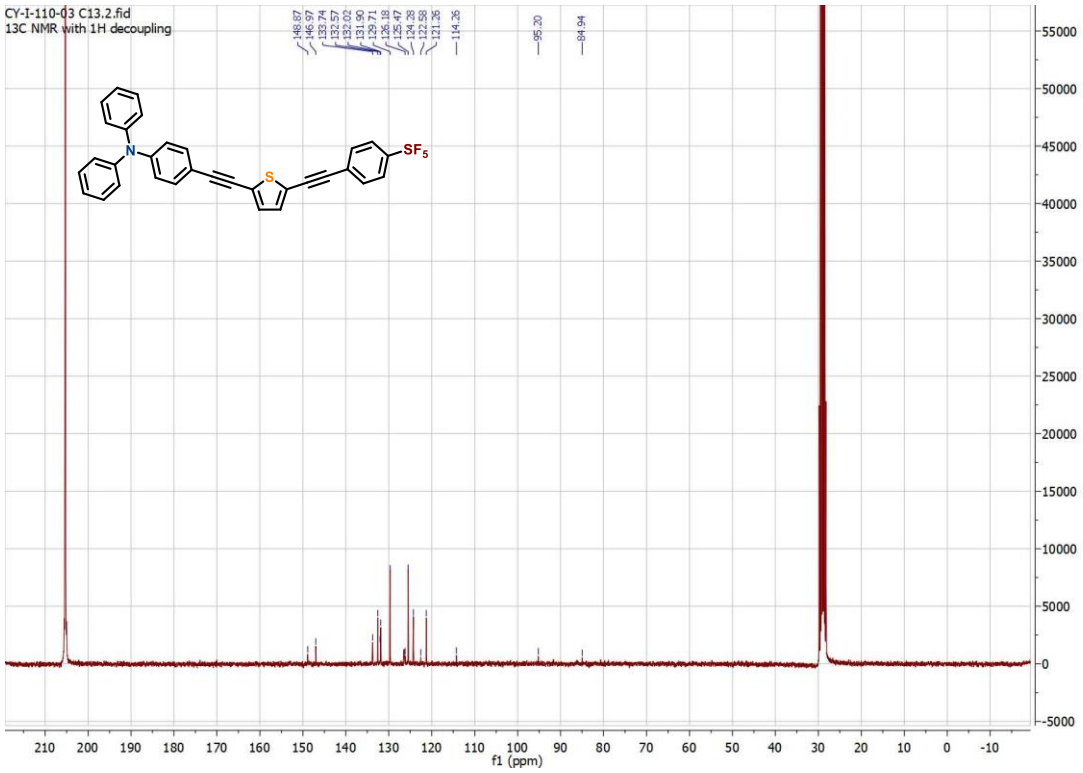

Figure 3.12. ^{1}H NMR of compound 3f.

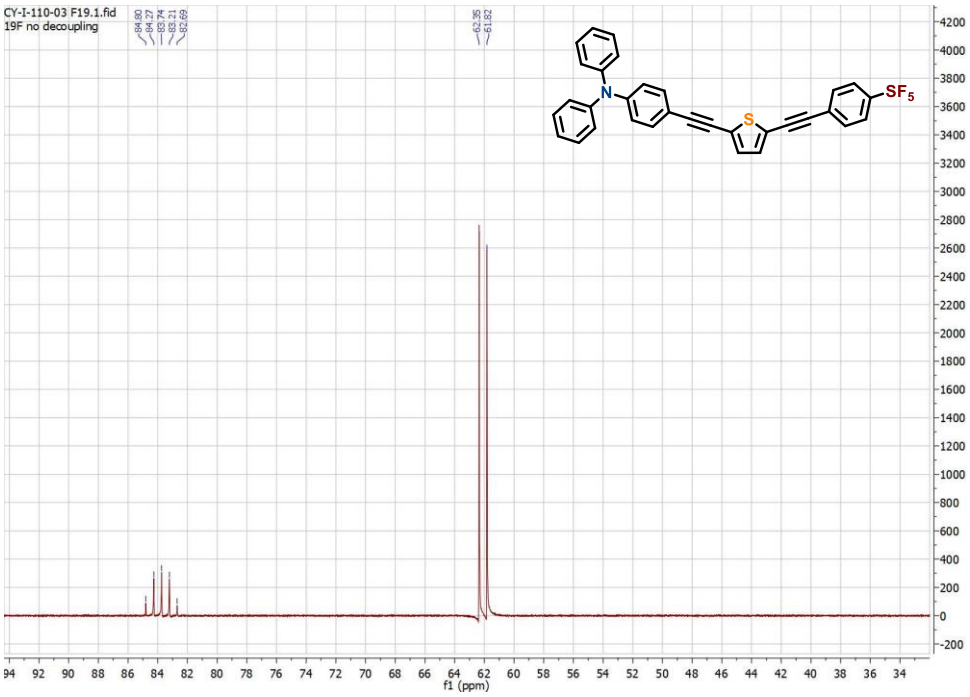

Figure 3.13. ^{13}C NMR of compound 3f.

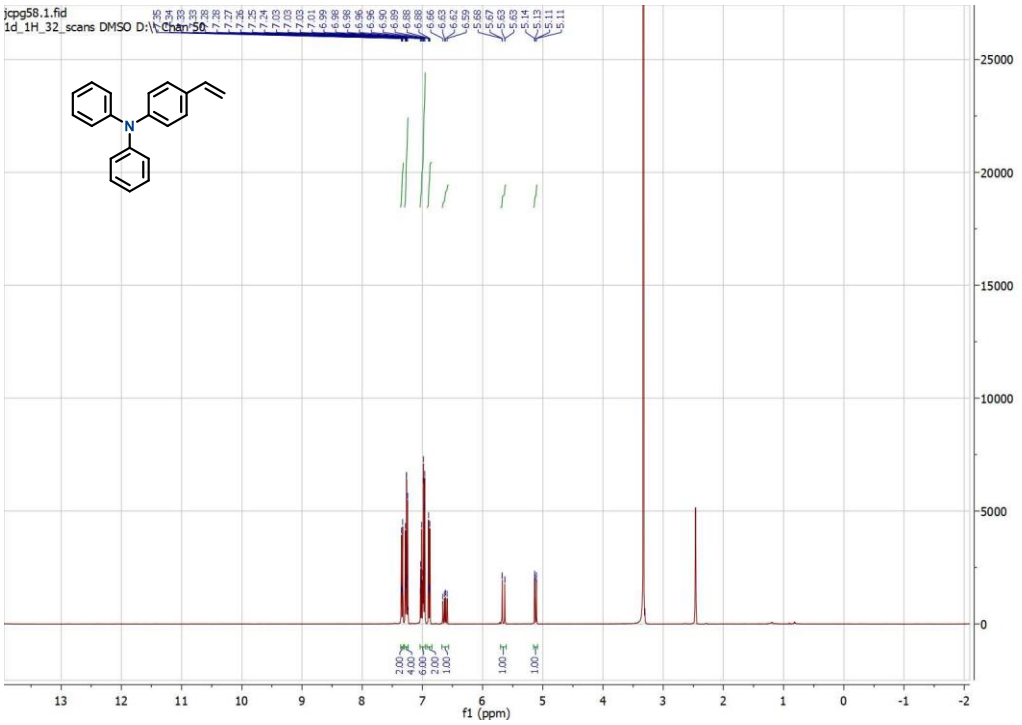

Figure 3.14. ^{1}H NMR of compound 12.

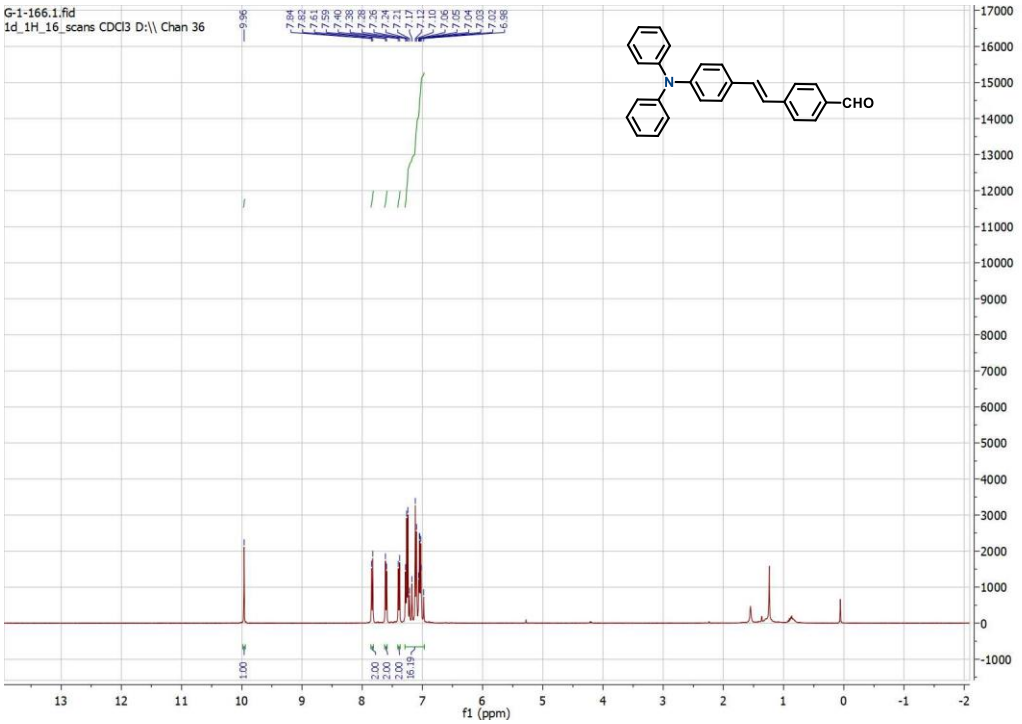

Figure 3.15. ^{1}H NMR of compound 13.

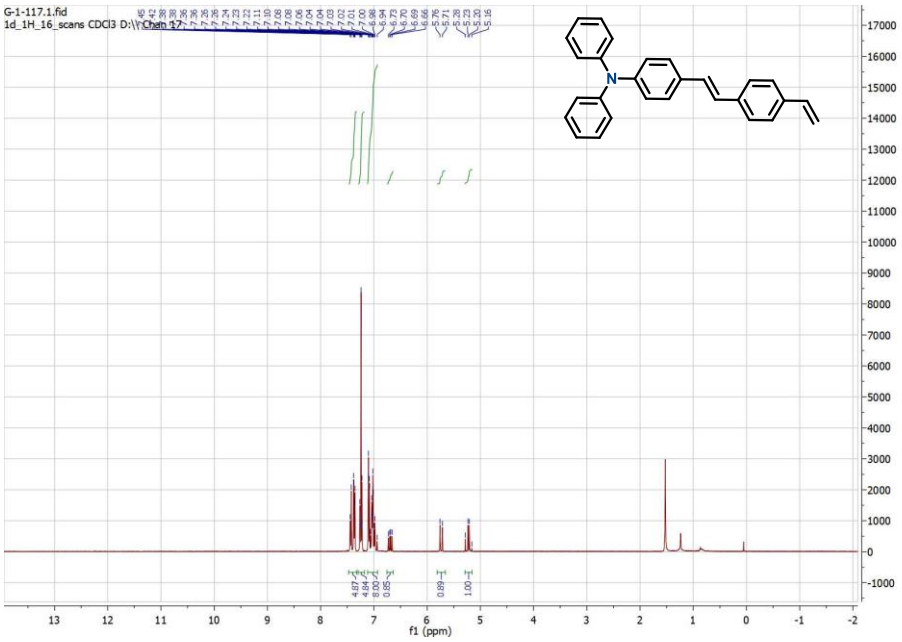

Figure 3.16. ^{1}H NMR of compound 14.

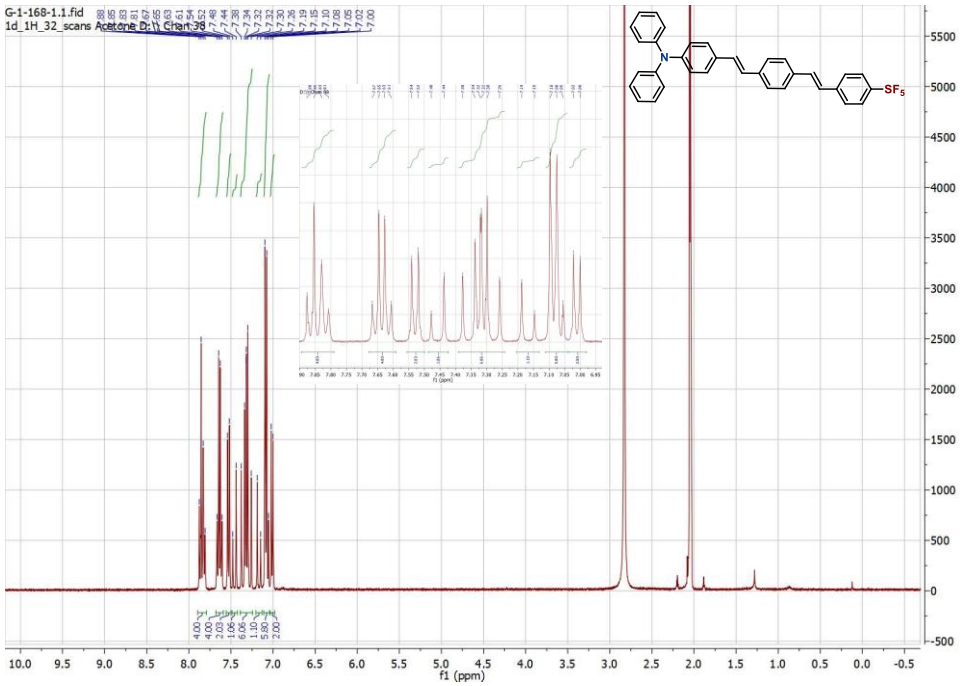

Figure 3.17. ^{1}H NMR of compound 3e.

Chapter 4. Pyrazine-Containing π-Conjugated Donor-Acceptor Polymers

4.1 Introduction

The π-conjugated D-A polymer systems have been a subject of intense study in the application of OFETs, OPVs, and OLEDs, due to their narrow HOMO-LUMO energy gaps.[1–3] Poly(pyridylvinylene phenylenevinylene) (PPyVPV) in particular, has attracted a considerable amount of attention due to its promising application in conductive and OLED materials.[4] PPyVPV can be considered as a π-conjugated D-A system, with the pyridine unit acting as an acceptor and the phenyl moiety acts the donor, although it is considered a weak D-A system due to the weakly electron-withdrawing nature of the pyridyl group.[5] However, the electronic property of the pyridyl unit can be readily tuned through protonation and quaternization of the nitrogen atom, which generates the more electron-deficient pyridinium unit, and the resulting poly(pyridiniumvinylenephenylenevinylene) (PPymVPV) shows a dramatic red-shift in optical absorption and improvement in electrical conductivity due to the narrowing of the HOMO-LUMO energy gap.[4]

The pyrazine group, on the other hand, is more electron deficient as compared to pyridine, and the incorporation of such a group in the poly(*p*-phenylenevinylene) (PPV) was first done by Galvin and co-workers, and the pyrazine-containing PPV showed good photophysical properties and OLED performance.[6] In 2009, Kertesz and co-workers reported a theoretical study on pyrazine-based polymers and showed that the electron-withdrawing nature of pyrazine and its ability to participate in inter- and intramolecular hydrogen bonding interactions could considerably narrow the HOMO-LUMO energy gap of the polymers.[7] Besides the direct incorporation of the pyrazine in a polymer, it can also be installed on units such as thiophene to make thieno[3,4-b]pyrazines units to tune the electronic properties of the polymer.[8] However, the overall number of studies of pyrazine-based materials has been scarce potentially due to the low reactivity of the pyrazine group,[9] and to the best of our knowledge, no study has reported on the direct co-polymerization of pyrazine-based polymers, which motivated our current study on pyrazine-based π-conjugated D-A polymer.

In this study, we synthesized a pyrazine-containing poly(*p*-arylenevinylene) (PAV) copolymer via metal-free Knoevenagel-type and aldol-type condensation reactions to avoid transition-metal impurities which could potentially have undesirable effects on the optoelectronic properties of the polymer. We also investigated the co-polymerization via Heck polycondensations. Protonation and quaternization of the pyrazine units in the PAV were attempted, and the photophysical properties upon the post-synthetic modification were studied.

4.2 Results and Discussion

4.21 Synthesis

The commercially available hydroquinone was treated with KOH and 1-bromododecane in ethanol and purified by recrystallization to give compound **1** as a fluffy white solid in 93% yield. The long dodecyl chain was employed to improve the solubility of the polymer. Compound **1** was then iodinated by iodine and periodic acid in methanol, the crude product was recrystallized in methanol to give compound **2** in excellent yield. Compound **2** was treated with *t*-BuLi in anhydrous THF at -78 ˚C, and anhydrous DMF was subsequently added to the reaction mixture to afford the dialdehyde **3**. We first investigated the polymerization of **P1** via a Knoevenagel-type condensation between compound **3** and the commercially available 2,5-dimethylpyrazine, anhydrous DMF was chosen as the solvent due to the required polarity for stabilizing the ionic transition state (**Scheme 4.1a**). The metal-free synthesis of **P1** allows the study of the intrinsic optoelectronic properties of the compound without the presence of metal catalyst impurities. The Knoevenagel polycondensation afforded **P1** in 28% yield. The synthesis of the desired polymer was investigated via another metal-free aldol-type polycondensation. The monomer **3** and the commercially available 2,5-dimethylpyrazine were reacted in acetic anhydride and the polymerization afforded **P2** in 38% yield (**Scheme 4.1b**).

Table 4.1. The polymerization and photophysical results of **P1** and **P2**.

Polymer	Yield	M_n (g/mol)	DP	Đ	λ_{max} (nm)	λ_{onset} (nm)	λ_{em} (nm)
P1	28%	5912	10	1.27	425	528	516
P2	38%	5910	10	1.40	425	528	516

Both **P1** and **P2** resulted in low number-average molecular weights with ten repeat units. To increase the chain length, we decided to employ the Heck polycondensation method since the Heck method was used to synthesize high molecular weight pyridine and pyrazine-containing polymers in the past.[4,6] Monomer **4** was synthesized from compound **3** through a Wittig reaction in 80% yield, and compound **4** was reacted with the commercially available 2,5-dibromopyrazine using different ligands in the Heck polymerization. Tetrakis(triphenylphosphine)palladium was first tested for the Heck reaction, and the reaction was run under a nitrogen atmosphere for 72 hours with no resulting polymers. A more reactive P(*o*-tol)$_3$ ligand for subsequently tested for the reaction, as it provides the steric bulk that increases the rate of the transmetallation step in the catalytic cycle. However, no polymer was afforded using the ligand. Other reactive ligands such as XPhos and SPhos have been used (**Scheme 4.1c**), but all Heck

polycondensation reactions failed to produce the desired polymer, possibly due to the low reactivity of the 2,5-dibromopyrazine towards Pd-catalyzed reactions. This finding can be supported by the previous work of Langer and coworkers on Heck cross-coupling with pyrazine units, where partial hydrogenation was observed in the product.[9] The exact reason for the low reactivity of pyrazine moieties towards Heck cross-coupling remains unknown due to its scarce reports in the literature.[10]

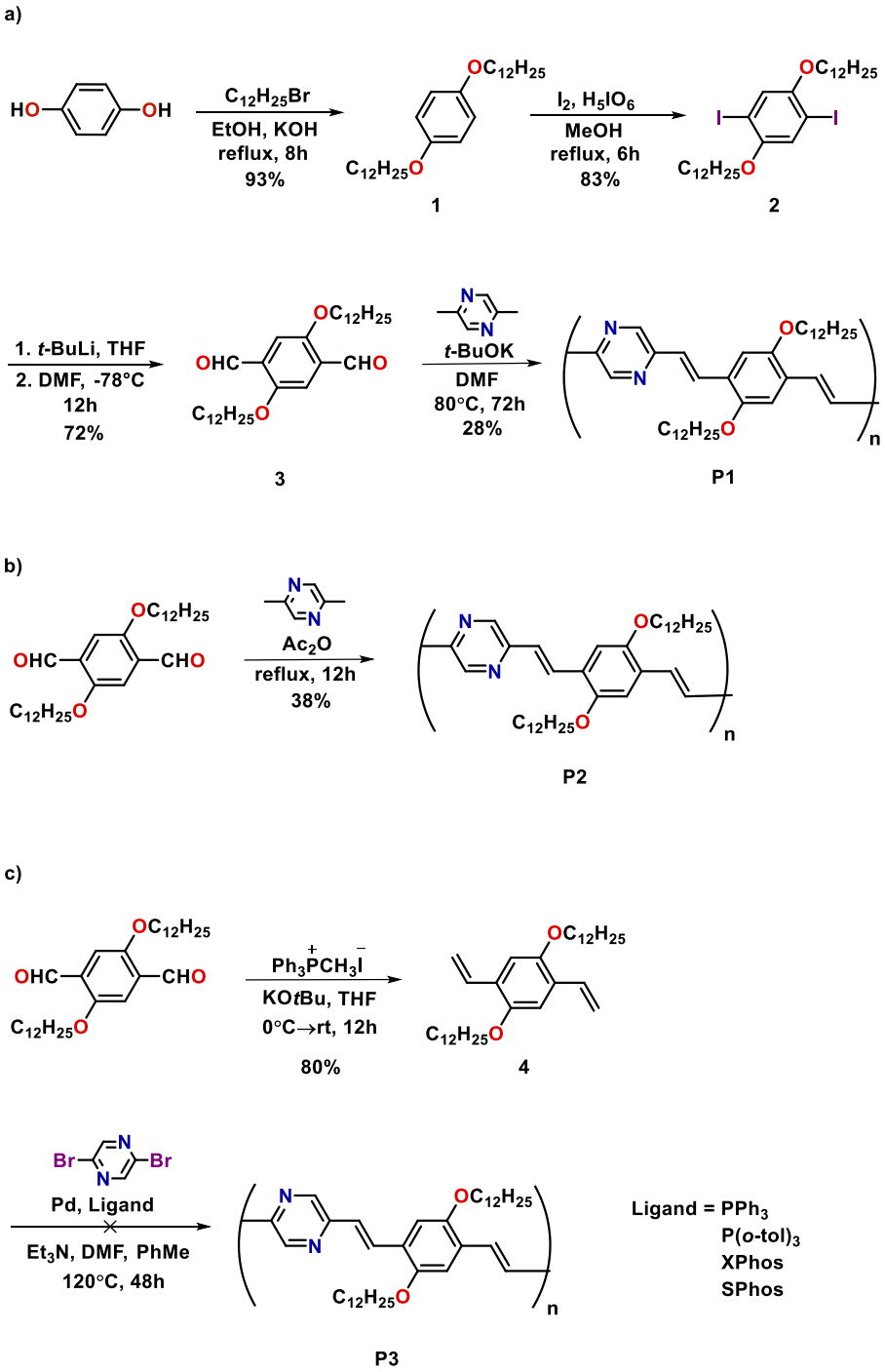

Scheme 4.1. The synthesis of a) **P1**, b) **P2**, and c) **P3**.

Protonation and quaternization of the pyrazine unit have been attempted to reduce the HOMO-LUMO energy gap of the D-A polymer (**Scheme 4.2**). The protonation of PAV was by effected treatment with TFA, and due to the low basicity of the pyrazine, 10,000 equivalents of TFA were added in order to protonate half of the pyrazine repeat units, and the protonation of the PAV was characterized by UV-vis spectroscopy. We also envisioned the quaternization of the pyrazine units by alkyl and zwitterionic chains to engineer the HOMO-LUMO energy gap of the polymer. Following similar nitrogen quaternization procedures in the literature, 1,3-propanesultone was refluxed with PAV in DMF. However, due to the low nucleophilicity of the pyrazine, the quaternization reaction did not occur, and the polymer was found decomposed at prolonged exposure to high temperature. Subsequently, 1-bromohexane was employed to quaternize the pyrazine in DMF, but no reaction occurred.

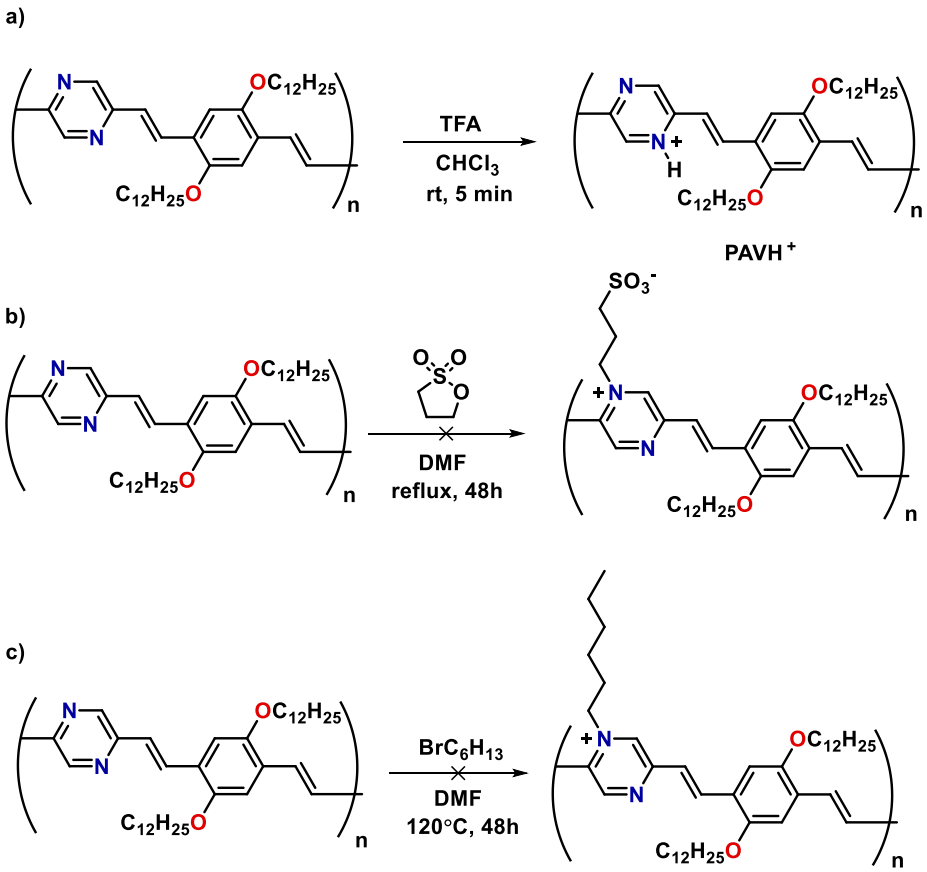

Scheme 4.2. The protonation and quaternization of PAV.

4.22 Photophysical Properties

To characterize the photophysical properties of PAV, solution-state and film-state UV-vis and fluorescence spectroscopy were carried out, and the data are reported in Table 4.1. The solution-state optical measurements of **P1** and **P2** were performed in chloroform, and the λ_{max} were both found at 425 nm. From the emission data, the λ_{em} of **P1** and **P2** were both measured to be 516 nm, showing a yellow emission

(**Figure 4.1a**). The PAV was spin-coated on the glass substrate to create a thin-film, and the film-state absorption maximum was recorded at 444 nm, which was red-shifted by 19 nm relative to that of the solution-state. The film-state λ_{em} also showed a 74 nm red-shift as compared to its solution-state (**Figure 4.1b**). The red-shifts observed in the film-state of the PAV were likely contributed by the enhanced solid-state packing effect resulting from the aggregation, and the film-state optical HOMO-LUMO energy gap was reduced to 2.13 eV from 2.92 eV of the solution-state, which are estimated from the λ_{onset} values. The solution-state relative quantum yield of PAV in chloroform was performed comparing against quinine sulfate in 0.5 M sulfuric acid, and it was measured to be 0.10. The quinine sulfate in 0.5 M sulfuric acid was co-dissolved with poly(methylmethacrylate) (PMMA) in chloroform and spin-coated on a glass substrate, and the relative quantum yield of PAV in the film-state was measured to be 0.22 relative to the quinine sulfate standard.

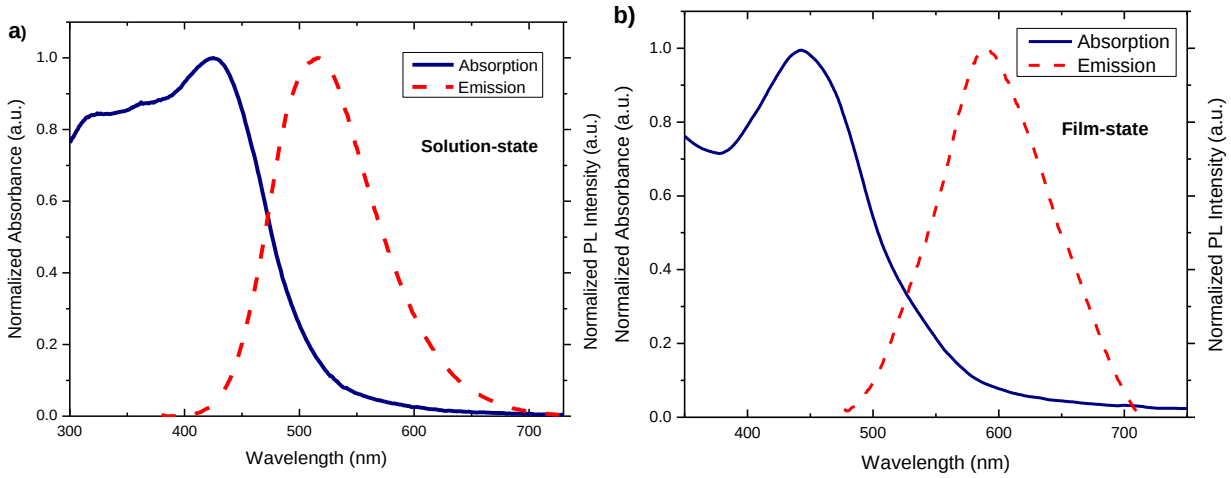

Figure 4.1. Normalized absorption and emission spectra of PAV in a) chloroform b**)** in the film-state.

The PAV compound was protonated by large equivalents of TFA to generate $PAVH^+$, and the protonation was evident from the absorption spectrum. Upon protonation, the λ_{max} of $PAVH^+$ was significantly red-shifted from 425 nm to 516 nm, and an additional absorption band at 374 nm appeared, which exhibited a dual-band absorption spectrum, which is commonly observed in π-conjugated D-A systems. The λ_{onset} of $PAVH^+$ was red-shifted from 528 nm to 685 nm, which corresponds to a HOMO-LUMO energy gap reduction from 2.9 eV to 1.8 eV upon protonation in chloroform.

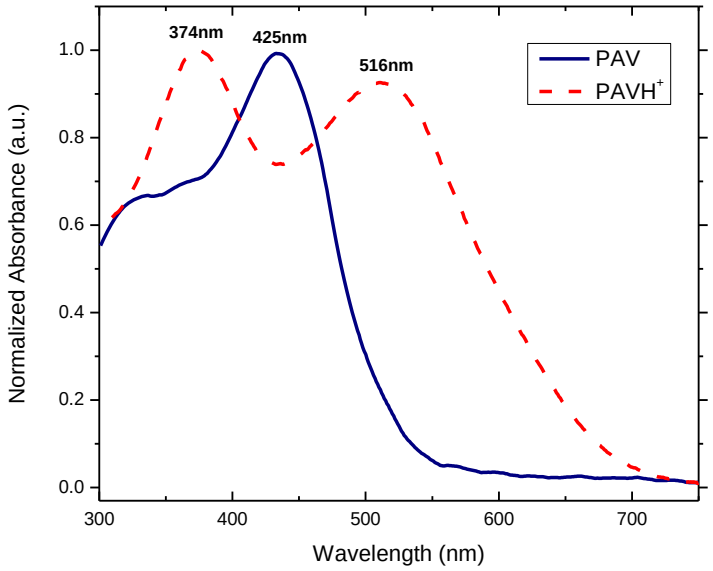

Figure 4.2. The UV-vis absorption spectra of PAV and $PAVH^+$.

4.3 Conclusion

In summary, we have investigated the synthesis of pyrazine-based π-conjugated D-A polymers via metal-free Knoevenagel- and aldol-type polycondensation. The obtained polymers showed low number-average molecular weights and low degree of polymerization, which suggested that the attempted metal-free polymerization methods were not robust. An alternative method such as Pd-catalyzed Heck polycondensation was investigated using various ligands; however, no polymers were successfully synthesized using this method, potentially due to the low reactivity of pyrazine towards the Pd catalyst. Future studies could be performed on optimizing the polymerization conditions, as well as alternative reactions such as the Wittig polycondensation. The photophysical properties of the PAV were studied, and the film-state absorption and emission showed significant red-shifts as compared to that in the solution-state. Quaternization with 1,3-propanesultone and 1-bromohexane of the pyrazine unit of PAV was unsuccessful, likely due to the low nucleophilicity of the pyrazine nitrogens. Protonation of the pyrazine units by TFA was successful, albeit requiring an excess of acid. The protonation of PAV gave rise to a significant red-shift in the absorption maximum of the $PAVH^+$.

4.4 Experimental Section

Synthesis of 1. To a suspension of hydroquinone (1.00 g, 9.08 mmol) and 1-bromodecane (4.77 g, 19.1 mmol) in 20 mL of EtOH, was added KOH (2.30 g, 40.9 mmol) under an atmosphere of N_2. The mixture was stirred under reflux for 8 hours, then cooled to room temperature. The precipitate was collected by vacuum filtration and washed with EtOH, and the crude product was purified by recrystallization from

MeOH to afford **1** as a white solid (3.8 g, 93% yield). ^{1}H NMR (400 MHz, $CDCl_3$): δ 6.80 (s, 4H), 3.87 (t, 4H), 1.75 (m, 4H), 1.42-1.24 (m, 36H), 0.86 (t, 6H).

Synthesis of 2. To a suspension of **1** (0.500 g, 1.12 mmol) in 2 mL of MeOH, was added iodine (0.280 g, 1.12 mmol) and periodic acid (0.260 g, 1.12 mmol) while stirring. The suspension was stirred at reflux under an atmosphere of N_2 for 6 hours, and the reaction was subsequently quenched by saturated KOH solution. The reaction was extracted with DCM, washed with H_2O and dried over anhydrous Na_2SO_4. The product was purified by recrystallization from a 1: 1 mixture of DCM/MeOH to afford **2** as a white solid (0.65 mg, 83% yield). ^{1}H NMR (400 MHz, $CDCl_3$): δ 7.15 (s, 2H), 3.90 (t, 4H), 1.78 (m, 4H), 1.40-1.25 (m, 36H), 0.86 (t, 6H).

Synthesis of 3. To 10 mL of anhydrous THF was added **2** (1.00 g, 1.43 mmol), and 1.6 M of *t*-BuLi in hexanes (0.320 g, 5.07 mmol) was added dropwise to the mixture under an atmosphere of N_2 at -78 ℃, and the mixture was slowly raised to 0 ℃ over 2 hours. Anhydrous DMF (1.05 g, 14.3 mmol) was added to the reaction mixture via a syringe at -78 ℃ and the mixture was slowly brought to room temperature and stirred for 12 hours. The reaction was quenched by saturated NH_4Cl solution and extracted with DCM and dried over anhydrous Na_2SO_4. The product was purified by column chromatography using DCM and hexanes as eluent (3: 7 v/v) to afford **3** as a yellow solid (0.52 g, 72% yield). ^{1}H NMR (400 MHz, $CDCl_3$): δ 10.50 (s, 2H), 7.41 (s, 2H), 4.06 (t, 4H), 1.79 (m, 4H), 1.43-1.24 (m, 36H), 0.86 (t, 6H).

Synthesis of 4. To a suspension of previously synthesized methyl triphenylphosphonium iodide in 20 mL of anhydrous THF was added *t*-BuOK (0.190 g, 1.67 mmol) at 0 ℃ and the suspension was slowly brought to room temperature over a period of 30 min. Subsequently, **3** (0.300 g, 0.600 mmol) was added to the suspension, and it was stirred at room temperature for 12 hours under an atmosphere of N_2. The reaction was quenched by H_2O and extracted with DCM and dried over anhydrous Na_2SO_4. After the evaporation of the solvent, the crude was purified by column chromatography using DCM/hexanes as eluent (2: 8 v/v) to afford **4** as a white solid (0.24 g, 80% yield). ^{1}H NMR (400 MHz, $CDCl_3$): δ 7.05-6.98 (dd, J_1 = 16 Hz, J_2 = 12 Hz, 2H), 6.96 (s, 2H), 5.73-5.68 (dd, J_1 = 20 Hz, J_2 = 4 Hz, 2H), 5.24-5.21 (dd, J = 12 Hz, 2H), 3.94 (t, 4H), 1.81-1.74 (m, 4H), 1.46-1.25 (m, 36H), 0.86 (t, 6H).

Synthesis of P1. To 6 mL of anhydrous DMF was added 2,5-dimethylpyrazine (0.050 g, 0.46 mmol) and the mixture was heated to 80 ℃ for 1 hour under an atmosphere of N_2. To the dark blue solution was then added **3** (0.23 g, 0.46 mmol) and the mixture was stirred for 48 hours at 80 ℃ then raised to 100 ℃ for 24 hours. The mixture was cooled to room temperature, extracted with DCM, and concentrated under vacuum. The viscous solution was slowly precipitated in cold MeOH, and the precipitate was collected by suction

filtration (process repeated 5 times) to afford **P1** as a dark red solid (0.29 g, 28% yield). ^{1}H NMR (400 MHz, $CDCl_3$): δ 10.49 (s, 1H, aldehyde proton), 8.69 (br, 1H, pyrazine proton), 8.03 (br, 1H, pyrazine proton), 7.46-7.35 (m, 4H, vinyl protons), 7.23 (br, 2H, phenyl protons), 4.14-4.05 (br, 4H), 1.88 (br, 4H), 1.41-1.20 (m, 36H), 0.88 (t, 6H).

Synthesis of P2. To 50 mL of Ac_2O was added **2** (0.700 g, 1.39 mmol) and 2,5-dimethylpyrazine (0.150 g, 1.39 mmol) under an atmosphere of N_2, and the reaction mixture was heated at reflux for 72 hours. The mixture was cooled to room temperature, extracted with DCM, and concentrated under vacuum. The viscous solution was slowly precipitated in cold MeOH, and the precipitate was collected by suction filtration (process repeated 5 times) to afford **P1** as a dark red solid (0.32 g, 38% yield). ^{1}H NMR (400 MHz, $CDCl_3$): δ 10.49 (s, 1H, aldehyde proton), 8.69 (br, 1H, pyrazine proton), 8.03 (br, 1H, pyrazine proton), 7.46-7.35 (m, 4H, vinyl protons), 7.23 (br, 2H, phenyl protons), 4.14-4.05 (br, 4H), 1.88 (br, 4H), 1.41-1.20 (m, 36H), 0.88 (t, 6H).

Synthesis of PAVH$^+$. To a mixture of **PAV** (0.010 g, 0.017 mmol) and 1 mL of chloroform-*d* was added TFA (19.0 g, 0.170 mmol) while stirring at room temperature. Aliquots of the resulting dark purple solution were characterized by UV-vis spectroscopy.

4.5 References

(1) Yuen, J. D.; Fan, J.; Seifter, J.; Lim, B.; Hufschmid, R.; Heeger, A. J.; Wudl, F. *J. Am. Chem. Soc.* **2011**, *133*, 20799–20807.

(2) Beaujuge, P. M.; Amb, C. M.; Reynolds, J. R. *Acc. Chem. Res.* **2010**, *43*, 1396–1407.

(3) Yao, L.; Zhang, S.; Wang, R.; Li, W.; Shen, F.; Yang, B.; Ma, Y. *Angew. Chem., Int. Ed.* **2014**, *53*, 2119–2123.

(4) Fu, D. K.; Xu, B.; Swager, T. M. *Tetrahedron* **1997**, *53*, 15487–15494.

(5) Zhou, Z.-H.; Maruyama, T.; Kanbara, T.; Ikeda, T.; Ichimura, K.; Yamamoto, T.; Tokuda, K. *J. Chem. Soc. Chem. Commun.* **1991**, *1460*, 1210-1212.

(6) Peng, Z.; Galvin, M. E. *Chem. Mater.* **1998**, *10*, 1785–1788.

(7) Tian, Y. H.; Kertesz, M. *Macromolecules* **2009**, *42*, 2309–2312.

(8) Wen, L.; Duck, B. C.; Dastoor, P. C.; Rasmussen, S. C. *Macromolecules* **2008**, *41*, 4576–4578.

(9) Nikishkin, N. I.; Huskens, J.; Verboom, W. *Org. Biomol. Chem.* **2013**, *11*, 3583.

(10) Malik, I.; Hussain, M.; Ali, A.; Tengho Toguem, S. M.; Basha, F. Z.; Fischer, C.; Langer, P. *Tetrahedron* **2010**, *66*, 1637-1642.

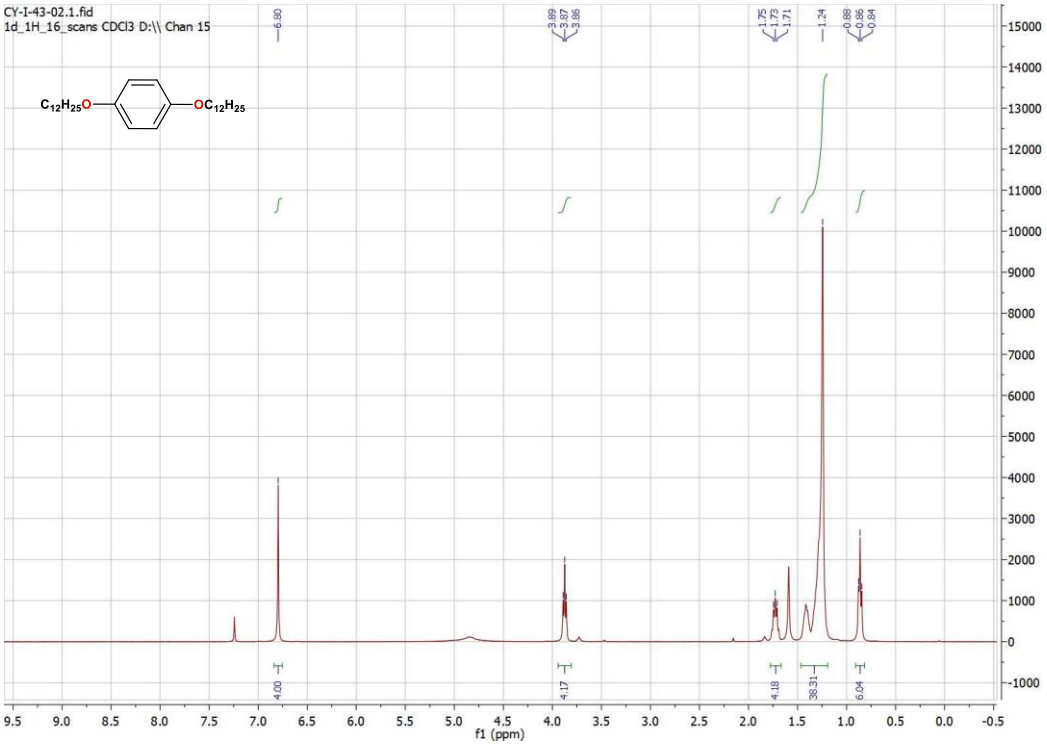

Figure 4.3. ^{1}H NMR of compound 1.

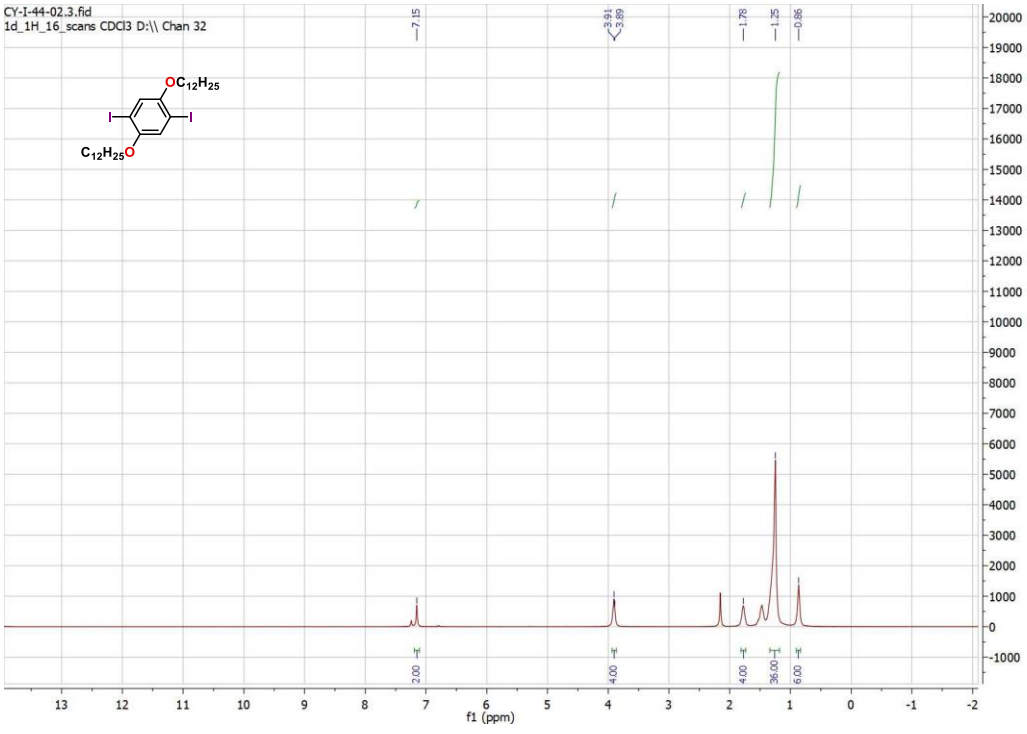

Figure 4.4. ^{1}H NMR of compound 2.

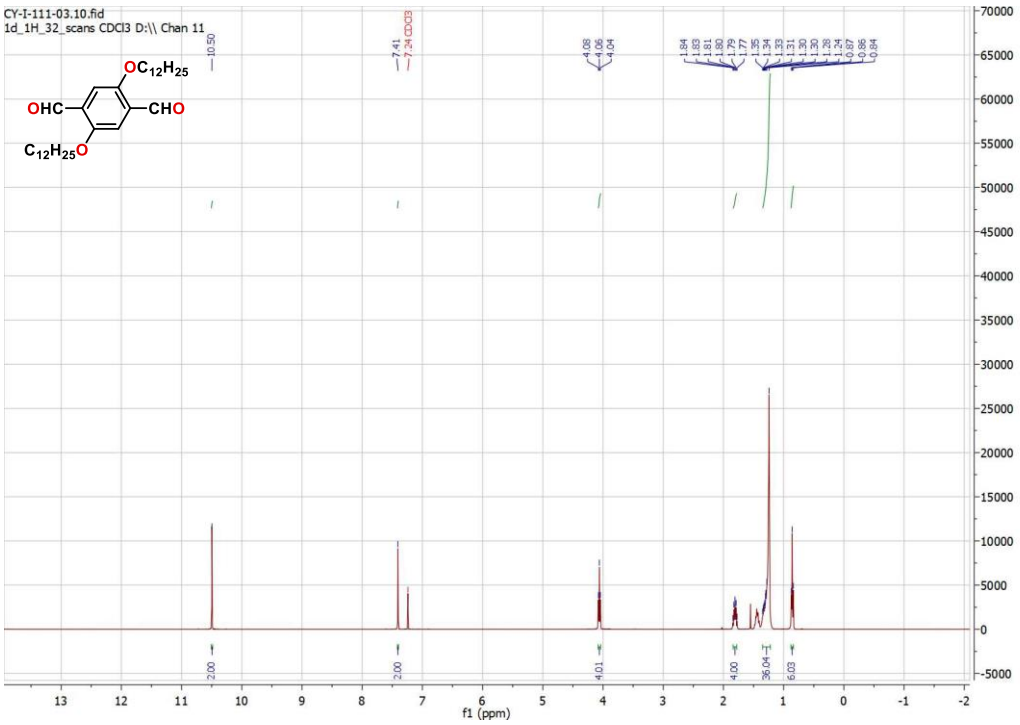

Figure 4.5. ^{1}H NMR of compound 3.

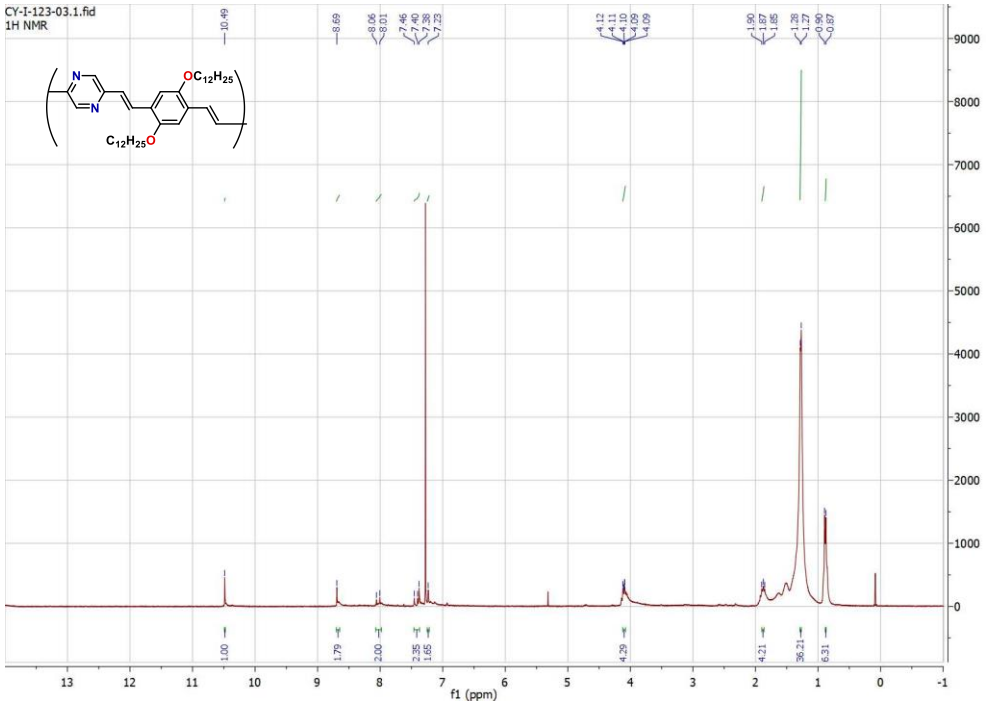

Figure 4.6. ^{1}H NMR of P1.

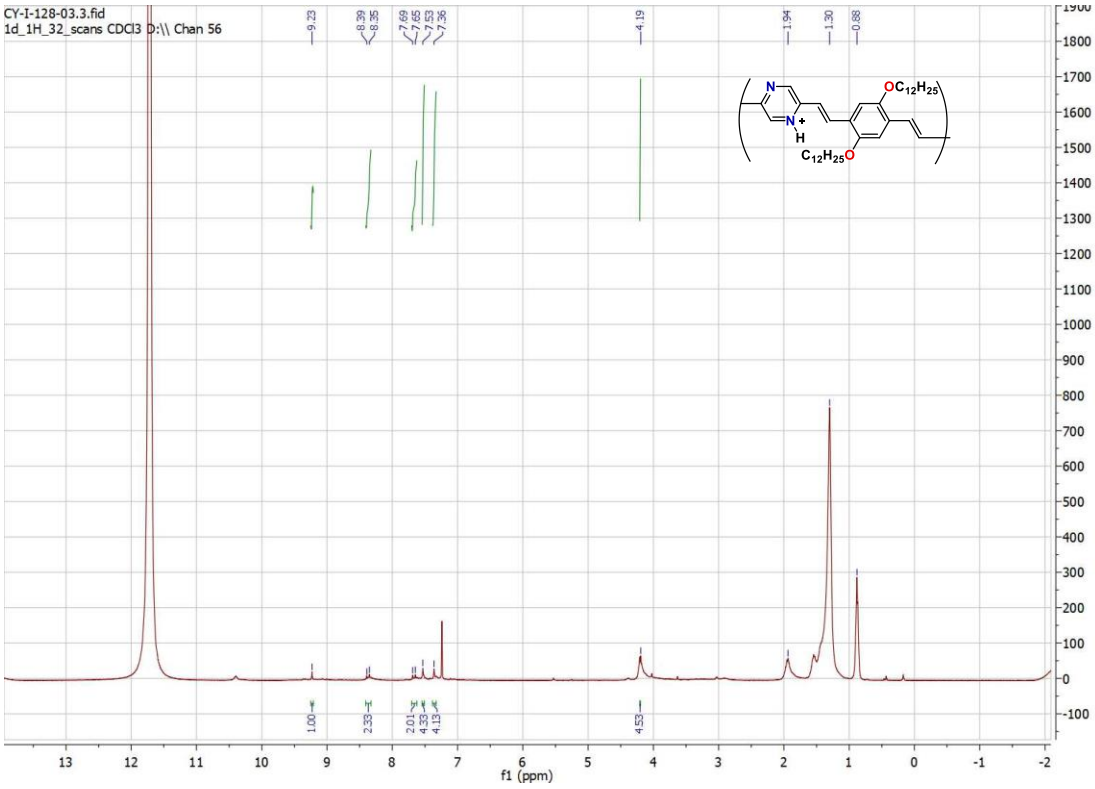

Figure 4.7. ^{1}H NMR of PAVH^{+}.

Chapter 5. Conclusions and Future Scope

5.1 Conclusions

The π-conjugated organic materials are of considerable interest due to their low cost of synthesis, tunability, and mechanical flexibility, compared to the traditional inorganic-based electronic materials such as silicon.[1] Current research in π-conjugated organic materials is focused on numerous forms including small molecules, oligomers, polymers, and organic frameworks. In the current thesis, we have investigated three types of π-conjugated organic systems: small molecules, polymers, and halogen-bonded (XB) organic frameworks, mainly regarding synthesis, theoretical, structural, and photophysical characterizations.

In Chapter 2, two series of XB organic frameworks were designed with 1,2,4,5-tetrafluoro-3,6-diiodobenzene (TFDIB) and 1,3,5-trifluoro-2,4,6-triiodobenzene (TFTIB) as the XB donors, and multiple π-conjugated *N*-heterocycles as the XB acceptor. These XB co-crystals have exhibited novel solid-state supramolecular assemblies which are significantly affected by the topicity of the XB donors. The MO energy levels of the crystals relative to their starting materials are influenced by the formation of intermolecular interactions such as XB and π-π stacking, suggested by DFT calculations and UV-vis spectroscopy. Two of the designed XB co-crystals have shown blue-shifts in emission upon mechanical grinding due to the loss in crystallinity, as evidenced by PXRD data.

In Chapter 3, a series of aryl-SF_5 containing π-conjugated D-A systems was designed, and the molecules were geometrically optimized by DFT calculations, whereupon the distribution of the molecular orbitals were obtained. The separation of the highest occupied molecular orbital (HOMO) and the lowest unoccupied molecular orbital (LUMO) indicates D-A systems. Two compounds of the designed aryl-SF_5 containing molecules were synthesized through Pd-catalyzed cross-coupling reactions, and their photophysical properties were studied in the solution, film, and solid-states.[2] The synthesized compounds exhibited large Stokes shifts that are potentially promising for applications such as bio-imaging.

In Chapter 4, a pyrazine-based π-conjugated D-A polymer was synthesized through metal-free Knoevenagel and aldol polycondensations. The photophysical properties of the polymer were studied in the solution and film-states. Post-synthetic modification including protonation and quaternization was performed on the polymer, and only protonation was successful due to the low nucleophilicity of the pyrazine unit. A significant red-shift was observed in the UV-vis absorption upon protonation compared to the unprotonated polymer.

As a general conclusion, diverse types of D-A systems were studied in this thesis, ranging from small molecules to supramolecular frameworks. We have shown that our designed D-A systems can be readily synthesized using available literature procedures. Many of these systems exhibited interesting photophysical properties that are promising for applications such as bio-imaging. Future studies may extend

the current molecular designs to more complex ones with improved optoelectronic properties. These materials can also potentially be tested in electronic devices such as OPVs and OFETs.

5.2 Future Scope

Regarding the XB work, although novel π-conjugated XB frameworks have been realized, the materials lack fascinating optoelectronic properties. Most co-crystal have shown weak to no fluorescence, and the UV-vis absorptions were not sufficiently enhanced by the formation of the XB interactions. Despite the formation of moderate to strong XB interactions in the co-crystals, other strong intermolecular interactions such as π-π stacking were found to be weak. The moderate optical properties exhibited by the co-crystals could be attributed to their insufficient intermolecular orbital interactions in the solid-state. Thus, the energy levels of the co-crystals can only be marginally modified through the current molecular design. For future studies, some drawbacks of the current co-crystals need to be addressed, such as weak intermolecular orbital interactions, poor optical properties, and low thermal stability, issues that are detrimental to their potential application in materials science.

To address these, XB acceptors with larger π-conjugation can be designed. Moieties such as anthracene and perylene diimide (PDI) have been reported as excellent optoelectronic materials that can form strong intermolecular orbital interactions in the solid-state (**Figure 5.1**).[3] These π-cores can be incorporated into the XB acceptor molecules, and improved molecular packing can potentially be achieved.

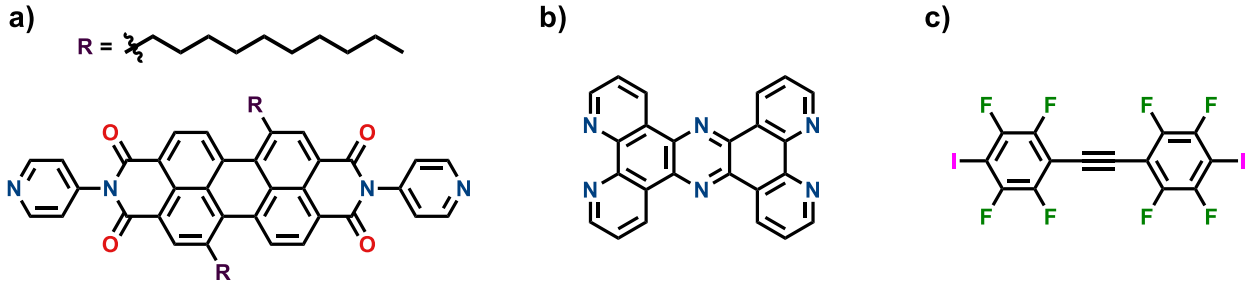

Figure 5.1. a) structure of proposed PDI XB acceptor, b) structure of fused ring XB acceptor, and c) structure of proposed XB donor.

Most of the pyridine units in our current XB acceptors are connected to the π-core through alkyne groups. Such a design offers molecular planarity which is a favorable feature for solid-state packing, but as indicated by our SCXRD data, they tend not to participate in intermolecular orbital interactions, and in some cases, only weak interactions are observed. To circumvent this problem, the pyridine unit can be fused into large π-cores to enable both the XB interactions and stronger π-π stacking (**Figure 5.1**).

By improving the intermolecular orbital interactions of the co-crystals, we can tune their MO energy levels more effectively, thus more pronounced changes in the solid-state optical properties compared to the starting materials can be realized. The relatively low thermal stability of the co-crystals can mainly

be attributed to the XB donors. The current XB donors are simple benzene systems which have low melting points. Therefore they limit the thermal stability of the resulting co-crystals. To improve this aspect of the material, we can further increase the π-conjugation of the XB donors (**Figure 5.1**). This strategy can elevate the thermal stability of the co-crystal, and it can also improve their packing and optical properties in the solid-state.

In addition to the optical studies of XB co-crystals, electronic studies can also be performed in the future. To date, single-crystal OFET devices based on halogen-bonded co-crystals have not been reported in the literature. Thus, XB co-crystals with excellent solid-state packing can be subjected to OFET measurements.

The molecular design in Chapter 3 showed an effective strategy to form π-conjugated D-A systems. Currently, a popular molecular design involves the incorporation of electron-withdrawing groups into π-cores to tune the electronic properties of the materials for applications such as OFETs and OPVs.[4] The SF_5 group can be directly incorporated into the π-systems for more effective tuning of the MO energy levels (**Figure 5.2**). The lipophilicity of the SF_5 group can also improve the solubility and solution-processability of the materials for potential electronic applications.

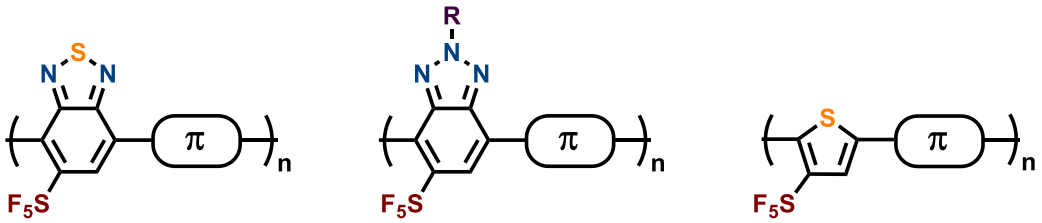

Figure 5.2. The proposed SF_5-containing π-conjugated polymers.

In Chapter 4, we encountered difficulties with protonation and quaternization of the pyrazine-containing polymer due to the low nucleophilicity of the pyrazine nitrogens. However, past reports in the literature suggest that the pyridine group can be efficiently protonated and quaternized,[5,6] therefore, pyridine-containing polymers can be designed and synthesized for post-synthetic modifications. To avoid similar molecular designs with the previous reports, other pyridine-containing electron-deficient π-cores can be introduced in the D-A polymer system, and protonation and quaternization should be possible for the pyridine nitrogen.

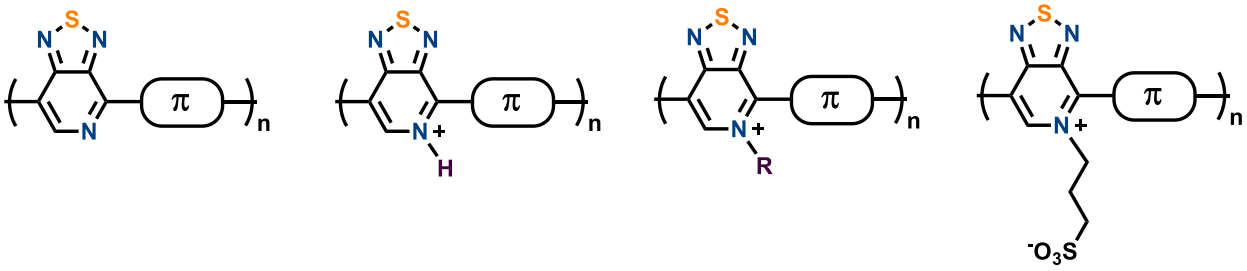

Figure 5.3. The proposed pyridine-containing π-conjugated polymers and their protonated, alkylated, and zwitterionic states.

With the successful postpolymerization modification of the pyridine-containing polymer, dramatic narrowing of the HOMO-LUMO energy gap and red-shift in optical absorption are expected. The broad absorption of the protonated/quaternized polymer can be studied for OPV devices; quaternization of the pyridine with zwitterionic chains would enable hydrophilicity which can be used as the interfacial layer between the metal electrodes and the organic semiconductor in various devices such as OFETs, OPVs, and OLEDs.[7] Another potential application for the protonated/quaternized polymer is in photocatalysis. The narrowing of the HOMO-LUMO energy gap of the polymer allows for facile photoexcitation by light, and the excited polymer can be studied for the decomposition of lignin.

References

(1) Kelley, T. W.; Baude, P. F.; Gerlach, C.; Ender, D. E.; Muyres, D.; Haase, M. A.; Vogel, D. E.; Theiss, S. D. *Chem. Mater*. **2004**, *16*, 4413–4422.

(2) Gautam, P.; Yu, C. P.; Zhang, G.; Hillier, V. E.; Chan, J. M. W. *J. Org. Chem.* **2017**, *82*, 11008–11020.

(3) Jones, B. A.; Ahrens, M. J.; Yoon, M. H.; Facchetti, A.; Marks, T. J.; Wasielewski, M. R. *Angew. Chem., Int. Ed.* **2004**, *43*, 6363–6366.

(4) Bronstein, H.; Frost, J. M.; Hadipour, A.; Kim, Y.; Nielsen, C. B.; Ashraf, R. S.; Rand, B. P.; Watkins, S.; McCulloch, I. *Chem. Mater.* **2013**, *25*, 277–285.

(5) Fu, D. K.; Xu, B.; Swager, T. M. *Tetrahedron* **1997**, *53*, 15487–15494.

(6) Marsella, M. J.; Fu, D. -K; Swager, T. M. *Adv. Mater.* **1995**, *7*, 145–147.

(7) Liu, Y.; Duzhko, V. V.; Page, Z. A.; Emrick, T.; Russell, T. P. *Acc. Chem. Res.* **2016**, *49*, 2478–2488.